NANO · MICRO small
www.small-journal.com

Design and Advanced Manufacturing of NU-1000 Metal–Organic Frameworks with Future Perspectives for Environmental and Renewable Energy Applications

Reza Abazari, Soheila Sanati, Majed A. Bajaber, Muhammad Sufyan Javed, Peter C. Junk, Ashok Kumar Nanjundan, Jinjie Qian,* and Deepak P. Dubal**

Metal–organic frameworks (MOFs) represent a relatively new family of materials that attract lots of attention thanks to their unique features such as hierarchical porosity, active metal centers, versatility of linkers/metal nodes, and large surface area. Among the extended list of MOFs, Zr-based-MOFs demonstrate comparably superior chemical and thermal stabilities, making them ideal candidates for energy and environmental applications. As a Zr-MOF, NU-1000 is first synthesized at Northwestern University. A comprehensive review of various approaches to the synthesis of NU-1000 MOFs for obtaining unique surface properties (e.g., diverse surface morphologies, large surface area, and particular pore size distribution) and their applications in the catalysis (electro-, and photo-catalysis), CO_2 reduction, batteries, hydrogen storage, gas storage/separation, and other environmental fields are presented. The review further outlines the current challenges in the development of NU-1000 MOFs and their derivatives in practical applications, revealing areas for future investigation.

1. Introduction

Increasing energy demand and attempts to resolve environmental concerns have resulted in researchers' work to find sustainable approaches for energy generation. The current research works are focused on the fast depletion of fossil fuel resources, environmental protection, and green and sustainable sources of energy development.[1,2] Efforts to find efficient methods of generation and storage of renewable energy have rapidly grown to innovative socioeconomic standards and the rise of environmental concerns, in addition to the technological advancements that enhanced energy consumption.[3] Researchers have made huge efforts to enhance energy efficiency by water purification at lower energies, developing high-power batteries using lower contents of heavy metals, and power generation with decremented carbon emission.[4,5]

Lithium-ion batteries, supercapacitors, and fuel cells are highly popular in electrochemical energy storage and conversion.[6] Additionally, industrialization and agricultural activities have deteriorated the environment, necessitating efficient control and elimination of environmental contaminants.[7] In addition, industrial effluents, pharmaceutical products, and

R. Abazari, S. Sanati
Department of Chemistry
Faculty of Science
University of Maragheh
Maragheh, Iran
E-mail: reza.abazari@maragheh.ac.ir

M. A. Bajaber
Chemistry Department
Faculty of Science
King Khalid University
Abha 61413, Saudi Arabia

M. S. Javed
School of Physical Science and Technology
Lanzhou University
Lanzhou 730000, China

P. C. Junk
College of Science and Engineering
James Cook University
Townsville 4811, Australia

A. K. Nanjundan
Schole of Engineering
University of Southern Queensland
Springfield, Queensland 4300, Australia

J. Qian
Key Laboratory of Carbon Materials of Zhejiang Province
College of Chemistry and Materials Engineering
Wenzhou University
Wenzhou, Zhejiang, China
E-mail: jinjieqian@wzu.edu.cn

D. P. Dubal
Centre for Materials Science
School of Chemistry & Physics
Queensland University of Technology
Brisbane, Queensland 4000, Australia
E-mail: deepak.dubal@qut.edu.au

The ORCID identification number(s) for the author(s) of this article can be found under https://doi.org/10.1002/smll.202306353

DOI: 10.1002/smll.202306353

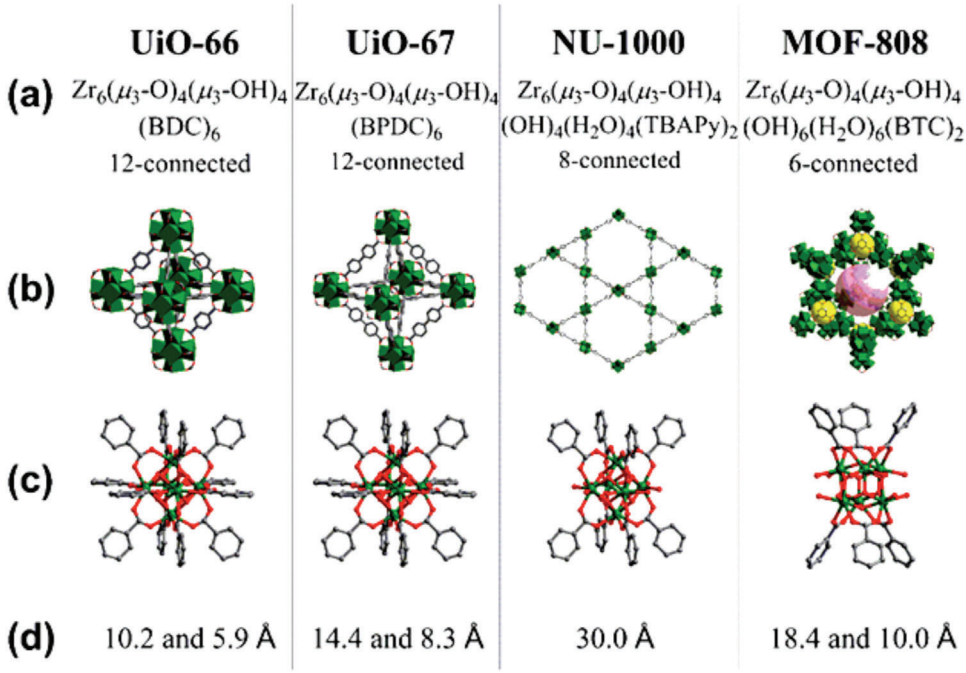

Figure 1. The character of Zr-MOFs structures: a) the selected MOFs formulae and denotations; b) their structures; c) types of coordination Zr_6 nodes; and d) their cage/window/pore diameter. Reproduced with permission.[51] Copyright 2019, American Chemical Society, (define BDC, BPDC, TBAPy, BTC).

organic pollutants are extremely damaging to the environment and are released into waterways and contribute to pollution. The traditional treatment techniques for wastewater are inefficient, energy-intensive, and uneconomical in removing such pollutants.[8,9] Despite other renewable energy sources, solar energy is a favorable option since it is reliable as well as economical to generate power, photocatalysis, production of hydrogen, reduction of CO_2, and treatment of water.[10,11] Therefore, it is a cleaner and more eco-friendly option, making it ideal for meeting the world's future requirements in terms of both the environment as well as energy. In this regard, efficient and sustainable routes are highly welcome in environmental protection measures. The fundamental role of materials science in this field lies in the design, fabrication, and evaluation of key functional materials.[12,13]

Metal–organic frameworks (MOFs) are a moderately new class of materials and bring exciting surface characteristics such as hierarchical pore structure, large specific surface area, good chemical stability, and ease of functionalization.[14–21] MOFs, composed of organic linkers binding cationic metal clusters, are a new generation of porous crystalline materials.[22–26] The cationic metal clusters that are located at the nodes are connected to one another *via* the use of coordinating metal ligands together with organic ligands.[27,28] The enormous surface area and vast structural tunability of MOFs, as well as their unique physiochemical characteristics, are well-known features of these materials.[29,30] Contrary to other porous materials like zeolites, MOFs can be easily synthesized and are modifiable under controlled conditions. MOFs have been used in various fields such as the degradation of pollutants, organic transformations, carbon dioxide reduction, splitting of water, drug delivery, chemical separation, gas storage, fuel, optoelectronic applications, catalysis, photocatalysis, and water remediation.[31–35] Furthermore, precise synthetic methods can facilitate the effective development of highly porous MOFs that possess targeted geometries and pore sizes for energy and environmental applications.[36–41] In particular, reticular chemistry is one of the most prominent approaches, as it allows the rational top-down design as well as precise structural assembly of MOF materials at the molecular level *via* corresponding organic and inorganic units.[42,43] For instance, edge-transfer nets which are networks containing only one type of edge, often exist in enlarged crystalline network architectures. This reticular design approach focusing on edge-transfer nets has led to the assembly of several important classes of MOF materials. Furthermore, exploiting reticular chemistry for exploring different combinations of molecular building blocks with dissimilar geometries can guide the unexpected finding of crystalline structures.[44] Such reticular chemistry-assisted synthetic methods have enabled Farha's group to successfully fabricate a series of MOF materials *via* a combination of rational design, directed synthesis, and occasionally unanticipated discovery.[45] Pearson's theory can be adopted in the development of MOFs to enhance metal node-organic linker interactions.[46] Hard acids such as metal ions of Al^{3+}, Cr^{3+}, and Zr^{4+} can be employed in reactions with hard ligands such as carboxylate linkers (e.g. MILs, UiO-67/66 and MOF-808, and so on) to achieve stable MOFs. Similarly, combination of soft Lewis bases and acids leads to correspondingly stable entities.[47,48]

Zr-MOFs have high stability in water and are used in different applications. **Figure 1** shows the structures of MOF-808,[49] UiO-67,[50] UiO-66,[51] and NU-1000[51] while **Table 1** lists the density, pore diameter, pore volume, and surface area of these Zr-based MOFs.[52–56] NU-1000 is one of the Zr-based MOFs, which comes with great surface area, hierarchical porosity, controllability, and

Table 1. Comparison of geometric properties for five Zr-MOFs.

Zr-MOF	pore volume [$cm^3\ g^{-1}$]	surface area [$m^2\ g^{-1}$]	small pore diameter [Å]	large pore diameter [Å]	References
UiO–66	1.18	1251	8	11	[52]
DUT–52	0.60	1399	4.36	8.59	[53]
MOF–808	0.84	1538.4	4.8	18.4	[54]
UiO–67	0.99	2500	11.5	23	[55]
NU–1000	1.46	2320	8	31	[56]

good chemical stability along with superior post-synthetic modification, which led to its applicability in electrochemical energy storage and conversion and environmental protection.[57] For example, it has been suggested that water-stable zirconium (Zr)-based MOFs (NU-1000) established on Zr_6O_8 clusters exhibit remarkable catalytic activity due to the existence of extremely Lewis acidic Zr centers.[58,59] The detected catalytic activity depends on pH, with the best efficiencies at alkaline pH conditions.[60] Using chemical warfare weapons and/or their mimics, Hupp and colleagues investigated the catalytic activity of NU-1000. The catalytic sites were nodes made of Zr_6 that have hydroxyl groups as well as terminal water ligands.[61] Currently, many review articles have been published that usually focus on the synthetic strategies of MOFs and brief overviews of their various applications. Nevertheless, relatively less attention has been paid to the development of Zr-MOFs and their energy and environmental applications. Some review articles have addressed Zr-MOFs,[62,63,64–66] however, a systematic and comprehensive summary of NU-1000 has never been provided. According to **Figure 2**, till 2023/05/31, 344 publications in the Web of Science addressed NU-1000. The popularity of this field has increased each year. The majority of studies on this material are related to energy and environment. This review will also summarize other applications of NU-1000.

This review summarizes and highlights the recent progress of energy and environmental applications of NU-1000. First, the structure of NU-1000 with computational linker design and role of a modulator in the synthesis have been described. Second, energy applications of NU-1000 including photocatalytic hydrogen evolution, electrochemical oxygen and hydrogen evolution, CO_2 reduction, and lithium–sulfur (Li–S) batteries are outlined. The third section addresses the recent progress in environmental applications of NU-1000 such as capture of heavy metals, toxic organic pollutants and gas adsorption, separation, oxidation of sulfur, luminescence sensing, catalysts, clean energy conversion, and pollutant degradation. Finally, concluding remarks and perspectives are addressed in energy and environmental applications of NU-1000. A synopsis of the current state-of-the-art highlights NU-1000 as a versatile platform for energy and environmental purposes.

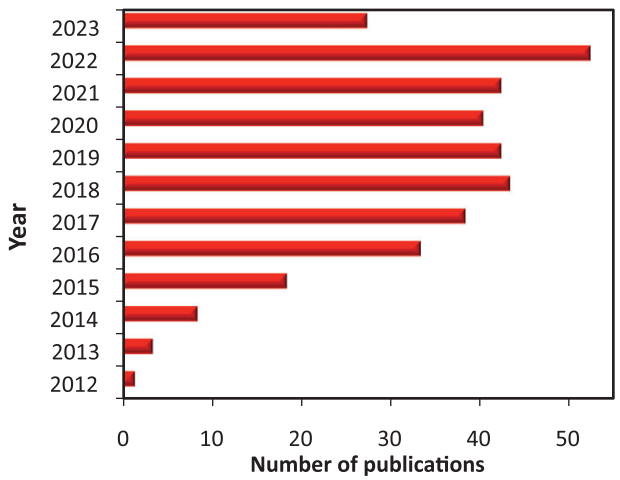

Figure 2. Increase in the number of published studies on NU-1000 (according to the Web of Science data, Jun 2023).

2. Structure of NU-1000

The ligands in the NU-1000 structure are tetratopic linkers of 1,3,6,8-tetrakis(*p*-benzoic-acid)pyrene (H_4TBAPy) and form triangular and hexagonal pores. The clusters of Zr_6 with linkers of $TBAPy^{4-}$ generate the thermally stable MOF NU-1000 as a mesoporous material.[67] The clusters of Zr_6 have an octahedral structure, and each of the cluster's triangular faces is covered by either μ_3-oxo or a μ_3-hydroxyl group.[68] Because of its very rigid construction, symmetry, and strong bonding between the linkers and nodes, NU-1000 has superior chemical as well as thermal stability compared to the majority of other MOFs.[69] The unsaturated behavior of the Zr_6 clusters, where only eight out of the twelve octahedron edges are coupled with linkers, is an advantage of NU-1000.[70] The mass transport issues that are often encountered in catalytic applications and allow for the rapid flow of substrates and reagents throughout the entire heterogeneous framework can be alleviated due to the exceptionally vast mesoporous channels extending throughout the structure of NU-1000. Therefore, NU-1000 is an ideal substrate for future enhancement, which has broadened its applications in CO_2 adsorption, catalysis, and toxic material cleanup due to the unoccupied sites on the cluster of Zr_6.[60,71] The structures of linker, node, and NU-1000 are presented in **Figure 3**.[72] Among different MOFs, NU-1000 is water-stable, environmentally friendly, and biocompatible which can be utilized in various energy applications.[62,63,73]

3. Computational Linker Design And Modulator Role

NU-1000 is a mesoporous MOF comprised of an oxo-Zr_6 $[Zr_6O_{16}H_{16}]^{8+}$ node. This MOF is prepared at high temperatures from a combination of $ZrOCl_2{\cdot}H_2O$ and benzoic acid as a modulator in the presence of a linker. The resultant crystals are mostly made by the NU-1000 domain, which crystallizes in a denser phase. Lu et al. prepared NU-601 hierarchical porous Zr-MOF (she-type)[74] by exchanging the linker $TBAPy^{4-}$ from NU-1000 with the TBAPy-2^{4-}. The six connecting nodes of NU-601 with overall 3D mesoporosity contribute significantly to the degrading hydrolysis of G-type nerve agent simulant. Using the linker, such as tetrakis(4-carboxyphenyl)-porphyrin (TCPP) (**Figure 4a**), with C_{2h} symmetry results in NU-902 (*scu*-type),[75] but with minor alteration in the torsion angle between the benzene ends and the central porphyrin rings, PCN-223 (*shp*-type).[76] The torsion angle φ_{cc} between the central plane (shown as green in Figure 4a)

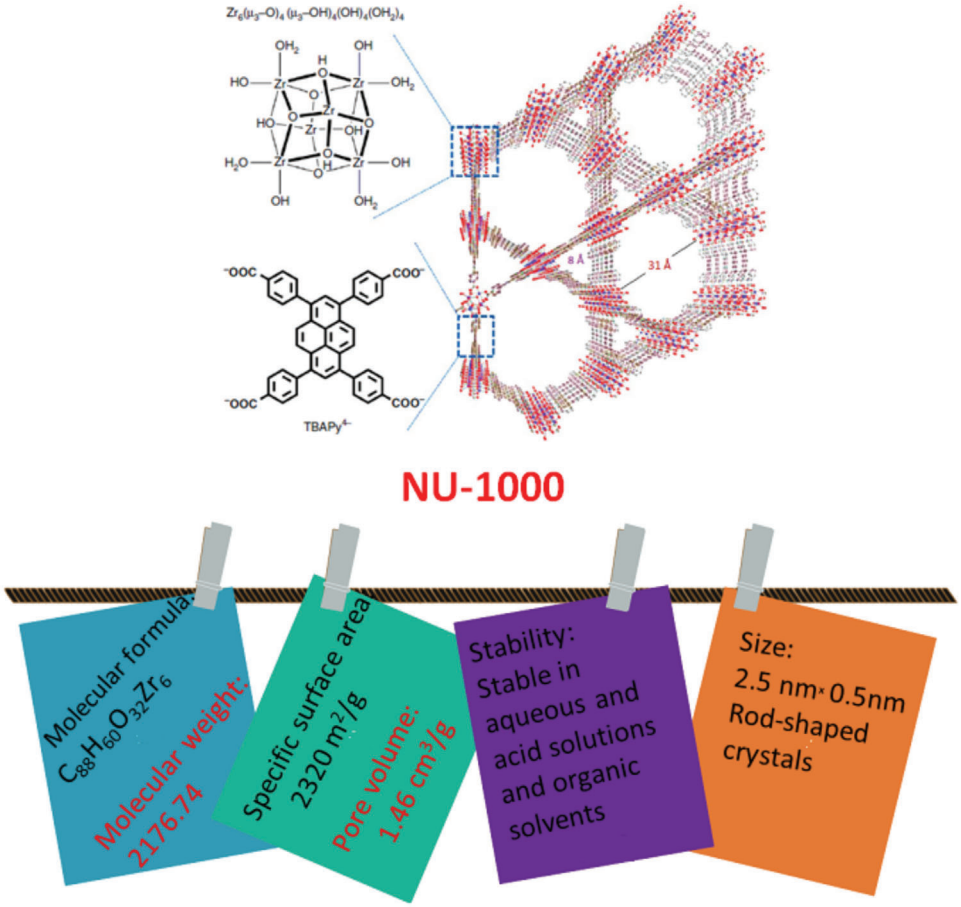

Figure 3. Schematic representation of the structure of NU-1000. Reproduced with permission.[72] Copyright 2015, Nature.

as well as the terminal carboxyl plane (shown as blue in Figure 4a) pushes the topology closer to csq or she when the linker is constructed with C_{2v} symmetry.

As depicted in Figure 4a, if φ_{cc} is close to or smaller than 60°, the overall dihedral angle between the neighboring joints will be 120°.[77] A *she*-type net will be formed if the angle φ_{cc} is large enough (≈ 80°).[78] This angle has a significant connection to the torsional angle φ_{cb} that exists between the central plane and the plane that contains the terminal benzene ring (Figure 4a, blue part). When φ_{cb} is sufficiently small (less than 60°), it is unlikely that φ_{cc} will surpass 80°, which is undesirable for a *she*-net. In TCCP, the neighboring pyrrole ring serves as an obstacle for the benzene ring, therefore, φ_{cc} always exceeds 60°. Webber et al. studied the role of modulators in phase-pure NU-1000 synthesis. $ZrOCl_2 \cdot H_2O$ as well as benzoic acid (BA) are commonly mixed with a TBAPy in DMF and aged at high degree of temperature to produce NU-1000.[79] In most cases, the product crystals (Figure 4b) are made up predominantly 0.486 g/cm^3 of NU-1000; however, the product also contains a denser phase that is structurally comparable to 0.704 g/cm^3 of NU-901 and possesses a greater density of node. The oxo-Zr_6 nodes of NU-1000 are rotated by 120 degrees with respect to one another, whereas the nodes of NU-901 are aligned parallel to each other (Figure 4b). The macropore part of NU-1000 is thought to be filled by oxo-Zr_6 nodes during the conventional synthesis of NU-1000, resulting in a structure similar to NU-901. Zr-atoms are mostly ligated to the modulator in both the $ZrOCl_2 \cdot H_2O$ solution and the modulator. By combining this solution with another solution that already contains linkers, it is possible to substitute the modulator molecule with the linker, resulting in the synthesis of MOFs.[80–82] When benzoic acid is replaced by biphenyl carboxylic acid, pure phase NU-1000 is produced. Comparing parallel reactions of products shows that use of BA or 4-phenylbenzoic acid as a modulator gives both pure phase and structurally heterogeneous crystals of NU-1000. The results obtained from the transmission electron microscope (TEM) images, can be seen in Figure 4c. This demonstrates the most compelling evidence that the generated crystals have a constant structural composition. The particles have a lattice spacing of 2.6 nm, the same as with NU-1000, and extend the full length of the particle. There was no evidence for any similar contrast of the denser materials or strain. As a result, it is possible to summarize the generated crystals are pure phase NU-1000, with no material comparable to NU-901.

In 2022, Rajasree et al. explored the significance of ligands designed in huge transition dipoles and their relative proper direction to MOF topology.[83] They described the size and vastness of the molecular excitons inside MOF-assembled chromophoric ligands by assessing the electron-hole correlation in their lowest energy density (optically allowed) transitions. Three

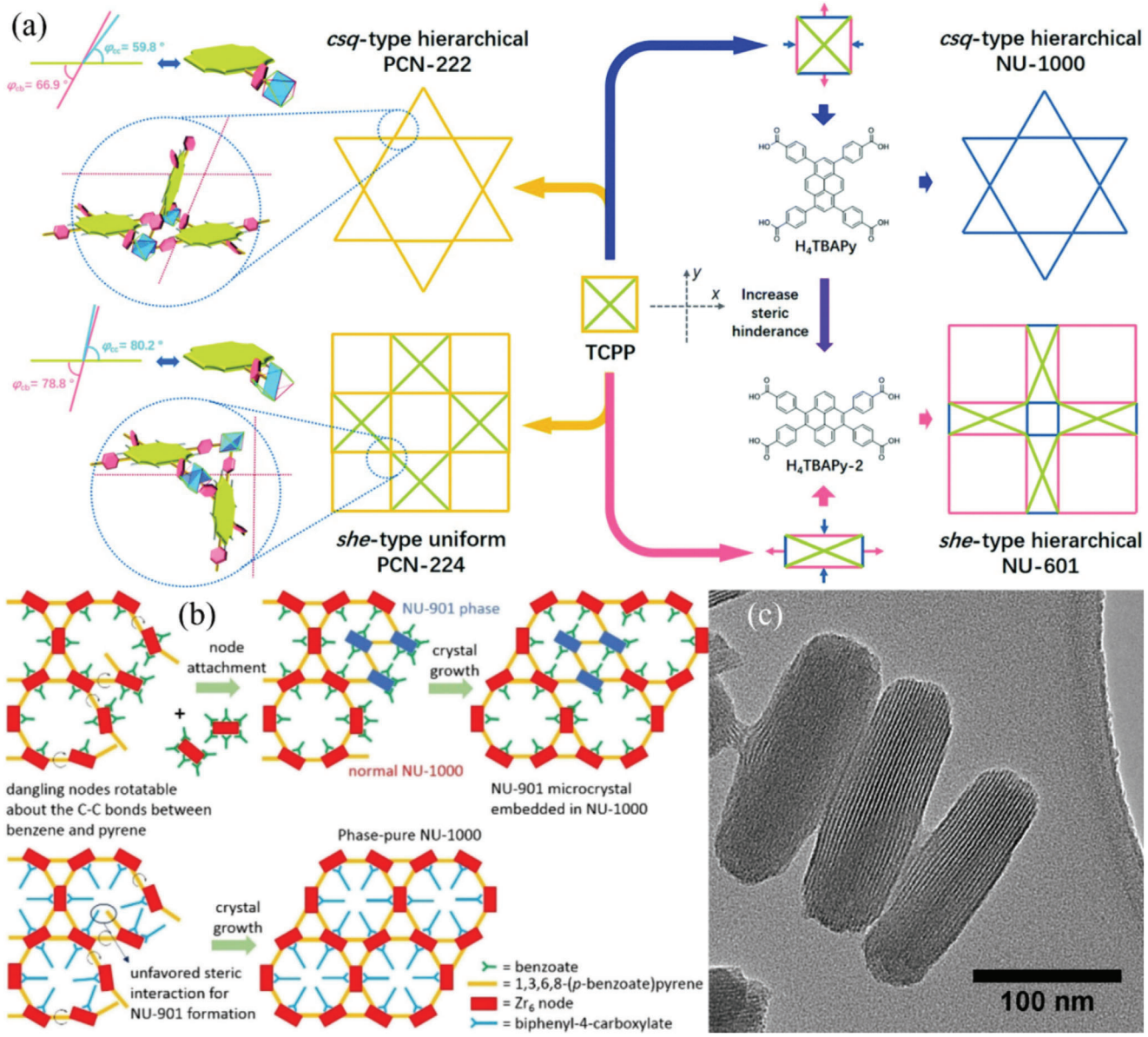

Figure 4. a) Zr-MOF hierarchies as a result of various linker configurations and geometries. Reproduced with permission.[74] Copyright 2021, Royal Society of Chemistry. b) Schematic representation of formation pathway of pure-phase NU-1000 and c) TEM image. Reproduced with permission.[79] Copyright 2017, American Chemical Society.

samples, namely, SIU-100, NU-1000, and *csq/xly* MOFs-PCN-222(Zn), were assessed which had asymmetrically oriented ligands around hexagonal mesopores and triangular micropores (**Figure 5**). They theoretically modeled and experimentally evaluated three zirconium MOFs with similar topologies but different linkers, and compared the dependency of size of such molecular excitons on the electronic symmetry of the ligands.

4. Water Stability of NU-1000 MOFs

For practical applications, MOFs with outstanding water stability are essential. There is often some amount of water or moisture involved in the majority of manufacturing processes, including CO_2 collection from combustion gas, proton conduction, purification of purification, and many other catalytic methods.[37,84,85] In the last ten years, there has been a significant acceleration in the research and development of water-stable MOFs. As a result of this, a number of well-known water-stable MOFs have been discovered, including MIL-100,[86] MIL-101,[87] ZIF-8,[88] and UiO-66.[68] In order to meet the needs of a wide range of new applications, many water-stable MOFs along with a diversity of functions have been produced.[89] Gas adsorption, scanning electron microscopy (SEM) as well as PXRD are three methods that are often employed for the evaluation of the stability of MOFs after they have been submerged in water. PXRD is useful for determining changes in crystallinity, but it is important to keep in

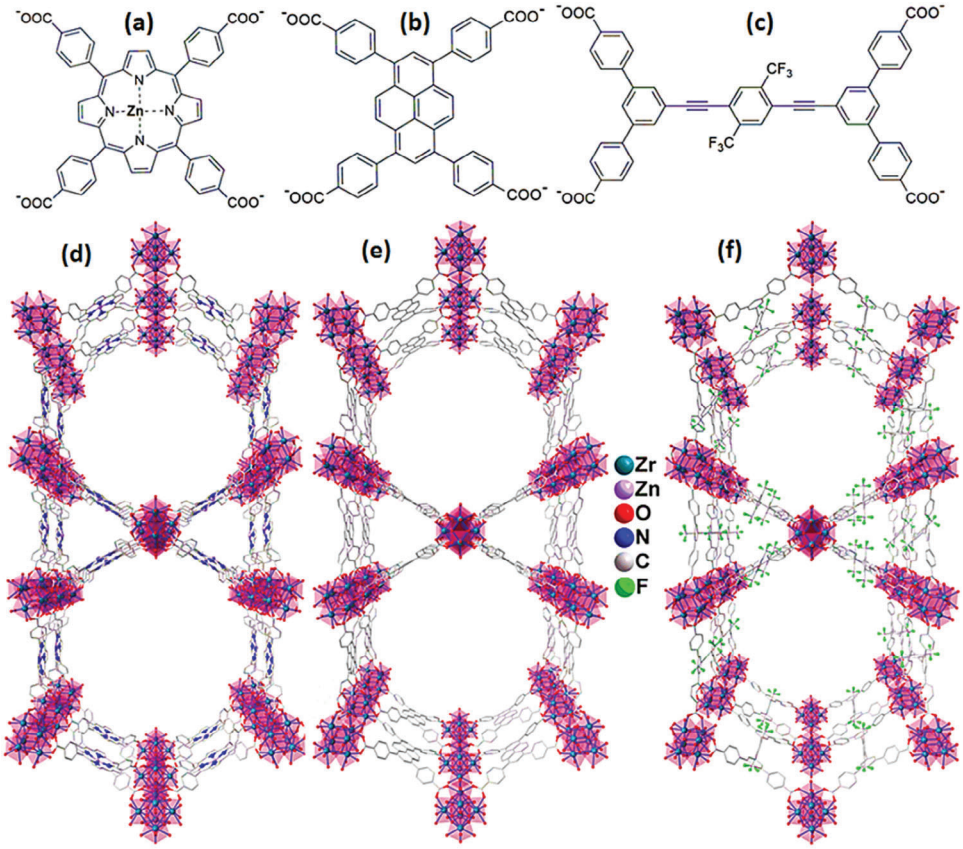

Figure 5. Deprotonated structures of a) TCPP(Zn), b) TBAPy, and c) PEPF linkers and their corresponding MOFs d) PCN-222(Zn),e) NU-1000, and f) SIU-100. Reproduced with permission.[83] Copyright 2022, American Chemical Society.

mind that the results may not be considerably different even if the MOF has undergone some degree of decomposition. In addition, CO_2/N_2 adsorption isotherms acquired at 195/77 K are often utilized in order to analyze changes in porosity as well as surface area following treatment with water. Bulk materials may be studied using PXRD and gas adsorption, while SEM can be utilized to observe minute morphological or crystal surface changes caused by MOF recrystallization.[90] These methods are desirable for determining whether MOFs are water-stable; yet, very little is known about the changes in architectures during the treatment with water. In recent work using in situ synchrotron powder diffraction, MOFs with high stability in an aqueous medium such as $Zn_2(BDC\text{-}TM)_2(DABCO)$ were studied and it was found that throughout the process of water adsorption, water induces bond rearrangement.[91] This defect caused by water adsorption, may create the porosity and the crystallinity of the materials.

Mandal's group synthesized NU-1000 in a variety of sizes ranging from 100 to 2000 nm,[59] with the reason of removing glyphosate from aqueous environments by the process of adsorptive removal (**Figure 6**a). The adsorption efficiency increases with decreasing particle size. The SEM image (Figure 6a) showed the formation of particles with 100 to 2000 nm average size. According to theoretical estimates, the greater adsorption energy of glyphosate makes for a better interaction with NU-1000. Yuan et al. have designed many M/Zr-MOFs with varying heterometallic cores/clusters ($M^+ = Cr^{3+}$, Cr^{6+}, Mn^{2+}, Ti^{4+}, Co^{2+}, Cu^{2+}, V^{3+}, V^{5+}, Fe^{2+}, Fe^{3+}, Zn^{2+} as well as Ni^{2+}) with framework topologies.[92] These M/Zr-MOFs were investigated in water at diverse pH values. In M/Zr-MOFs, it was revealed that an increase in the oxidation state of the hetero-metal cations led to an improvement in their stability. In addition, Zr-MOF aids in the stability of the matrix by supporting Zr clusters with limited connection. The rate constant of water exchange (*kex*) of the cation and p*K*a of the hydrated cation $[M(H_2O)_m]^{n+}$ were examined in order to provide a description of the stability of the metal cation.[61] This constant measures how quickly water in solution replaces the coordinated water on a metal cation. When the least well-balanced pH of M/Zr-MOFs was plotted versus the p*K*a of the hydrated cation $[M(H_2O)_m]^{n+}$ or the rate constant of water exchange (logarithmic scale) of M^+, correlations were seen in both cases. According to the definitions of p*K*a and *kex*, the bond strength of the O-H link is described through p*K*a of the hydrated cation $[M(H_2O)_m]^{n+}$, while inertness of the M-O link is reflected by the value of *kex*. (Figure 6c). The breakdown of M—O bonds is responsible for the heterometals leaching from M/Zr-MOFs. (Figure 6c).

Therefore, the lowest stable pH should be connected to *kex* to provide an accurate description of the M/Zr-MOF dissolution rate constant (k_d). In point of fact, *kex* and p*K*a are related to one another as well due to the fact that the strong M—O bond that exists inside $[M(H_2O)_m]^{n+}$ is anticipated for the polarization of the O-H via an inductive effect, thereby enabling O—H bond simple

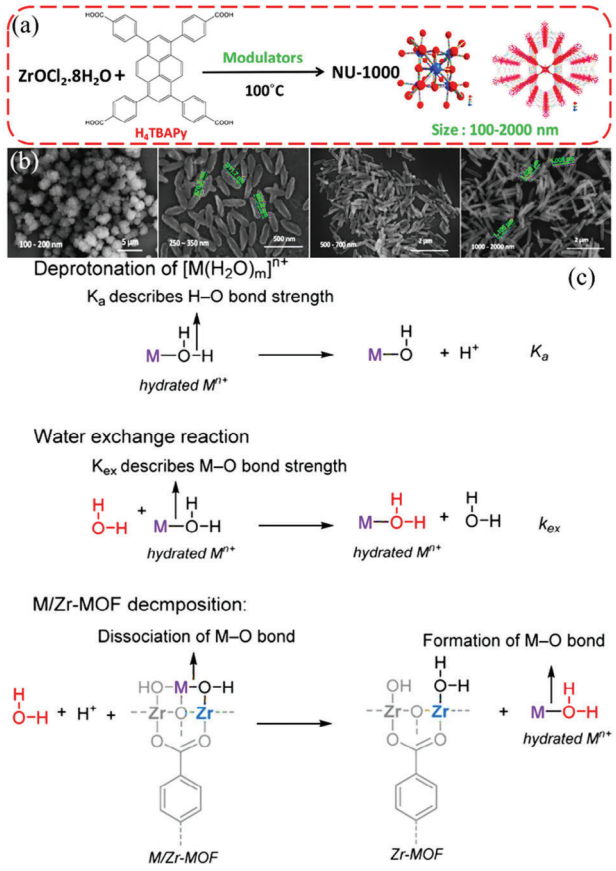

Figure 6. a) Synthesis process of NU-1000, b) SEM images. Reproduced with permission.[59] Copyright 2018, American Chemical Society. c) Equations in a simplified form demonstrate the deprotonation of $[M(H_2O)_m]^{n+}$, the water exchange, and the breakdown of M/Zr-MOF. Reproduced with permission.[92] Copyright 2019, American Chemical Society.

to break. This is because of the inductive effect of the strong M—O bond. It is simple to utilize the rate constant water exchange of cations as a descriptor to roughly estimate MOF stability because this rate constant has been thoroughly researched and published.

5. Applications of NU-1000

While researchers keep seeking new materials for different applications, NU-1000-containing materials have indicated fantastic performance in different applications such as energy storage and conversion, catalysis, adsorption, and environmental applications. Because of uniform and tunable pore sizes, accessible and large specific surface area, and high stability, researchers looked toward the discovery of new NU-1000 applications. In this section, we discuss the applications of NU-1000 such as energy and environmental applications.

5.1. Energy Applications of NU-1000

Coping with future energy crises, as well as the development of energy generation, storage, and conversion technologies, are among the main priorities of researchers around the globe.[93,94] Some of these technologies require materials with high hydrolytic stability. MOFs are of crucial significance as they possess high-valent cations such as Zr^{4+}. NU-1000 is one of the members of this class of MOFs with high structural stability due to the strength of Zr—O bonds. Due to the presence of Lewis acidic Zr clusters, it exhibits great catalytic activity. In comparison with other MOFs, NU-1000 also benefits from the great internal surface area, synthetic tunability, chemical stability, and diverse topologies, making it a promising candidate for energy applications such as hydrogen generation, CO_2 reduction, and batteries.[95–97] This section provides recent progress on NU-1000 for energy applications.

5.1.1. Photocatalytic Water Splitting

Among the renewable sources of energy, solar energy is one of the most promising alternatives. In this context, the use of solar energy for its conversion into fuel or chemical energy through the photocatalytic splitting of water has gained a considerable deal of attention.[98–100] Excited state lifetime, charge mobility, strong absorption of visible light, and high efficiency of charge-separated states are among the major features in the evaluation of the performance of a photocatalyst. Light absorption may occur in organic linkers, nodes, or both. The superiority of light absorption in the linker lies in LMCT and longer lifetime of the excited states which provides a path for charge separation. Electron-hole separation facilitates the reduction reaction by the catalyst in the hole and oxidation reaction with the help of an electron.[14,101] The presence of pores in the structure of MOFs enables the reactants to penetrate the active sites, resolving the mobility of charge issue in many semiconductors. NU-1000 (as a MOF structure) has been recently regarded as a proper photocatalyst due to its large pores and tunability and stability of its structure.

Z-scheme photocatalysts are composite semiconductor catalysts that operate through the Z-scheme path with no need for an additional electron mediator.[102] The Z-scheme design strategy of a photocatalyst can improve the performance of the photocatalyst, outperforming a single-component photocatalyst. The advantages of these photocatalysts include high charge separation efficiency and a wide light absorption range. Accordingly, Li et al. employed an engineering strategy for the integration of BiOl in NU-1000; the developed BioI@NU-1000 Z-scheme heterojunction photocatalyst was utilized in photocatalytic hydrogen evolution (**Figure 7**a(i)).[103] BiOl@NU-1000 exhibited the best performance with a hydrogen generation rate of 610 μmol h^{-1} g^{-1}. Such a great performance can be assigned to a highly dispersed heterojunction, high surface area, and Z-scheme photocatalyst construction. Due to the respective roles of BiOI and NU-1000 as p-type and n-type semiconductors, a *p-n* heterojunction was formed which resulted in the photocatalytic activity as depicted in Figure 7a(ii).

Thanks to their versatile features such as multi-electron transfer ability and tunable physicochemical properties, polyoxometalates (POMs) have been regarded as promising photocatalysts for splitting water.[104] The recycling of POMs is, however, difficult which can be resolved by the use of heterogeneous photocatalysts and some support materials such as MOFs. For

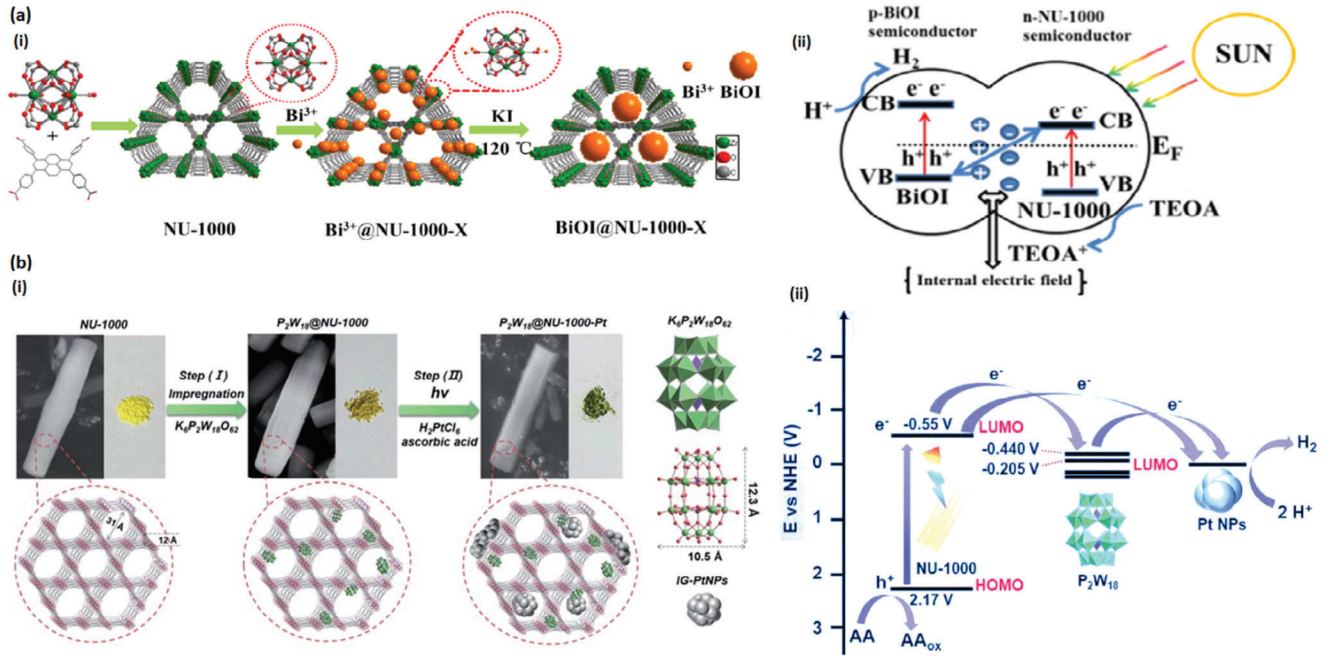

Figure 7. a) i) Synthetic protocol of BiOI@NU-1000-X Heterostructures, ii) the mechanism of Z-scheme charge transfer between BiOI and NU-1000 under light irradiation. Reproduced with permission.[103] Copyright 2021, American Chemical Society. b) i) synthetic method of the P_2W_{18}@NU-1000-Pt composite. The red circles are the microscopic illustration of the structure, ii) the diagram of energy level for photocatalytic hydrogen generation by P_2W_{18}@NU-1000-Pt photocatalyst. Reproduced with permission.[105] Copyright 2021, Royal Society of Chemistry.

instance, Jiao et al. used P_2W_{18}@NU-1000-pt as a photocatalyst for hydrogen evolution.[105] They assigned the good performance of this composite photocatalyst to the synergistic effects of photo absorbing of NU-1000, catalytic activities of Pt nanoparticles, and multi-electron transfer in P_2W_{18} (Figure 7b(i,ii)). In another study, Jiao et al. successfully synthesized Ni_3PW_{10}@NU-1000 and $Ni_3P_2W_{16}$@NU-1000 and used them as a photocatalyst for hydrogen evolution (**Figure** 8a(i)).[106] Their results revealed the high photocatalytic activities of $Ni_3P_2W_{16}$@NU-1000. $Ni_3P_2W_{16}$ POM has the proper molecular size and structure to maximize the interactions with NU-1000. According to the crystal structure of these two composites, cubane $\{WNi_3O_4\}$ serves as an active site and is stabilized in these two composites by ligands of tri-lacunary $\{P_2W_{15}O_{56}\}$ and $\{PW_9O_{34}\}$, respectively. As $\{P_2W_{15}O_{56}\}$ in the $Ni_3P_2W_{16}$@NU-1000 can store more electrons and deliver them to the active sites compared to the other composite, it can reduce protons to hydrogen, showing higher activities (Figure 8a(ii,iii)).

The low cost of the photocatalyst is one of the major factors in the selection of photocatalysts for solar fuel production processes such as water splitting. In this regard, metal sulfides have drawn a considerable deal of attention in photocatalytic hydrogen generation. Some metal sulfides have shown performances comparable to those of expensive metals.[107] Maintenance of the photocatalyst stability during the reaction is one of the challenges that can be resolved by engineering the surface sites or template growth. Peter et al. deposited nickel sulfide in NU-1000 and used it as a photocatalyst to evaluate the water reduction to hydrogen gas (Figure 8b(i,ii)).[108] The presence of Ni^{+2} and S^{-2} sites in NU-1000 was confirmed by Raman spectroscopy and X-ray photoelectron spectroscopy. Hydrogen gas generation at the rate of 3.1 mmol $g^{-1}h^{-1}$ was detected at pH = 7 and under ultraviolet light (390 nm). This performance was attributed to the efficient UV absorption by photosensitizer linker of pyrene. The performance of the photocatalyst under visible light is also important in the practical application of solar fuel photocatalysts. This investigation was carried out in the presence of Rose Bengal dye which showed an improvement in hydrogen generation at high rates. Another report stated that MoS_x-modified NU-1000 (named MoS_x-SIM) contains sulfhydryl groups whose protons can react with metal hydrides and form H_2 which included MoX edge active sites.[109] In this study, Noh et al. reported that tetraphenyl-pyrene linkers in the NU-1000 structure served as light harvesters which played the role of photo-excited reactant and delivered electrons to Mo sites, hence, contributing to photocatalytic water reduction to H_2. Bag et al. indicated the advantages of using NU-1000 in the preparation of CdS@NU-1000/RGO composite photocatalyst to improve the performance of CdS in hydrogen generation. Since CdS can be employed as a visible light photocatalyst, it has gained increasing attention in the field of water splitting. It, however, suffers from fast recombination of electron-hole and agglomeration of CdS nanoparticles. The mentioned drawbacks were resolved in a study conducted by this research group and their CdS@NU-1000/RGO composite exhibited ideal hydrogen generation performance under visible light.[110] The results of this study showed that the performance of CdS@NU-1000/1%RGO was ≈15 times better than that of commercial CdS which could be because of more active sites and a reduction in the recombination of charge carriers.

Thanks to its pores, NU-1000 allows many reactants to diffuse, hence resolving the problem of charge mobility in the active sites of many semiconductors. NU-1000 can serve as a

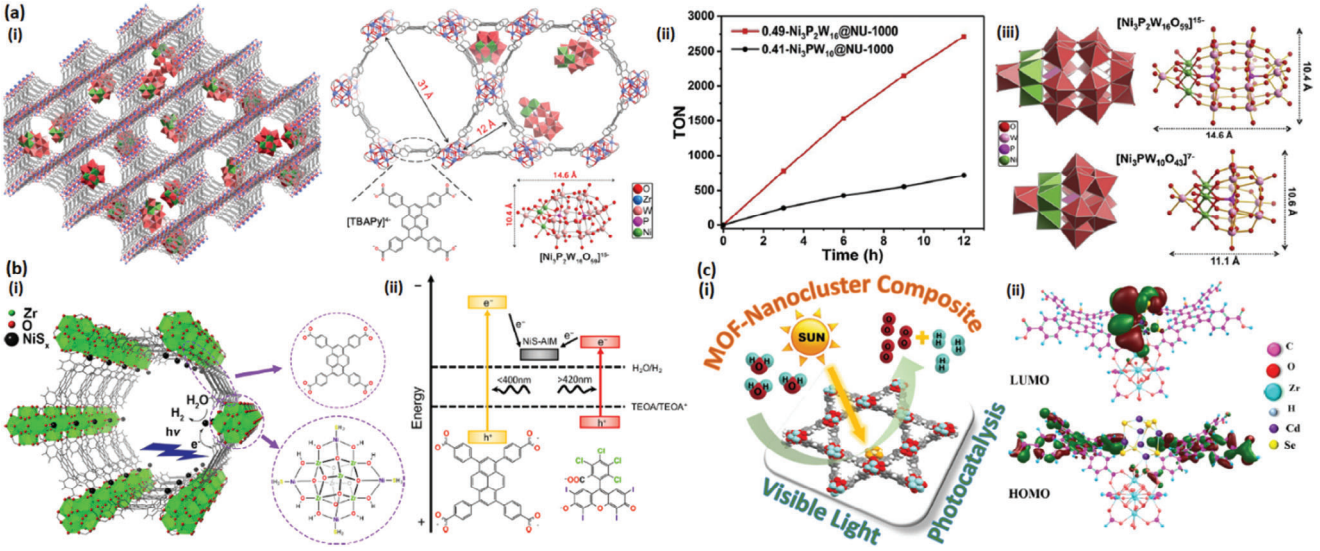

Figure 8. a) i) The proposed structure for $Ni_3P_2W_{16}$@NU-1000 composite, ii) TONs comparison under optimal photocatalytic reaction conditions. $Ni_3P_2W_{16}$@NU-1000: 1 mg 0.49- $Ni_3P_2W_{16}$@NU-1000, pH = 6.0, Xe-light radiation with full-optical wavelength. Ni_3PW_{10}@NU-1000: 5 mg 0.41-Ni_3PW_{10}@NU-1000, pH = 6.0, Xe-light radiation with full-optical wavelength, iii) Size, Ball-stick model and polyhedral crystal structures of two different tri-Ni-substituted POMs. Reproduced with permission.[106] Copyright 2021, Elsevier. b) i) NU-1000 idealized demonstration after imparting functionality of NiS_x by AIM. The pyrene-based linker in the role of a UV sensitizer, transfers an electron to NiS_x node (dotted circle) and then reduces H^+/H_2O to H_2 (g), ii) energy diagram of related Photocatalytic system. Reproduced with permission.[108] Copyright 2017, American Chemical Society. c) i) schematic representation of Cd_6Se_6@NU-1000 as photocatalyst for splitting of water, ii) the molecular model of HOMO and LUMO of the Cd_6Se_6@NH_2-NU-1000. Reproduced with permission.[111] Copyright 2020, American Chemical Society.

photo-activator in photocatalytic reactions and improve the performance of the photocatalysts through encapsulation of photoredox species in their structure. Choudhuri et al. computationally evaluated the encapsulation of CdSe in the structure of NU-1000 (Cd_6Se_6@NU-1000) (Figure 8c(i,ii)).[111] In this structure, the electron is transferred from the organic ligands to the LUMO in the inorganic cluster, giving rise to charger separation which can prolong the lifetime of excited states and improve photocatalytic performance. This composite photocatalyst has band edges that enable photocatalysis of oxygen evolution reaction (OER) under visible light.

5.1.2. Electrocatalytic Water Splitting

Electrochemical splitting of water encompasses two half-reactions hydrogen evolution reaction (HER) occurs at the cathode and OER occurs at the anode. Electrode material plays a decisive role in these half-reactions.[112–114] Various materials have been examined to be used as electrodes and researchers are seeking efficient solutions for these challenges. MOFs are unique materials with specific advantages in this field. For instance, NU-1000 has a large surface area, thermal and chemical stability, and large volume of pore which can facilitate electron transfer in the electrochemical reactions; therefore, NU-1000 could be a potential electrode material in electrochemical water splitting.

To decline carbon emissions and due to the significance of solar fuel technologies, the development of HER electrocatalysts has found increasing significance among researchers. Commercialization and large-scale hydrogen generation have further added to the significance of this problem.[115] Based on the relevant literature, metal chalcogenides have shown acceptable performance as a HER electrocatalyst.[116,117] Among these materials, MoS_2 has a 2D layered structure which has been widely explored in the field of HER. In this structure, the presence of undercoordinated Mo edge sites leads to the formation of molybdenum-hydride species during electrocatalysis, hence improving the electrocatalytic performance. The role of MOFs as catalyst support is important as they can resolve structural issues such as site uniformity and facilitate the atomic scale activity of the catalyst. The three-dimensional nature of the MOFs can provide a large internal surface area, enhancing the catalyst accessibility. Moreover, organic linkers of MOFs can significantly prevent the agglomeration of installed catalysts.[118] Noh et al. evaluated the functionalization of NU-1000 with MoS_x through solvothermal deposition of solution-phase in MOFs labeled as MoS_x-SIM which was employed as an HER photocatalyst. Thanks to its hydrothermal stability and the presence of several catalyst grafting points in the NU-1000 structure, this MOF was reported as the ideal support for electrocatalytic HER.[69] The problem with NU-1000 lies in its poor conductivity which can decrease the installation of electrocatalysts on them. This group used redox mediators (RMs) (**Figure** 9a(i,ii)) and found that RMs could easily diffuse the MOF-affixed MOS_x due to the porosity of NU-1000 and continuously entered electrons to the catalytic sites, hence improving and enhancing the performance of the electrocatalyst for HER from acidified water. According to the structure depicted in Figure 9a(ii), the environment of the catalyst includes a channel connecting micropores and hexagonal mesopores. The presence of a catalyst in the mesopores can guide the catalyst toward solvent-rich channels while the localization of the catalyst in micropores will guide it toward hydroxo ligands on the

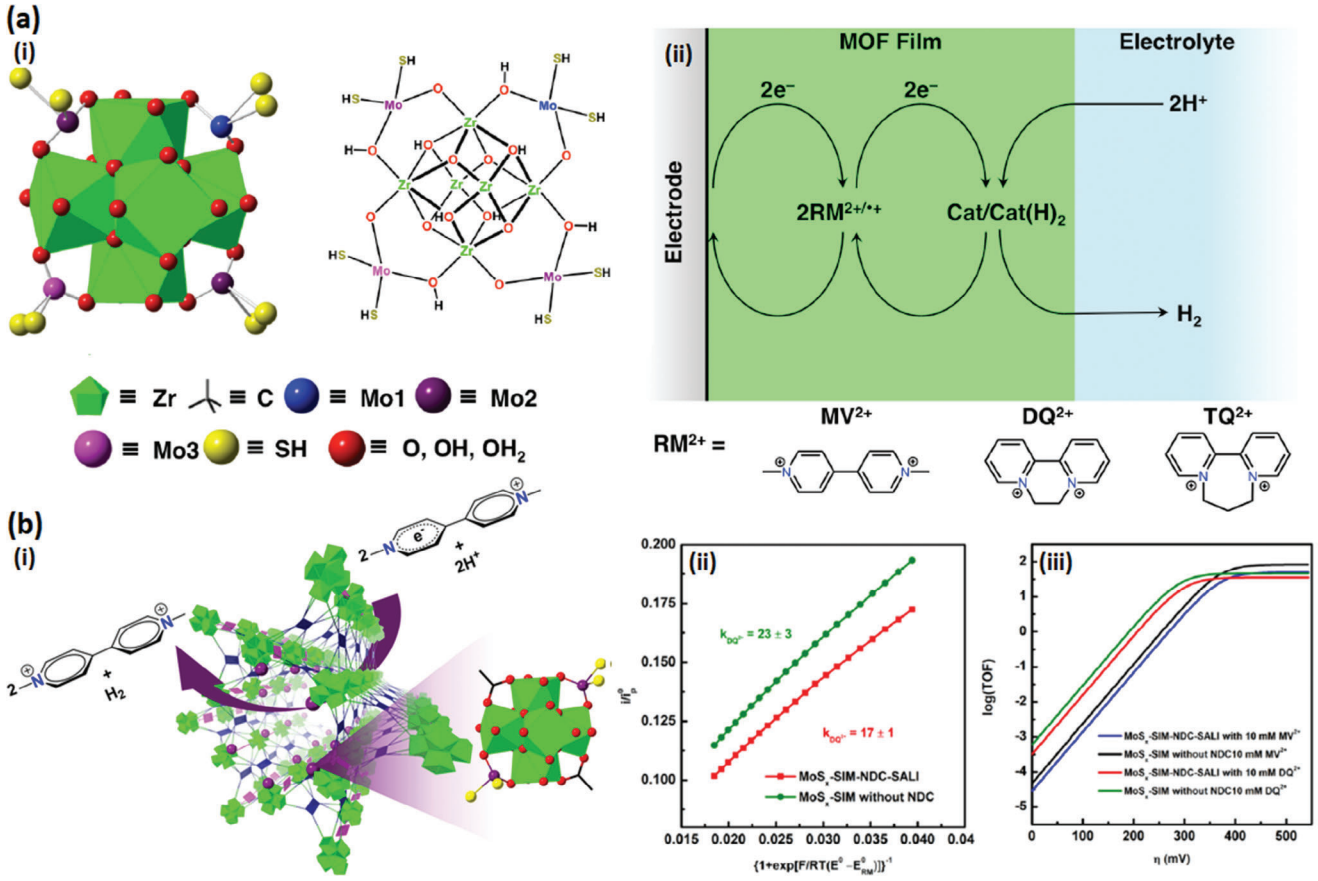

Figure 9. a) i) The MoS_x-anchored Zr_6 node of the representative structure of MoS_x-SIM showing all the crystallographically distinct MoS_x units (Mo1-03) and the framework viewed along the *c*-axis (the minor structure Mo3 is omitted for clarity), ii) proposed redox mediator-assisted electrocatalytic system with various redox mediators. Reproduced with permission.[69] Copyright 2018, American Chemical Society. b) i) structure of NDC deposited NU-1000 as an electrocatalyst for HER, ii) Foot-of-the-wave analysis on MoS_x-SIM-NDC-SALI and the analogous system without NDC, iii) log(TOF) vs. overpotential plots. Reproduced with permission.[120] Copyright 2019, WILEY-VCH.

node walls. In the continuation of their studies, this group decided to clarify and determine the site-specific catalytic activities. They concluded that one of the environments would block the catalyst by the installation of single metal atoms. As Peter et al. had proven (by crystallographic data) that naphthalene dicarboxylate (NDC) occupies micropores upon entrance into the NU-1000 structure, they inferred that $Mo(SH)_2$ units should be only allocated to mesopores if using NDC (Figure 9b(i)).[119] The same group prepared the single-site electrocatalyst of MoS_x-SIM-NDC-SALI through solvent-assisted ligand incorporation (SALI). Their electrochemical findings indicated that the performance of MoS_x-SIM-NDC-SALI was similar to NDC-free MoS_x-SIM which had been previously reported by this group.[120] A comparison of these two studies indicated the better performance of $Mo(SH)_2$ units at micropores rather than mesopores which can be attributed to the narrow hydrogen bond network in the micropore (Figure 9b(ii,iii)). Application of the MOFs as a porous supporting scaffold to form a composite electrode could be an efficient strategy to achieve better HER electrocatalysts.[121–123] These composites can offer improved conductivity and increased density of electrocatalytically active surface sites due to their porous scaffolds and facilitated proton delivery; therefore, lower overpotential would be needed for the electrochemical reactions. Hod et al. used NU-1000 to prepare a composite electrode for HER. As MOFs have exhibited substantial resistance under hydrolysis conditions, even at high temperatures and in the presence of hydroxide ions, thus, they have sufficient chemical stability to be applied in HER. This group reported a composite electrode for electrocatalytic HER based on NU-1000-Ni-S under pH 1 conditions.[72] The mentioned electrocatalyst exhibited the overpotential of 238 mV at the current density of 10 $mAcm^{-2}$ which is a low value compared to its constituents.

Howe et al. recently developed an interesting strategy for designing an MOF-based electrocatalyst for water oxidation by providing oxidizing equivalents through the use of redox-active colinkers. Their strategy led to more electrocatalytic active sites with optimal charge transfer. On the other hand, the MOF could further affect the catalytic activities due to higher active sites. Regarding the structural similarity of metallo-linker $Ru(tda)(py(PhCOOH)_2)_2$ with H_4TBAPy native linker in NU-1000, this group synthesized NU-1000-Ru mixed linker MOF and evaluated it for water splitting purposes. Interestingly, ruthenium metals within the structure are more oxidized by anodic potential while Ru linkers on the surface of the crystal are directly

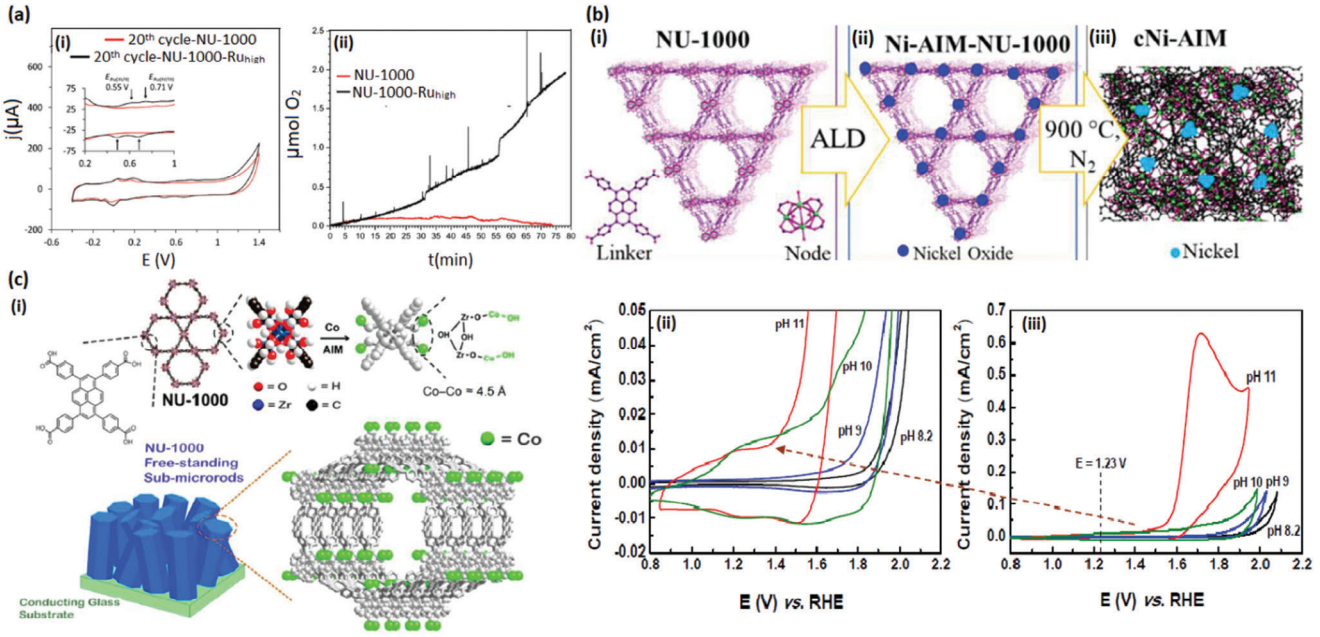

Figure 10. a) i) CV curves of NU-1000 and NU-1000-Ru_{high} (20th cycle, inset: a zoom into the Ru-based oxidations of NU-1000-Ru_{high}), ii) oxygen evolution measurement coupled to controlled potential electrolysis (CPE) of NU-1000 (red) and NU-1000-Ru_{high} (black). Reproduced with permission.[124] Copyright 2022, WILEY-VCH. b) i) The structure of NU-1000 including the Zr_6O_8 node and the pyrene linker, ii) Ni-AIM-NU-1000 after nickel oxide deposition on the NU-1000 clusters by ALD, iii) cNi- AIM-NU-1000_900 °C after heating to 900 °C under N_2. Reproduced with permission.[125] Copyright 2018, American Chemical Society. c) i) NU-1000 structure and cobalt ions possible configuration on the node after AIM, ii) CV curves of the Co-AIM NU-1000 thin film in 0.1 M Na_2SO_4/NaOH aqueous solutions adjusted to various pHs and iii) The panel was obtained by plotting on a finer current-density scale data in the panel at right. Reproduced with permission.[126] Copyright 2015, American Chemical Society.

oxidized through the interfacial transfer of holes. The presence of Ru linkers in NU-1000 was also confirmed by cyclic voltammetry in addition to characterization tests (**Figure 10**a(i)). In this work, NU-1000-$Ru_{high(5.7\%)}$ was employed as the working electrode for water oxidation which produced 1.94 μmol O_2 after 80 min of controlled potential electrolysis (Figure 10a(ii)).[124]

As mentioned earlier, the low conductivity and stability of MOFs are among the major problems of this class of unique materials; as one of the members of MOFs, NU-1000 is not an exception. The stability of NU-1000 is higher at pH values of 11 and more. Some researchers have resolved this issue using a smart strategy. Palmer et al. claimed to resolve these two problems by pyrolysis of Oxy-Ni atomic layer deposition of Oxy-Ni-AIM in NU-1000 at high temperatures. They reported that cNi-AIM-NU-1000_900 has improved conductivity and stability which managed to effectively play the role of electrocatalyst for water oxidation at a pH of 13.8 (1 M NaOH) (Figure 10b(i–iii)).[125]

Another group prepared NU-1000 thin films by the chemical growth method and used them as a porous scaffold. They deposited Co ions as an atomic deposition layer on this support and labeled the product as Co-AIM-NU-1000 (Figure 10c(i)). As NU-1000 has large channels and high thermal stability, the accessibility of OH^- and OH_2^- ions in its layers facilitated the installation of Co ions using AIM. They, thus, predicted that this 3D array could further improve the performance of the electrocatalyst in water splitting due to the concentration of catalyst sites on the surface of the electrode or higher catalyst site's areal density compared to the monolayer coatings. On the other hand, the presence of the porous NU-1000 in the electrocatalyst can provide equivalent monolayers with abundant electrocatalytic sites which may significantly contribute to the electrocatalytic reactions. An electrochemical study of these electrocatalysts indicated partial water oxidation at pH levels of 8.2, 9, and 10. At pH = 11, however, a four-electron mechanism led to water oxidation (Figure 10c(ii,iii)).[126] Sanati et al. used NU-1000@NiMn-LDHS composite as an electrode material for HER and OER in a basic solution. They reported the excellent performance of this electrode material was due to the high surface area and porosity of NU-1000 and the layered structure of NiMn-LDH with more active sites. In KOH 2 M solution, this electrode showed an overpotential of 129 and 39 mV for HER and OER at the current density of 10 $mAcm^{-2}$, respectively.[127]

5.1.3. CO_2 Reduction

The ever-increasing application of fossil fuels not only enhanced the energy demand of the world but also increased the emission of CO_2 to the atmosphere causing climate and environmental change.[128,129] In this regard, CO_2 conversion into useful fuels could be a solution to reduce greenhouse gas accumulation and its adverse impacts on the environment.[130,131] Electrocatalytic CO_2 reduction is one of the methods of CO_2 conversion in which the electrode material plays a decisive role. An ideal electrocatalyst requires the lowest overpotential for the reaction. Thanks to their high stability and feasibility of separation of electrocatalyst products, heterogeneous electrocatalysts have gained extensive industrial applications and are considered superior to

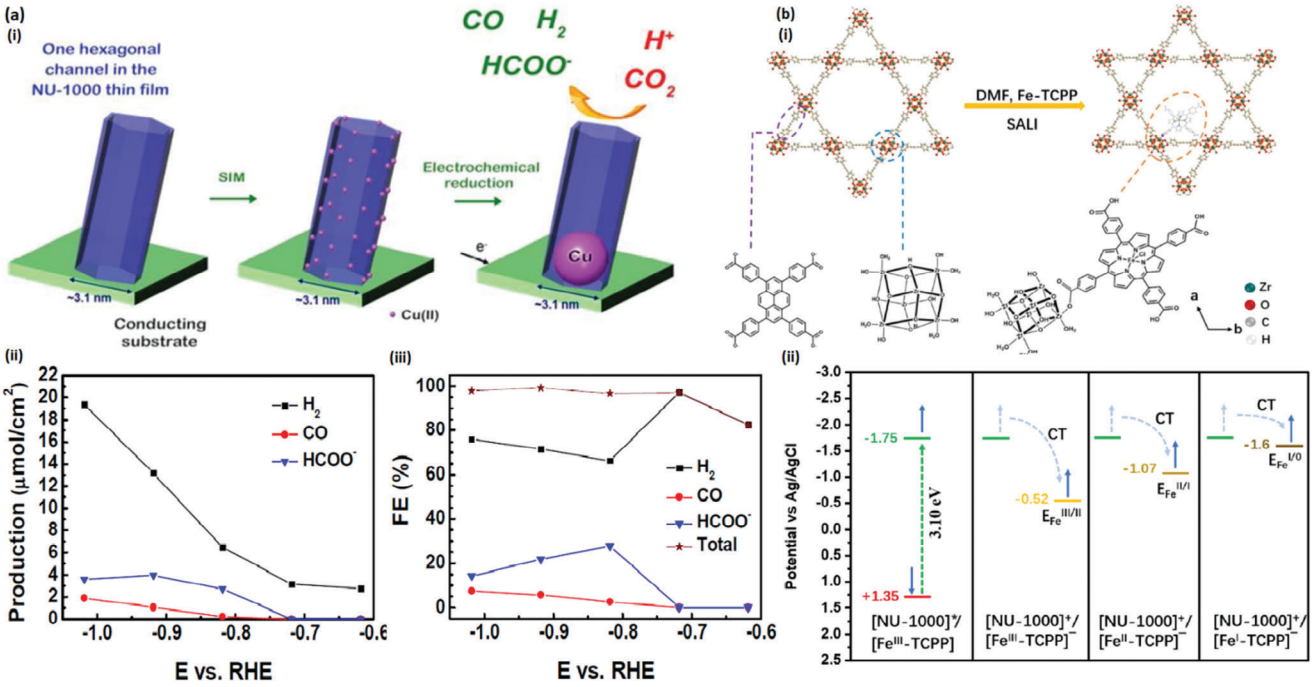

Figure 11. a) i) Schematic illustration of SIM to install single-site Cu(II) into the NU-1000 thin film and the electrochemical reduction of Cu(II) to produce nanoparticles of metallic Cu, ii) generation rates and iii) Faradaic Efficiency (FE) of products by Cu-SIM NU-1000 thin films. Reproduced with permission.[133] Copyright 2017, American Chemical Society. b) i) Structure of the Fe-TCPP@NU-1000, ii) Energy diagrams illustrating the estimated $\{NU\text{-}1000\}^{+/0*}$ excited-state redox potential (green), and the $\{NU\text{-}1000\}^{+/0}$ redox potential (red), reduction potentials of catalyst. Conduction (green) and Valence (red) band energies. Photo-excitation (pale arrows) and excited-state electron-transfer processes (blue arrows). Reproduced with permission.[136] Copyright 2022, Elsevier.

homogeneous ones. Copper has been utilized in metallic electrocatalysts for CO_2 reduction due to its low costs and tendency to generate oxygenated products and different hydrocarbons.[132] The high specific surface area feature allows the installation of active sites within the MOF. By increasing active site density, the current density also rises, enhancing the electro-catalytic performance of the MOF. Therefore, Kung et al. argued that MOF thin films containing Cu nanoparticles could be an ideal candidate for CO_2 reduction. In their work, they installed Cu(II) clusters on the NU-1000 using the SIM method and named it Cu-SIM NU-1000. The obtained products were analyzed using gas chromatography and ^1H nuclear magnetic resonance. The results indicated good performance of this electrocatalyst in CO_2 reduction and formate was the main product of this reaction at −0.92 V vs. RHE applied potential, with CO and hydrogen as the gas-phase products (**Figure 11**a(i–iii)).[133]

MOFs are ideal photocatalysts for carbon dioxide reduction due to their improved electron–hole (e–h) separation and high stability in UV–vis light.[134] In particular, Zr-based MOFs ensure photocatalyst stability and largely prevent chromophore aggregation due to their very strong bonds.[135] A group of researchers utilized NU-1000 as a photosensitizer to prepare a heterogenous photocatalyst with Fe-TCPP for photocatalytic CO_2 reduction (Figure 11b(i)).[136] Linkers of pyrene in the NU-1000 structure absorb photons and transfer electrons to the porphyrin to form a self-contained photocatalyst; this Fe-TCPP@NU-1000 photocatalyst exhibited acceptable CO_2 reduction to CO at light irradiation of 390 nm while H_2 was formed as a byproduct. Thermodynamic studies showed that the photo-excited NU-1000 could reduce Fe^{III}-TCPP, Fe^{II}-TCPP, and Fe^{I}-TCPP (Figure 11b(ii)).

5.1.4. Lithium–Sulfur (Li–S) Batteries

Li–S batteries are a group of energy storage devices, which rely on reversible electrochemical reactions. Many researchers have utilized Li–S batteries as energy storage systems in electric vehicles and portable devices due to the high density of energy and being inexpensive.[137,138] However, there are some challenges in the use of these systems; for instance, sulfur reduction occurs during the discharge process leading to the formation of polysulfides which migrate from the anode to the cathode, causing the shuttle effect, hence, inactivating the electrode surface. One approach to overcome such challenges is the use of porous matrices. Another important point in Li–S batteries is ionic and electronic transport.[139] Regarding the low conductivity of MOFs, measures should be considered to solve this problem by applying MOFs as an electrocatalyst in the Li–S batteries. Redox-active MOFs could be a good choice in such cases, either in the form of active sites in the scaffold, i.e. metal nodes or ligands, or by importing redox-active species post-synthetically. This approach was applied by Liu et al. using an anthraquinone (AQ)based linker in the NU-1000 structure. Through a post-synthetic method, they achieved a redox-active NU-1000 structure by substituting the carboxylate ligand in the NU-1000 structure with anthraquinone-2-carboxylate (AQ-COOH) (**Figure 12**a).[140] They predicted that the

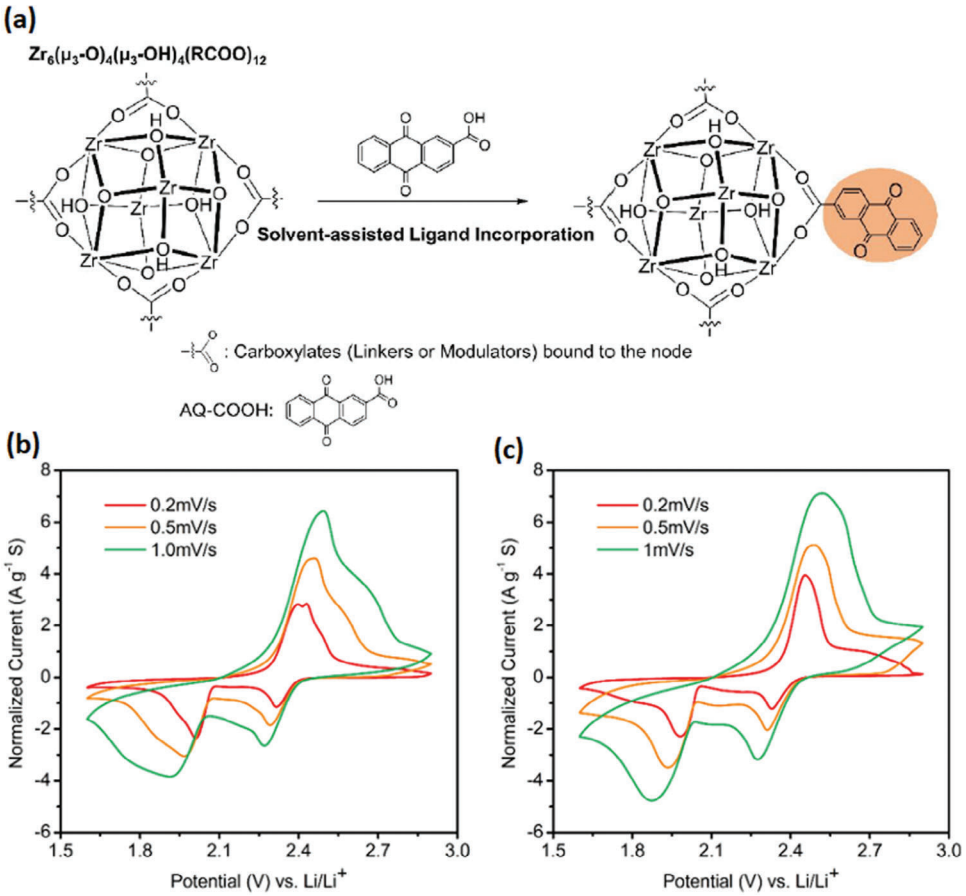

Figure 12. a) Schematic representation of solvent-assisted ligand incorporation treatment to substitute bound modulators with AQ-COOH. Only 1/3 of the carboxylates are shown for simplicity, b) Cyclic curves of coin cells constructed with NU-1000+S, and c) NU1000-AQ+S composite cathodes. Reproduced with permission.[140] Copyright 2020, American Chemical Society.

presence of AQ in the structure can increase and facilitate charge mobility, enhance the concentration of local Li-ions during cycling, and facilitate the transfer of charge and polysulfide redox. Their studies showed that there must be a balance between pore volume and AQ loading to accelerate charge–discharge and optimize charge transfer. Reduction and oxidation peaks were observed in cyclic voltammetry curves for NU-1000-AQ and NU-1000, with cathodic peaks corresponding to S_8 to Li_2S_x reduction and Li_2S_x to Li_2S (Figure 12b,c).

5.1.5. Hydrogen Storage

The application and development of sustainable and clean energy sources such as solar and wind in energy storage are among the urgent needs to resolve our dependence on fossil fuels. Hydrogen is a promising candidate in this field as it could be generated from renewable sources while producing environmentally compatible byproducts. Nonetheless, molecular hydrogen has low volumetric energy density at ambient conditions, necessitating its compression to achieve a good energy density for energy-demanding purposes such as transportation.[141,142] Bobbitt and colleagues explored the effect of NU-1000 functionalization on the improvement of its H_2 storage capacity. Accordingly, ultra-flexible alkane chains fail to improve the hydrogen storage capacity of NU-1000 as they do not diffuse into the pores. On the other hand, rigid chains like alkyne-containing groups enhanced the surface area and the achievable H_2 capacity of NU-1000 from 39.0 to 44 g L^{-1} (at the respective storage pressure and temperature of 50 bar and 350 °C, and desorption pressure of 10 bar and 430 °C) by decorating the pores with long and rigid alkyne chains.[143]

5.2. Adsorption

5.2.1. SO_2 Adsorption

Sulfur dioxide (SO_2) has been regarded as one of the most dangerous air pollutants by the World Health Organization. This colorless gas causes breathing problems and even death.[144,145] One of the capabilities of MOFs is their ability to capture gases, thus, they can also be employed in SO_2 capture.[146] Nonetheless, some MOFs suffer from poor chemical stability and degradation upon exposure to sulfur dioxide.[147,148] For the application of MOFs to selectively adsorb SO_2 traces, the low-pressure SO_2 adsorption is more suitable than the total capacity obtained at ambient pressure. The development of adsorbents for the elimination of SO_2 is a demanding challenge, necessitating a deep

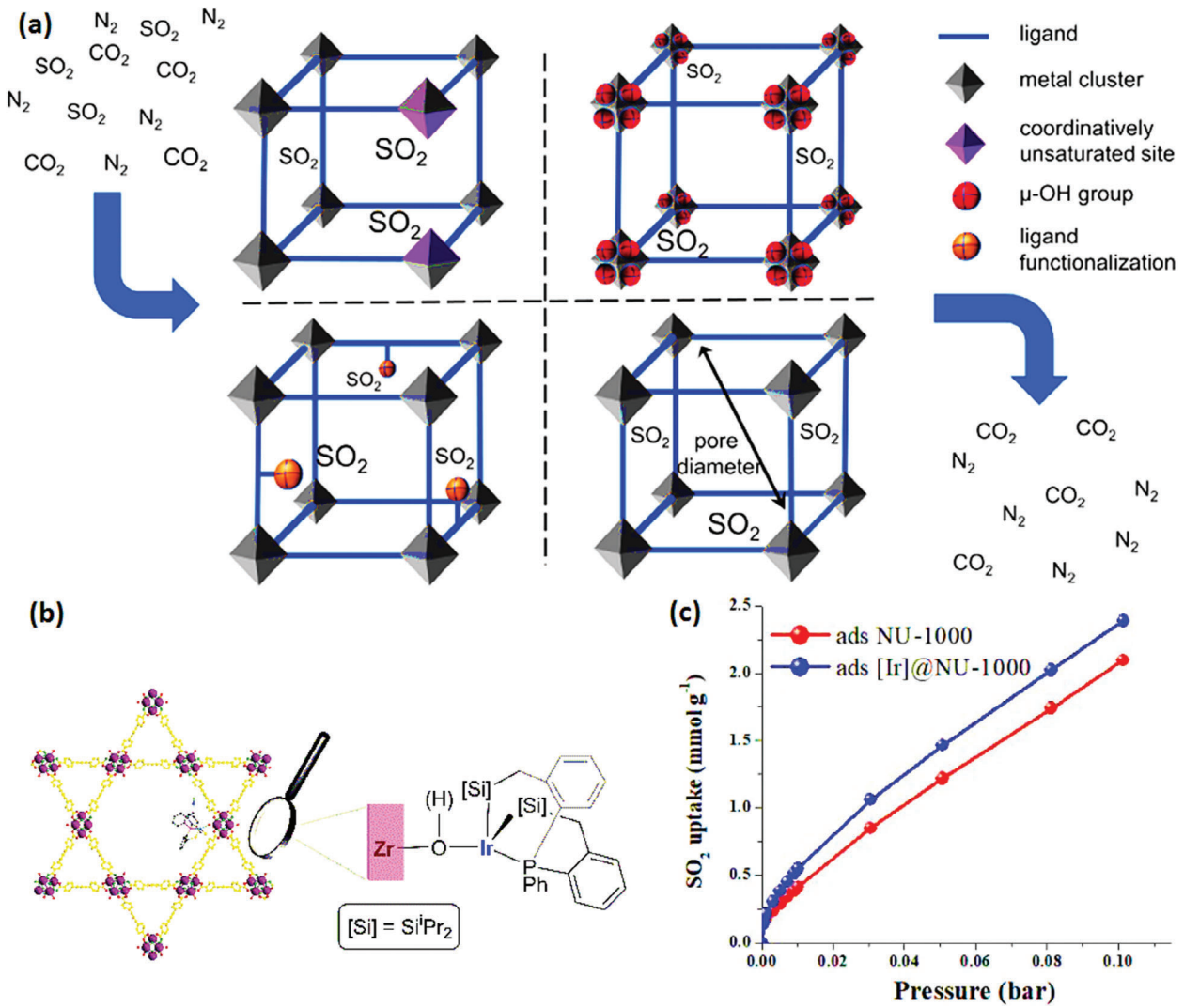

Figure 13. a) Schematic imagination of potential influencing factors for SO_2 adsorption at low pressure in porous materials. Reproduced with permission.[149] Copyright 2021, American Chemical Society. b) Proposed bonding of [Ir{κ$_3$(P,Si,Si)PhP(o-$C_6H_4CH_2Si^iPr_2)_2$}] into NU-1000 to produce [Ir]@NU-1000 novel material and c) The isotherms of adsorption-desorption of SO_2 collected for both of samples. Reproduced with permission.[150] Copyright 2020, American Chemical Society.

understanding of the underlying mechanisms to optimize MOF SO_2 adsorbents.[149] **Figure** 13a presents possible effective factors in selective SO_2 adsorption. Gorla et al. developed [Ir]@NU-1000 by incorporating [Ir{κ$_3$(P,Si,Si)PhP(o-$C_6H_4CH_2Si^iPr_2)_2$}] into NU-1000.[150] Such a slight modification significantly enhanced the SO_2 adsorption by NU-1000, mostly at low pressures while maintaining the structure. These findings highlight the promise of NU-1000 as an SO_2 sensor (Figure 13b).

5.2.2. Adsorption of Both CO_2/ N_2O

The incorporation of polar linkers into NU-1000 can promote N_2O uptake, as observed in the case of CO_2. Mercuriet et al. anchored the ditopic thiazolium carboxylate salt 5-carboxy-3-(4-carboxybenzyl)thiazolium bromide (H_2PhTz)Br onto the NU-1000 nodes through solvent-assisted ligand incorporation in a manner of bridging between adjacent [Zr_6] clusters. The insertion of the thiazolium pillar has improved the pristine MOF capacity for gas adsorption, reflecting its outstanding behavior in both CO_2 and N_2O adsorption. Moreover, the functionalized MOF could forejudge between gases pollutants by selective adsorption at various temperatures, enriching a CO_2/N_2O mixture in each component just by a simple temperature switch.[151]

5.2.3. Enhancement and Decline of CO_2 Adsorption

Farha et al. utilized the SALI approach to append different chain lengths (C_1−C_9) of perfluoroalkane carboxylates on the NU-1000 clusters.[51] CO_2 adsorption investigations revealed the synergistic action of perfluoroalkane-functionalized nodes in this system as the primary binding sites of CO_2, manifested by greater isosteric adsorption heats (Q_{st}) values with incrementing chain

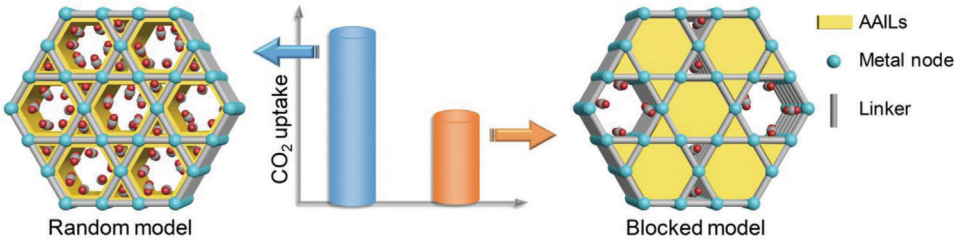

Figure 14. The channels blocking by loaded ionic liquids for reduced CO_2 uptake. Reproduced with permission.[152] Copyright 2019, American Chemical Society.

length. To synthesize ionic liquid/MOF composites, Xia et al. employed ionic liquids of [Emim][Gly] and [Emim][Phe]) and MOFs of UiO-66 and NU-1000. The blockage of MOF channels upon introduction of ILs the CO_2 uptake compared to the model encompassing random distribution of ILs (**Figure 14**).[152]

Luconi and colleagues functionalized NU-1000 with a monocarboxylic acid grafted with a benzothiazolium (BzTz) tail through SALI functionalization. The obtained NU-1000-BzTz composite was utilized for the storage of CO_2 (because of its boosted thermodynamic affinity for CO_2 in comparison with pristine MOF) and sensing of luminescent pollutant ions in aqueous media.[153]

5.2.4. Selective Adsorption of CH_4/N_2

The development of nanoporous structures for gas storage and separation is a prominent challenge in contemporary material science.[154] The separation of methane (CH_4) from other gases is crucial in the reduction of greenhouse gas emissions.[155] The performance of CH_4/N_2 separation for UiO-66, NU-1000, UiO-67 adsorbents, and other conventional samples such as Zeolite-13X were assessed by Kim et al. NU-1000 exhibited great CH_4/N_2 selectivity based on the ideal adsorbed solution theory due to its micro-/meso-porosity and large surface area in addition to polar surface hydroxyl groups. NU-1000 shows great CH_4 working capacity (4.79) under the pressure of the swing adsorption process.[156] Vandenbrande and colleagues explored methane adsorption of several Zr-based MOFs to examine the sensitivity of diverse sets of force fields in the generation of isotherms and single-molecule adsorption energy. MOF-808, DUT-52, UiO-66, NU-1000, and UiO-67 exhibited different pore volumes and surface areas, resulting in the following order of methane uptake values UiO 66 ˂ MOF 808 ˂ DUT 52 ˂ UiO 67 ˂ NU 1000.[157] Equilibrium adsorption isotherms of NU-1000 were examined at low coverage (0.0-0.2 monolayer) for nitrogen, carbon monoxide, argon, and methane gases at temperatures above 371 °C which led to differential (Q_{st}) as a coverage function.[158] The heat shows a more decreasing trend with coverage for CO and N_2 gases compared to CH_4 and Ar, as predicted by DFT calculations.

5.2.5. Selective Adsorption of CO_2/N_2

In a study by Bao et al. on the CO_2/N_2 selectivity, NU-1000 pores were impregnated with polyethyleneimine (PEI). The NU-100 structure includes free hydroxyl groups which offer acidic sites for impregnating PEI.[159] At low pressures, the highest CO_2/N_2 selectivity was reported for PEI(50)@NU-1000. The selectivity for gases of N_2 and CO_2 at 1 bar flue gas was excellent compared to NU-1000. Such an excellent performance can be attributed to the lack of open-metal sites in NU-1000 which led to very low N_2 adsorption. The CO_2/N_2 separation was also desirable for PEI(50)@NU-1000 under the dynamic mixture flow.

5.2.6. Ammonia Adsorption

Ammonia adsorption by high-capacity and porous sorbents could be an ideal method for its mitigation, release, storage, and capture as well as chemical separation. Liu et al. assessed ammonia sorption by various NU-1000-a structures.[160] They summarized the local node compositions for most NU-1000 variants (**Figure 15**) in addition to their corresponding experimental preparation routes. Figure 15 (bottom row) shows the ammonia chemisorption modes of the four variants. The interactions of red NH_3 and green NH_3 with bridging OH^- protons and terminal OH^- hydrogen atoms create reversible NH_4^+. The purple NH_3 also shows the coordination of NH_3 to open sites of Zr in which, the purple dashed line signifies H-bonding between NH_3 and the adjacent terminal hydroxyl group (i.e. $Zr{-}NH_3{\cdots}O(H){-}Zr$). The blue NH_2^- and H^+ represent dissociation of the blue-coordinated NH_3 on open sites of Zr. Before measuring the adsorption according to the treatment performance, this group found that the physisorption of NH_3 on NU-1000 occurs through London-dispersion interaction and hydrogen-bonding while its chemisorption takes place by coordination in open metal sites, acid-base reactions with μ_3-hydroxo groups, or node-based μ_3-oxo protonation.

5.2.7. Propane and Isobutane Adsorption

Chen et.al explored the adsorption of isobutane and propane in NU-1000 and NU-1003 with different widths of channels.[161] The adsorption performance can be affected by the widths of the channel, hence, the cooling capacity for diverse adsorption cooling purposes. In comparison with MIL-101, NU-1000 and NU-1003 led to a 2-4-fold increment in cooling capacities.

5.2.8. Iodine Adsorption

Radioiodine capture is one of the efficient approaches for progress in the field of nuclear energy. It occurs following nuclear

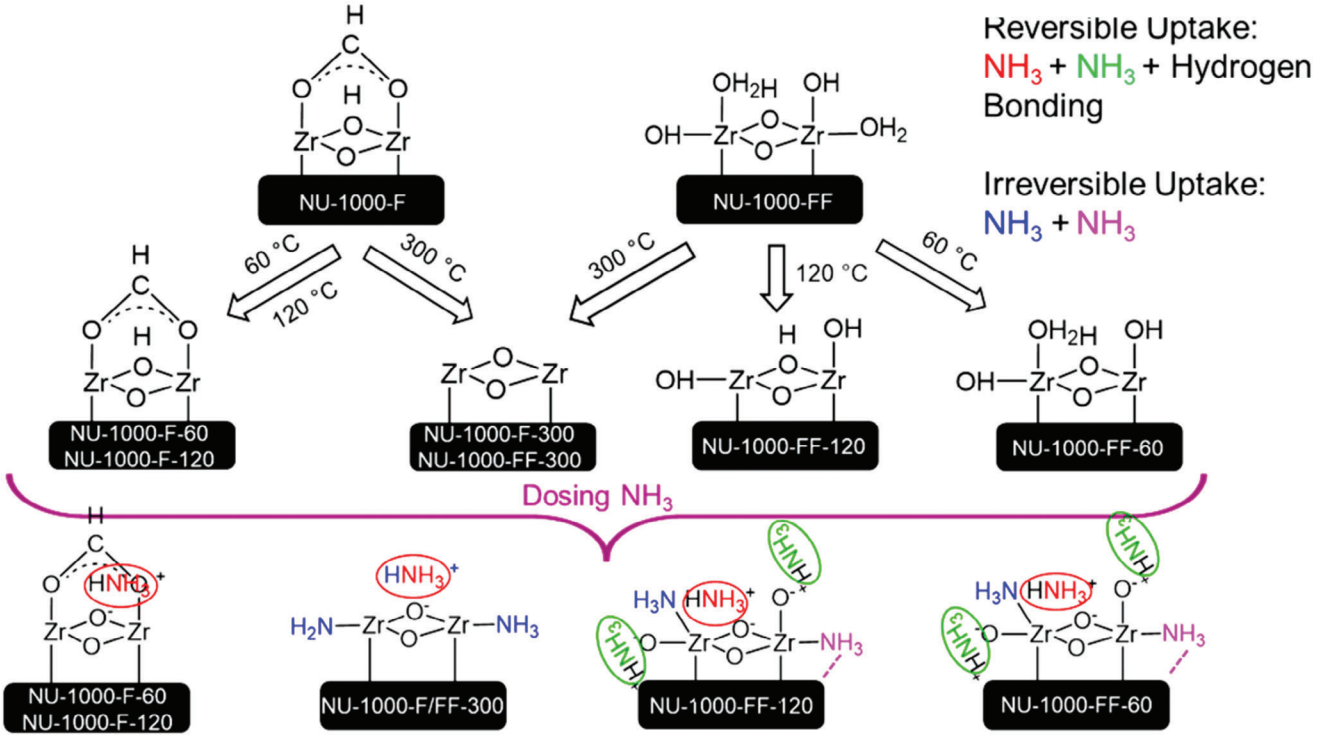

Figure 15. Local structures of clusters for different NU-1000 compounds after dosing with NH_3 vapor and thermal treatment. Reproduced with permission.[160] Copyright 2021, American Chemical Society.

functions.[162] Chen and coworkers assessed several Zr-MOFs with different types of carboxylate ligands and Zr_6 nodes for capturing volatile iodine and found a relationship between adsorption performance and structural stability, in addition to the host-guest interactions (i.e. linkers and Zr clusters).[163]

5.2.9. Adsorption Chillers

Due to their low electricity consumption and environmental compatibility, low-grade thermal energy/solar-powered adsorption chillers have received growing research popularity.[164] In 2021, UiO-66, DUT-67, and NU-1000 water-stable Zr-MOFs were employed by Li and colleagues using water as a working fluid.[165] The low-grade waste heat and solar that have low carbon emission and low electricity consumption can power adsorption chillers. Ammonia has been commonly employed as the working fluid due to its high evaporation enthalpy and high pressure of vapor, promoting heat and mass transfer in adsorption chillers. Liu et al. investigated ammonia adsorption of MOFs using MOFs with potential ammonia stability. Their study aimed to achieve the best performance of working pairs of MOF/ammonia for adsorptive cooling.[166] The results of this study indicated the best behavior of the working pairs of NU-1000/ammonia whose value was estimated at 560 KJ kg^{-1} specific cooling effect.

5.2.10. Adsorption of Organic Compounds

The separation of aromatic pollutants from their sugar mixtures is one of the essential steps that should be considered in the second generation of biorefineries. Regarding the decisive role of these biocatalysts in biomass conversion into fuel and chemicals, they are deactivated in the presence of these compounds.[167] The weak nature of physisorption interactions of NU-1000 can lead to high-selective separation of relevant sugars.[168] Yabushita and coworkers reported extraordinary selectivity in the furanics adsorption such as 5-hydroxymethylfurfural and furfural, by exclusive adsorption of simple sugar constituents of furanics in aqueous media using NU-1000 adsorbents.[169] They concluded that in the pyrene-containing MOFs, π–π interactions occur on aromatic units in furanic compounds. As sugars do not possess aromatic moieties, these interactions were not observed in sugars. These results highlight the importance of synthetic adsorption sites in materials competing with enzymes in selective molecular recognition. NU-1000 also exhibited remarkable selectivity in the removal of biomass-derived aromatic compounds with no sugar adsorption, even in concentrated sugar solutions.[170] The influence of ionic liquid (IL) cosolvent was also examined on the efficiency of separation.[171] The unprecedented monomeric sugar adsorption by NU-1000 can be assigned to the co-adsorption of IL into the MOF spaces which alters the adsorption site nature of NU-1000 (pyrene linker). Yabushita et al. reported similar findings concerning the selective separation of aromatics from sugars.[167]

The challenge that remains is the detection and remediation of harmful per- and PFAS in aqueous medium.[172] In 2021, Li et al. utilized ZIF-8, NU-1000, and UiO-66 to assess the MOF structure influence, and properties of PFAS and H_2O matrix on the adsorption of PFAS@MOF.[173] Accordingly, NU-1000 exhibited great affinity to anionic and non-ionic PFAS. Electrostatic interactions between Zr metal nodes and anionic PFAS in NU-1000 can

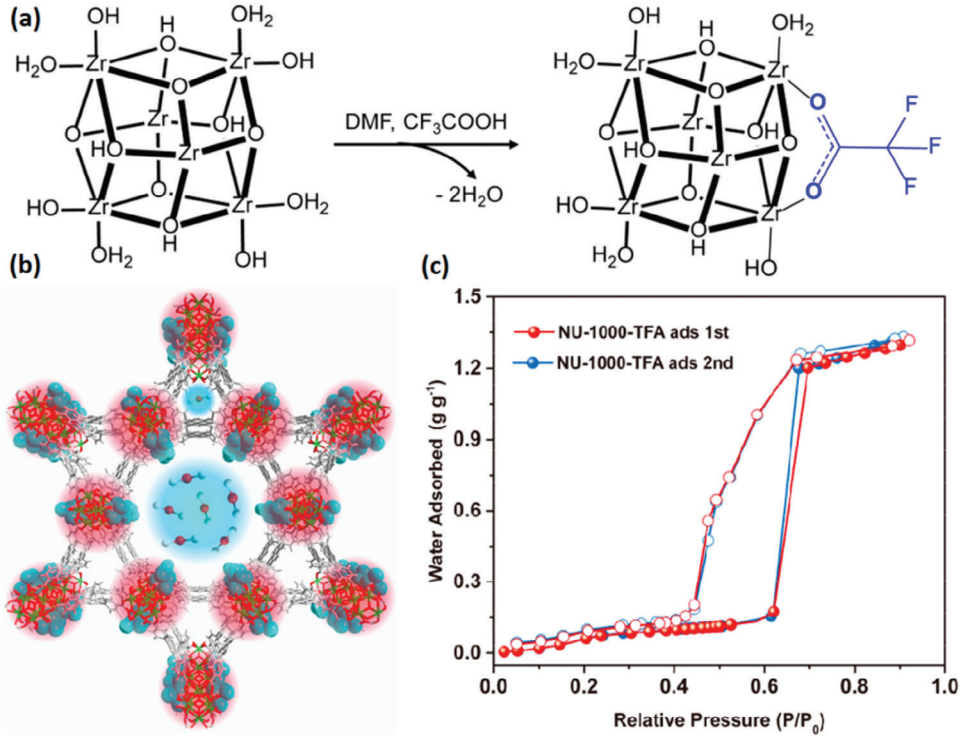

Figure 16. a) Post-synthetic modification of NU-1000 with TFA for water adsorption, b) topology of NU-1000-TFA structure, and c) first and second water adsorption performances of NU-1000-TFA. Reproduced with permission.[176] Copyright 2021, American Chemical Society.

be considered as the prominent mechanism in the adsorption of anionic PFAS. Moreover, acid–base interactions occurring between Zr nodes in NU-1000 and the amine groups of non-ionic polyfluoroalkyl substances dominate non-ionic polyfluoroalkyl substances removal mechanisms.

Applications involving water adsorption such as heating and cooling pumps, control of humidity, purification of water, and water harvesting are prominent players in industrial and environmental protection. In the mentioned fields, MOFs with sufficient water resistance are required.[174] The water-adverse role is due to its invasion of the metal node to break the coordination bonds between the linker and node, leading to collapse of the framework.[175] In 2021, a novel nanoporous MOF, NU-950, was designed by Yang et al. with *sqc* topology for sorption of water by NU-950 (*sqc*), NU-1000 (*csq*), and NU-901 (*scu*) materials.[176] Their study confirmed the topological effects on structural stability of these compounds in aqueous environments. Moreover, a feasible and generalizable route was described to increase stability in aquatic environments in these compounds by using a trifluoroacetic acid (TFA) hydrophobic capping agent. Due to the water-forbidden areas due to the new NU-950- TFA, the decorated TFA groups and NU-1000-TFA with *csq* and *sqc* relatively stable topologies showed a drastic improvement in water stability. The NU-1000-TFA structure is shown in **Figure 16** which exhibited drastic water absorption of ≈1.32 g g^{-1} in addition to surviving successive adsorption–desorption cycles with almost no decline.

Snurr et al. conducted a molecular dynamics simulation on alkanes in the hierarchical NU-1000.[177] Small molecules could diffuse from one channel type to another due to the specific topology and the interconnected channels. The mean squared displacement of molecules was plotted vs. time for different NU-1000 channels. Occupation of the larger hexagonal mesochannels reflects fast diffusion preferably along the axial direction. The slower diffusion in the smaller triangular microchannels also depends on the molecular size.

5.3. Catalytic Reactions

5.3.1. Alcohol Oxidation

MOFs benefit from well-defined catalyst-supporting sites such as reactive hydroxyl groups and well-defined structural periodicity introducing them as a promising support for single-site heterogeneous catalysts.[178] However, the residual organic moieties potential role should not be overlooked, especially, formate ions capable of occupying the catalyst anchoring sites in the course of MOF synthesis. Yang et al. described the role of the residual formate species in altering the NU-1000 catalytic activity, structure, and redox capability which is post-synthetically incorporated with copper(II) ions.[179] They indicated that in NU-1000 with formate, copper (II) ions only bind to ions in the node via bridging μ_3–OH groups, whereas, in the formate-free samples, copper (II) ions transfer protons from ligands to the terminal –OH_2 ligands Testing two MOFs for the oxidation of benzyl alcohol, residual formate boosted the turnover frequency of catalyst. According to the DFT calculation results, a sacrificial two-electron donor (e.g. node-bound formate) contributed to reducing copper(II) to copper(0) by nonradical pathways (**Figure 17**). Otake et al. reported an enhancement in the oxidation catalytic performance of the

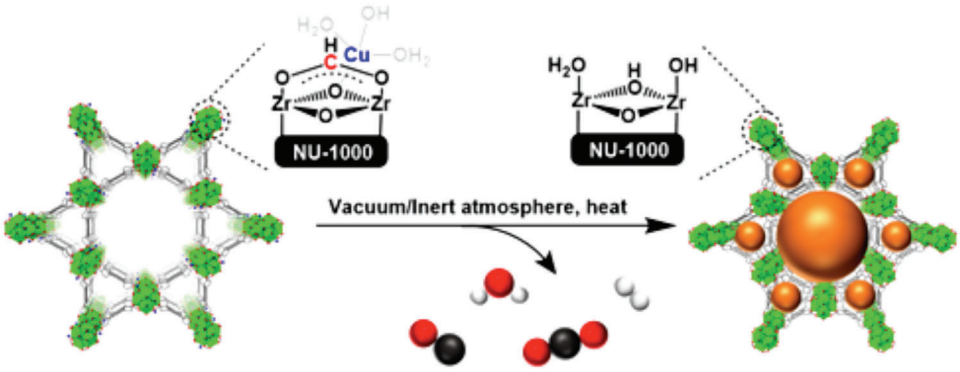

Figure 17. Reduction of Zr_6-cluster-supported mononuclear copper(II) to copper(0) nanoparticles as heterogeneous catalysts for benzyl alcohol oxidation by molecular oxygen. Reproduced with permission.[180] Copyright 2018, American Chemical Society.

NU-1000 incorporated with single-atom-based vanadium oxide for 4-methoxybenzyl alcohol under an O_2 atmosphere.[180]

5.3.2. Ethylene dimerization

The interest in ethylene dimerization lies in its product, 1-butene, which is a key building block for various commercial products such as plastics, surfactants, liquid fuels, and lubricants.[181] A properly-dispersed Ni_4-hydroxo cluster-containing NU-1000 catalyst was prepared by ALD which exhibited high activities in ethylene dimerization.[182] Bernales et al. applied Rh(I) complexes to the NU-1000 clusters to obtain high catalytic performance and selectivity for ethylene hydrogenation and dimerization.[183] Ye et.al employed various transition metals supported on NU-1000 clusters to assess their ability in dimerization of ethylene. Accordingly, the rate-determining step varied for different catalysts, reflecting the significance of taking more than one step for comparison of catalytic cycles across diverse metals. These findings agree with the ethylene dimerization activity of supported Ni^{II}, therefore, Cr^{II} and Pd^{II} could be high-potential catalysts in this process.[184] Pellizzeri et al. also explored metal cations grafted on Zr_6 nodes for catalyzed ethene dimerization to 1-butene.[185] To enhance the activity, Liu et al. incorporated electron-withdrawing (hexafluoroacetylacetonate) and electron-donating (acetylacetonate) ligands into NU-1000 as catalysts for modification of its steric and electronic properties in ethylene dimerization.[186]

5.3.3. Ethylene polymerization

High-efficiency and high-selectivity preparation of polymers, in particular, polyethylene of diverse grades, is vital in cost-effective production procedures.[187] In 2022, Goetjen et al. utilized the Cr-SIM-NU-1000 catalyst for this reaction.[188] At room temperature and using $(C_2H_5)_2AlCl$ as a cocatalyst, Cr-SIM-NU-1000 forms a linear polyethylene product in the presence of pure C_2H_4.

5.3.4. Ethylene hydrogenation

Wang et al. explored eight MOFs (M-NU-1000, M-NU-1200, M-NU-1010, and M-NU-1008 (M = zirconium and hafnium)) with 8-connected clusters with pore characteristics and various topologies and as a support for the deposition of Ni catalyst to be used in ethylene hydrogenation under controlled catalysis.[189] The linkers, nodes, and MOFs topologies are presented in **Figure 18**. Ni-containing materials grafted on Hf-MOFs showed better catalytic performance than those anchored on isostructural Zr-MOFs. Such an enhancement could be attributed to the deposition of Ni on a more active bridging oxygen site in the case of hafnium-based catalysts.

Desai et al. selectively catalyzed the semi-hydrogenation of alkynes to alkenes by heterobimetallic Rh-Ga active sites anchored onto the NU-1000 clusters (**Figure 19a**).[190] Redfern reported an NU-1000-Cu–oxo cluster composite (CuNPs@NU-1000) as a precatalyst which showed high activity and selectivity along with great stability in the catalyzed semi-hydrogenation of acetylene to ethylene.[191] The CuNPs@NU-1000 catalytic activity was assigned to the prevention of nanoparticle aggregation and the active sites of copper with uniform size as a consequence of the structurally well-defined NU-1000 support template effect (Figure 19b).

The NU-1000 nodes could be post-synthetically modified for installing metal cation catalysts.[67] Several other examples also highlighted the prominence of dispersed metal atoms or nodes (M@NU-1000 catalysts, M = metal ion) in NU-1000 as a catalyst.[71,118,192–194] Shabbir et al. examined the hydrogenation of ethene mechanism on metal ion catalysts supported on NU-1000 through microkinetic modeling and studies of high throughput reactors.[195] According to their results, metal cations with less unpaired electrons utilized the active sites of metal hydride and followed the mechanism proposed for hydrogenation on catalysts of M@NU-1000 and homogeneous photocatalysts of metal ions. On the other hand, metal cations with more unpaired electrons use the active sites of the bare metal cation to utilize proximal oxo ligands to form bonds with hydrogen species. Concerning catalytic hydrogenation, it results in more effective H_2 binding.

5.3.5. Activation of Carbon–Hydrogen Bonds

The conversion of feedstocks of low-cost hydrocarbons to other valuable materials is achievable through the selective activation of carbon–hydrogen bonds.[196] Gaggioli et al. evaluated

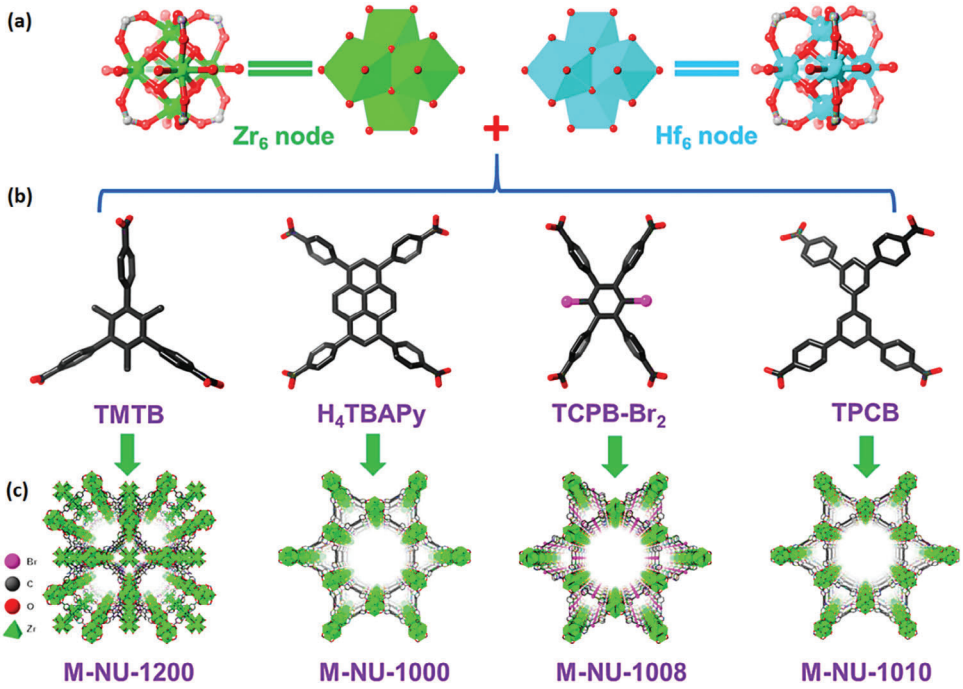

Figure 18. a) Metal nodes, b) Linkers, and c) framework topologies for M-NU-1200, M-NU-1000, M-NU-1008, and M-NU-1010 (M = zirconium and hafnium). Reproduced with permission.[189] Copyright 2020, American Chemical Society.

the activation of carbon–hydrogen bonds during the propane oxidative dehydrogenation by first-row transition metals containing hetero-bimetallic oxide clusters, anchored on the NU-1000 nodes.[197] The energy required for transferring H from propane to the metal oxide lies in the range of −27 kcal mol^{-1} for copper and zinc atoms to 86 kcal mol^{-1} for titanium atoms. Pahls and colleagues assessed the activation of methane carbon–hydrogen bonds through bimetallic NU-1000 clusters. Accordingly, materials encompassing copper and metals with Lewis acid sites improved carbon–hydrogen bond activation processes.[198] Based on Simons et al., doped Co-M oxide clusters supported on NU-1000 clusters can cleave carbon–hydrogen bonds, offering target species to synthesize improved catalysts.[199] Huang and colleagues employed perfluoroalkane-functionalized NU-1000 for ultrafine Pd NPs encapsulation to activate carbon–hydrogen bonds as a hydrophobic platform. The obtained perfluoroalkane-stabilized nanoparticles of Pd showed great regioselectivity and activity for direct carbon–hydrogen arylation of indoles in aqueous media. Moreover, the incorporation of perfluoroalkane chains into the NU-1000 mesopores facilitated the reactants' access to the active sites by providing hydrophobic surfaces, which enhanced the activity.[200]

5.3.6. Epoxidation of Alkenes

Noh et al. exploited the superior activity and cyclohexene selectivity for the ring-opened diol and the cyclohexene epoxide by molybdenum(VI) oxide deposited on NU-1000 (**Figure 20**).[201] Hupp et al. also prepared NU-1000 with L-tartaric acid to obtain a chiral catalyst that can be utilized as an asymmetric support for molybdenum catalytic active centers as Lewis acid sites to

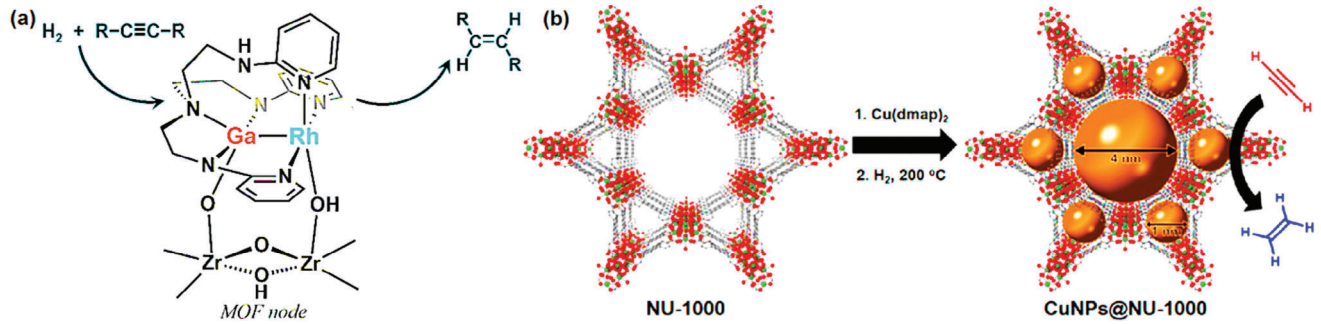

Figure 19. a) The Rh-Ga active site structure onto nodes of the NU-1000 in alkyne semi-hydrogenation. Reproduced with permission.[190] Copyright 2019, American Chemical Society. b) Installation of Cu–oxo clusters in NU-1000, followed by a mild reduction for the semi-hydrogenation of acetylene to ethylene. Reproduced with permission.[191] Copyright 2018, American Chemical Society.

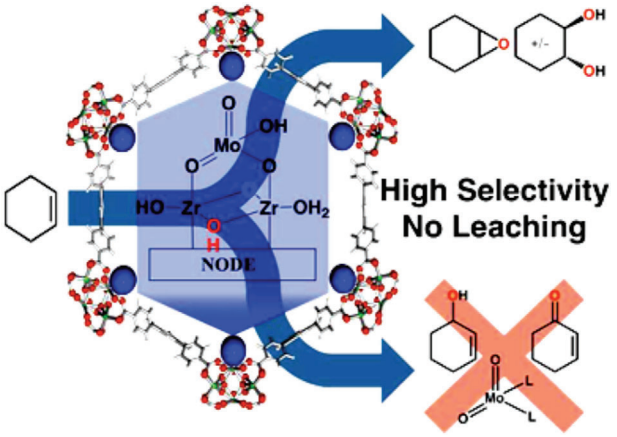

Figure 20. Reaction scheme of cyclohexene epoxidation with high selectivity by MO-NU-1000 catalyst. Reproduced with permission.[201] Copyright 2016, American Chemical Society.

transform alkenes to epoxides along with up to 100% excellent selectivity and enantiomeric excess.[202]

5.3.7. Oxidative Dehydrogenation

Co(II) cations were installed into the NU-1000 nodes through two different methods: ALD in a MOF (AIM) labeled as Co-AIM+NU-1000 and solvothermal deposition in a MOF (SIM) labeled as Co-SIM+NU-1000.[203] Formation of propene from propane during reaction of the oxidative dehydrogenation (ODH) showed different catalytic behaviors under the same conditions, possibly due to the different distributions of the Co sites in these two systems (**Figure 21**). Similar results were reported by the same group.[204] Based on Gates et al., the nodes of NU-1000 can serve as molecular catalyst supports chemisorbing highly uniform catalytic metal complexes.[205]

5.3.8. Hydrogen Elimination

Several basic steps in catalytic cycles are the elimination of hydrogen from a metal alkyl complex and its reverse reaction.[206] A deep understanding of the catalytic cycles requires proper knowledge of the role of the active site and other influential factors.[207] Yang et al. introduced a catalyst named V-functionalized yttria-decorated NU-1000 in the reactions of β-H elimination. The results showed that the linkers of carboxylate and yttria can promote the transfer of electrons between NU-1000 linkers and transition metals.[208]

5.3.9. Other Catalytic Reactions

NU-1000 has exhibited the highest stability with transition-metal nodes, making it a promising catalyst or catalytic support upon modification with other metals. Its large pores and water/thermal stability facilitate metal loading through ALD as well as metal exchange which might be otherwise limited by mass transport of vapor-phase and degradation of framework.[70,209,210] Mondloch et al. employed XRD findings and indicated that the loading of the nodes with Zn and Al through the ALD process did not dramatically alter the crystallinity of NU-1000.[70] They confirmed the reaction of Zn and Al with free hydroxyl groups on the clusters by DRIFTS spectroscopy. In another report by Kim et al. X-ray PDF and XRD techniques were applied to study the indium loading effect on NU-1000 nodes using ALD.[211] Farha et al. studied the bonding energies of vapor adsorption of calcium on NU-1000 at 300 K in an oven vacuum through a series of analyses and DFT calculations. Accordingly, the calcium atoms were transiently and weakly adsorbed, allowing their deep diffusion (≈10 to 20 nm) into the NU-1000 structure.[212]

Thornburg and coworkers prepared NU-1000 via post-synthesis modification with silica to reach active catalysts possessing excellent selectivity in the ring-opening reactions at high rates and yields. According to their results, active sites in NU-1000 nodes could be stabilized on other substances.[213] Furthermore, NU-1000 can act as a good support to activate methyltrioxorhenium for olefin metathesis. Methyltrioxorhenium is converted into a catalyst with active sites upon immobilization on the dehydrated NU-1000 strongly Lewis acidic acid sites.[214]

Porous materials can be utilized for the encapsulation of enzymes to not only protect the enzymes against denaturation in nonbiological media but also to facilitate the enzymatic reaction rates under desirable reaction conditions.[215] Chen and his research team considered the model of cytochrome c to assess the structure and behavior of enzymes encapsulated in NU-1000.[216] Based on them, encapsulation altered the enzyme structure around the active centers, improving the access of reaction substrates to the active centers. Such a variation in enzyme structure and enhancement in the catalytic activity could be assigned to the hydrophilic/hydrophobic interactions occurring between the organic linkers and the enzymes (**Figure 22**).

Enzyme-like substances with proteolytic potential can be introduced as promising alternatives to natural enzymes.[217] In 2021, Parac-Vogt et al. reported that the Hf_6O_8-based NU-1000 can serve as a heterogeneous catalyst to hydrolyze peptide bonds under mild conditions.[218] This system showed great selectivity for the cleavage of protein substrates, i.e. hen egg white lysozyme (HEWL). Their results showed that the insertion of oxo-clusters of Hf_6O_8 is an efficient approach for preserving the hydrolytic function. Their previous studies indicated that in the isolated oxo-cluster of Hf, strong substrate adsorption smoothing prevented the development of proteolytic potential. Li et.al further improved the NU-1000 catalytic activity by synthesis of NU-1000 nanoparticles whose larger relative external surface area can accelerate the reaction. The methyl paraoxon catalytic hydrolysis was explored versus crystallite size of NU-1000 which indicated a remarkable rise in the rate of the nano-sized crystals in comparison with microcrystals.[219]

One of the main challenges in catalysis research is to design catalysts capable of converting light hydrocarbons of the shale gas into platform molecules or denser compounds for their further conversion into chemicals and fuels.[220,221] Hydrocarbon catalytic oxidation with H_2O_2 has been one of the most prominent ideas. Ahn and coworkers developed a customized reactor to elucidate the activation and selective oxidation of H_2O_2 in the vapor phase.[222] Their findings suggest highly selective

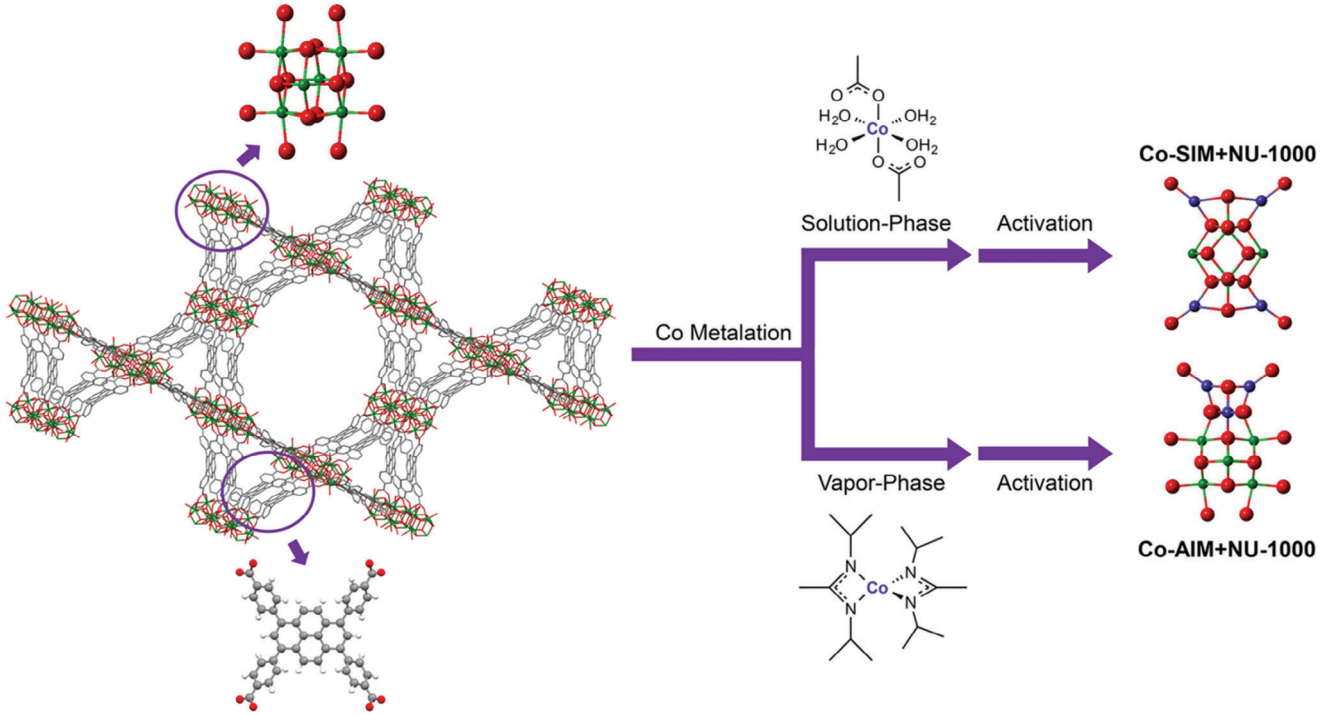

Figure 21. MOF supports structural representation, NU-1000, and two routes for the synthesis of Co-based catalysts for catalyzing the ODH of propane to propene. Reproduced with permission.[204] Copyright 2017, American Chemical Society.

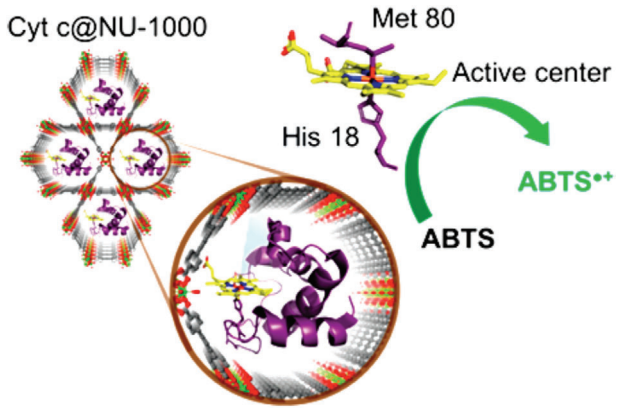

Figure 22. Schematic illustration of cytochrome c encapsulated in the mesopores of NU-1000 and its oxidation of ABTS. Reproduced with permission.[216] Copyright 2020, American Chemical Society.

cyclohexene epoxidation with hydrogen peroxide over catalysts of metal oxide with Lewis-acid sites including niobium and titanium grafted on NU-1000 and SiO_2.

MOFs can also serve as selective catalysts for hydrocarbon transformation.[223] Hackler et al. reported the incorporation of different clusters of metal oxide upward of 8 atoms into the pores of the NU-1000 through ALD to selectively catalyze propyne hydrogenation and isomerization.[224] They reported copper and cobalt as the most active elements for hydrogenation of propyne into propylene (**Figure 23**). Moreover, the zinc and cobalt combination in NU-1000 could diminish the propensity for coking and overall hydrogenation to propane in comparison to its individual components. Liu and coworkers also emphasized the applicability of metal-oxide-cluster-based NU-1000 nodes as well-defined supports for heterogeneous catalysis of ethylene hydrogenation.[225]

Yabushita et al. managed to synthesize selective Lewis-acid sites in a phosphate-modified NU-1000 to transform glucose into 5-hydroxymethylfurfural (HMF) (**Figure 24a**).[226] HMF can be employed as a building block of polymers and a small-molecule clinical agent in sickle-cell disease. Strong Lewis-acid sites can be obtained through phosphate modification of NU-1000 nodes which may result in undesired side reactions. The atmospheric catalytic activation of dioxygen to achieve sustainable oxidation processes has gained a great deal of popularity.[227] Farha et al. immobilized $H_3PW_{12}O_{40}$ in NU-1000 frameworks, i.e. PW_{12}@NU-1000 composites to oxidize CEES, a mustard gas simulant, with no use of light and sacrificial reductants (Figure 24b).[228]

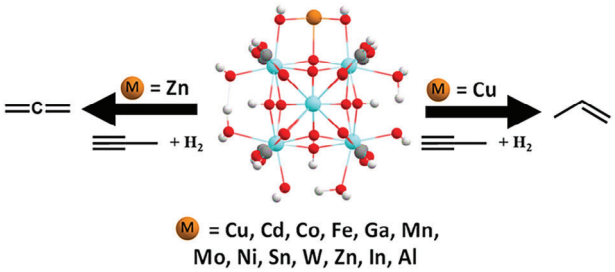

Figure 23. Reaction scheme for selective hydrogenation and isomerization of propyne to alkenes through metal ions attached to the node. Reproduced with permission.[224] Copyright 2017, Royal Society of Chemistry.

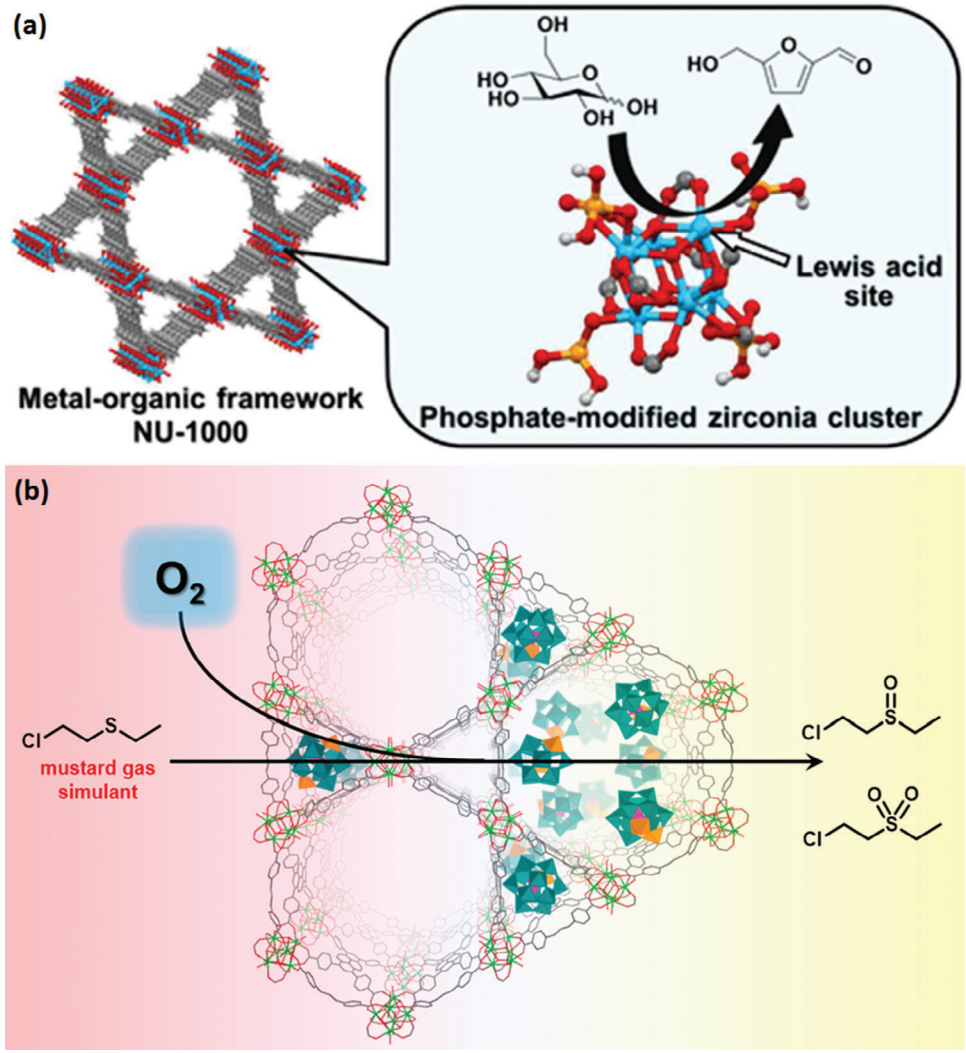

Figure 24. a) Glucose transformation to 5-hydroxymethylfurfural using functionalized NU-1000 with strong Lewis-acid sites. Reproduced with permission.[226] Copyright 2017, American Chemical Society. b) The immobilization of POMs in the NU-1000 channels for aerobic oxidation. Reproduced with permission.[228] Copyright 2019, American Chemical Society.

Interestingly, the PW_{12}@NU-1000 composites could be fully recycled, while the PW_{12} decomposed and led to other products.

Eddaoudi et al. presented the step-by-step anchoring of $W(\equiv C^tBu)(CH_2{}^tBu)_3$ inside the mesopores of NU-1000.[229] The initial carbyne moiety was quantitatively converted into W = O because of the special surface characteristics of the Zr_6 nodes, which resulted in better catalytic activity relative to the corresponding catalysts prepared through other grafting routes. Biomass-derived ethanol has attracted a considerable deal of attention as a promising substitute for petroleum for the production of value-added hydrocarbons.[230,231] Paluka et al. conducted a DFT investigation to evaluate the dehydrogenation reactions on Fe/Zr-NU-1000 in the presence or absence of an oxidizing agent (i.e. N_2O). The supported NU-1000 framework facilitated the e^- transfers and stabilized all species along the reaction coordinate.[232] Cramer et al. assessed the deposition of transition metals on NU-1000 by using DFT calculations for the acceptor-free dehydrogenation of alcohol, a prominent reaction for hydrogen generation and storage.[233] Based on their proposed mechanism, the MOF support is actively involved in the proton transfer process. Moreover, Co and Ni-containing catalysts could serve as good candidates in the reaction.

Isomerization of C-C bonds is among the prominent petrochemical reactions. The *o*-xylene isomerization/disproportionation can be regarded as a probe reaction for strong Brønsted acid catalysis which also exhibits sensitivities to pore topology and the local acid site density.[234] Notestein and colleagues encapsulated phosphotungstic acid (PTA) within NU-1000 to obtain a strong catalyst for isomerization of *o*-xylene at 523 K (**Figure 25a**).[235] Similarly, the contribution of the Brønsted acidity could enhance the reactivity of Hf_6O_8-based NU-1000 (Hf-NU-1000) for the chemical CO_2 fixation into five-membered cyclic carbonates relative to its corresponding Zr-NU-1000 counterpart (Figure 25b).[236] The practical application of nanoporous solids for adsorptive separations and catalysis requires thorough knowledge of the mass transfer

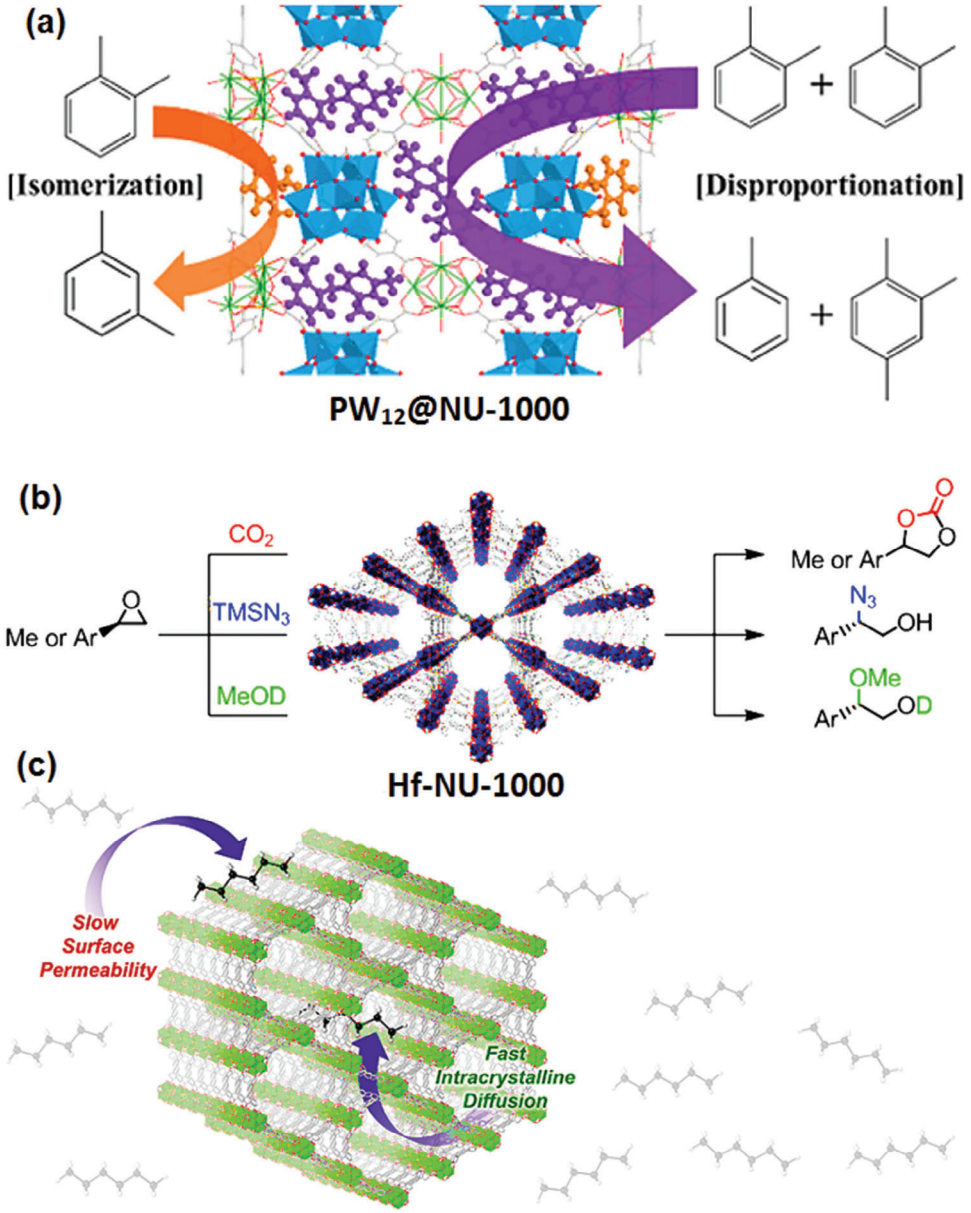

Figure 25. a) *o*-Xylene isomerization over PW_{12}@NU-1000. Reproduced with permission.[235] Copyright 2018, American Chemical Society. b) CO_2 fixation over Hf-NU-1000. Reproduced with permission.[236] Copyright 2014, American Chemical Society. c) Mass transfer process within NU-1000. Reproduced with permission.[238] Copyright 2022, American Chemical Society.

limitations.[237] In 2022, Farha et al. assessed the *n*-hexane mass transfer in Zr-MOFs by considering both intracrystalline and surface transfer of mass mechanisms (Figure 25c). NU-1000 and NU-1200 outperformed the other MOFs. They assigned the loading dependence to the local content of adsorbates at the boundary of the crystal which might affect the permeation from the pores into the crystallite. Moreover, they reported higher surface permeabilities in the MOFs with hierarchical micro/mesopores as well as those with cubic crystal structures.[238]

The influence of the pore structure of the catalysts on substrates of interest for investigation of the catalytic activity has been the subject of numerous studies.[239] The results of Dai et al. revealed the possibility of upgrading the selectivity of ethanol by many Zr-MOFs such as NU-1000, if guest molecules can be stabilized inside the pore during the catalytic process.[240] Chen and Snurr explored the self-diffusion of *n*-hexane in several hierarchical MOFs of similar topologies as NU-1000 but various pore sizes under the same conditions. They intended to establish a relationship between the structure and properties of the adsorbate diffusion into MOFs.[241] Accordingly, the microchannel diameter and the window size connecting these microchannels and meso-channels were decisive factors.

Post-synthesis routes for the incorporation of additional metal sites inside the MOFs have been the subject of various works including those conducted by Lercher et al.,[242] Ahn et al.,[203] Li et al.,[118] Yaghi et al.,[243] Zhang et al.[244] and Lu et al.[71,190,245]

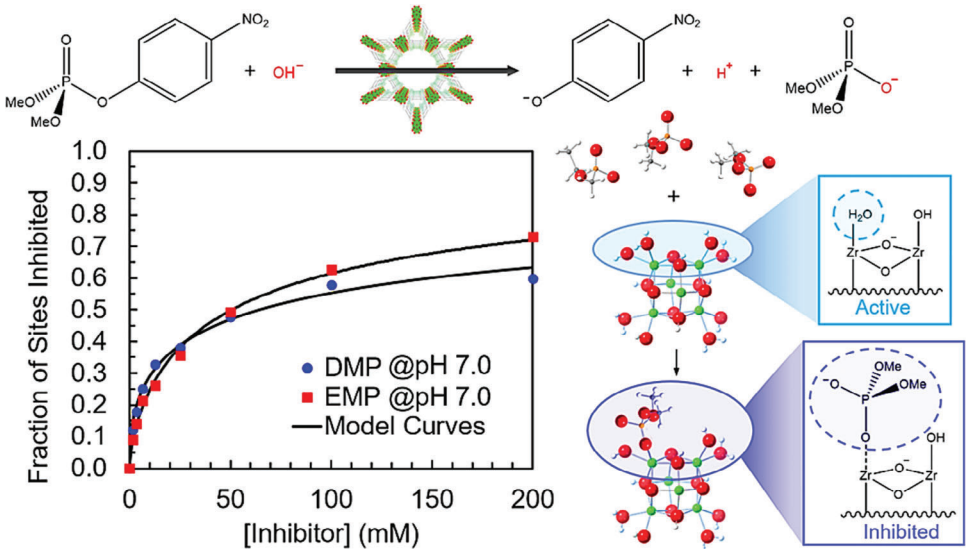

Figure 26. The hypothetical node structure of NU-1000 for hydrolysis reaction of DMNP with Langmuir–Freundlich model fitting curves at pH 7.0. Reproduced with permission.[253] Copyright 2021, American Chemical Society.

Farha and Hupp proposed a high-efficiency vapor-phase metalation approach for the incorporation of Zn(II) and Al(III) into the NU-1000 mesopores.[70] The modified system exhibited better catalytic behavior; in some cases, the elusive methane oxidation into methanol was achieved.[242,243]

5.4. Degradation/Destruction of Chemical Warfare Agents

Given the serious toxicity and rapid human incapacitation rate of chemical warfare agents (CWA), the development of a process for their fast degradation/destruction is highly welcome, particularly for those containing phosphorus–fluorine bonds.[246–248] A great number of research works have addressed the application of Zr-MOFs as catalysts for hydrolyzing organophosphate CWAs. In the mentioned process, Zr atoms play the role of Lewis acids and increment the phosphorus centers reactivity, while the hydroxyl groups on the clusters and/or linkers with different functional groups further promote the reaction via the activation of the nucleophile or contribution to the release of the leaving groups.[60,249–252] The catalytic hydrolytic destruction of DMNP, a key nerve agent was assessed in 2021, using NU-1000.[253] The interaction of NU-1000 in DMNP hydrolysis and the nerve agent ethyl methylphosphonofluoridate (EMPF) was explored which resembled the G-series nerve agents hydrolysis degradation product, Sarin (GB), for deconvolution of the impact of product inhibition from other influences on catalytic activities. Based on them, the accessibility of considerably labile node aqua ligands is a critical factor in the Lewis-acid catalytic hydrolysis of the stimulants or nerve agents because the primary step in the catalysis involves displacing ligated H_2O by a phosphorus bond, terminal oxygen atoms of the reactants (**Figure 26**). Wang and coworkers revealed the impact of the water content of Zr-MOF on its hydrolysis rates. They evaluated solid-phase decontamination of DMNP by NU-1000, UiO-66, and UiO-66-NH_2 to indicate the full slower hydrolysis and various reactivity trends in comparison with the solution decontamination. Such a difference can be attributed to diversity in the structural design of Zr-MOF.[254] Atilgan et al. introduced a halogenated-BODIPY ligand as a strong photosensitizer that can be post-synthetically appended to NU-1000 clusters to augment the generation of singlet oxygens by the MOF which can act as a heterogeneous photocatalyst in the generation of $^1O_2$ upon exposure to green LED light. These singlet oxygens managed to selectively detoxify the sulfur mustard simulants of CEES to lower-toxicity sulfoxide derivatives of CEESO with an approximate half-life of 2 min.[255] Howarth et al. reported NU-1000-PCBA by the incorporation of fullerene-based photosensitizers ([6,6]-phenyl-C_{61}-butyric acid (PCBA)) into NU-1000 by SALI and the post-synthetic process to the rapidly and selectively oxidize of CEES and sulfur mustard.[256]

Nerve agents act by inhibiting the acetylcholinesterase enzyme, which breaks down the neurotransmitter acetylcholine, which makes the neurotransmitters continue sending signals, while none of them are broken down.[257] Acetylcholine formation in the synaptic cleft between muscle cells and nerve cells can lead to muscular contraction and death.[258] The results of recent studies have shown that the use of Zr-MOFs can effectively prevent the formation of this product such that the hydrolysis products form a strong bidentate binding with nodes to prevent acetylcholine.[259] The mentioned problem can be avoided by depositing single-atom catalysts on the nodes to promote more favorable monodentate binding modes of the products. These active sites can be evaluated at the atomic level, allowing detailed computational mechanistic investigations.[60,260] Snurr et al. used the DFT approach to comprehensively investigate the effect of catalysts with single-atom metals on the nodes of Zr_6 at various oxidation states in the sarin nerve agent's gas-phase hydrolysis.[261] Previous works to increment the MOF-catalyzed nerve agent hydrolysis addressed either the incorporation of defect sites or the preparation of MOFs with diverse functionalized ligands and/or metal nodes.[262] The single atom systems were assessed to promote monodentate binding of the products to the

active sites, thus, preventing undesirable bidentate binding which resulted in the prevention of product in the previous works on nerve agents gas-phase degradation on Zr_6 nodes.

Mendonca and Q. Snurr conducted DFT studies to investigate the effect of catalysts with single-atom metals on the nodes of Zr_6 for sarin gas-phase hydrolysis. The results of this study revealed that the deposition of these catalysts on Zr-MOFs can accelerate the hydrolysis of nerve agents.[261] Grissom et al. addressed the diffusion, adsorption, and reaction of CWAs in a series of Zr-MOFs, including NU-1000 in combination with polyoxometalates, to examine the influence of the common ambient gases (e.g. carbon dioxide, sulfur dioxide, and nitrogen dioxide) on the efficacy of the NU-1000 and polyoxometalate in CWAs degradation.[263]

Farha et al. presented the catalyzed degradation of CWAs by open-metal sites in NU-1000 which served as Lewis acids.[60] Their system showed high potential as a support for the diverse metal species deposition on the ordered sites of the framework. In the ALD of NU-1000, organometallic precursors react with the hydroxyl sites on the clusters, enabling the deposition of diverse metal-oxo clusters inside the tiny pores of NU-1000.[70,264] Platero-Prats et al. examined the dynamic structure and reactivity of NU-1000-supported copper species.[265] According to their results, the Cu^0-NU-1000 system had catalytical activity for ethylene hydrogenation in the gas phase. Nevertheless, to improve the efficiency of catalyst in the gas-phase hydrolysis, the product desorption barrier should be decreased.[266] In this context, Chen and Snurr assessed the catalytic gas-phase hydrolysis of a model simulant of organophosphate CWAs (dimethyl *p*-nitrophenyl phosphate) via mono- and bi-metallic NU-1000.[267] They indicated that to facilitate the reaction the active metal−oxygen−metal motifs can serve as acids and bases in relevant enzymes.

According to Gil-San-Millan et al., reactivity and the detoxification of UiO-66, MOF-808, and NU-1000 to the bulky reagent $[Mg(OMe)_2(MeOH)_2]_4$ (is this really a bulky reagent? Seems rather small to me!) strongly depend on the size of pore and distribution in the relevant MOFs. The modification drastically improved catalytic destruction of P—S and P—F bonds of toxic nerve agents.[268] MOF-808, PCN-777, UiO-66/67, NU-1400, NU-1002, and NU-1000 were prepared based on an octahedral Zr_6 cluster to degrade organophosphorus (OP) nerve agents.[249,269,270] De Koning and his team showed the potential of DTNB@NU-1000 for the degradation of VX (i.e. highly persistent and extremely toxic nerve agents with hard detectability) in neutral buffers.[271] They detected a color response with the degradation of VX whose intensity was linearly related to the VX concentration.

As extremely noxious substances, organophosphorus compounds (OPs)[272] are not only involved in eutrophication induction but they can also bind to the neurotransmitters, acetylcholinesterase, leading to nerve paralysis and death.[273] Such a deadly action further emphasizes the significance of the removal of OPs from water. Zr_6O_8 cluster-based MOFs have shown remarkable catalytic performance against compounds based on organophosphate like pesticides, stimulants, and real warfare agents which can be assigned to their highly Lewis acidic zirconium centers.[58,60,274] repetition??? Chen et al. explored the NU-1000-catalyzed phosphate ester hydrolysis by DFT calculations.[275] The distorted node-catalyzed reaction examination indicated that during catalysis, dehydrated NU-1000 remained in the distorted form. The rate enhancement upon high-temperature treatment of NU-1000 can be attributed to the distortion and dehydration of nodes regarding the water-exchange step absence and the smaller barriers on the distorted nodes. Koning et al. also evaluated the diverse chemical warfare agents based on organophosphate degradation rates by NU-1000.[269] Their results confirmed the great potential of NU-1000 in the destruction of diverse agents in alkaline-buffered systems.

Despite the significant contribution of organophosphate-based pesticides to the agricultural industries, their toxicity has posed adverse impacts on the environment and humans.[276] In 2022, According to Bondzic et al., organophosphate pesticides possessing aromatic heterocyclic moieties can be effectively eliminated by NU-1000 in <3 min average time.[277] Based on their experimental and computational results, the enhanced chlorpyrifos removal (after only 1 min) by NU-1000 can be assigned to the hydrolysis and sorption synergic effects. The physisorption on the pyrene linkers and the chemisorption on the Zr node followed pseudo-first-order kinetics within the first minute, whereas the pseudo-second-order model describes the entire time range. Additionally, the pyridine moiety content of the chlorpyrifos offers adequate basicity for facilitating the bridging of the Zr_2OH ligands to the catalyst (**Figure 27**).

Organophosphate CWA works by inhibiting the enzyme acetylcholinesterase (AChE), which is essential for nerve function in the body,[278] and is one of the most harmful substances on the globe. Examples of CWAs containing organophosphates, such as Sarin, Soman, and Novichok, are well known.[279] Over the course of several years, a significant amount of time and energy has been invested in the development of catalytic materials that are capable of effectively breaking down organophosphate CWAs. Because of their outstanding stability and activity, Zr-MOFs have received the most attention in this application.[69,280,259] The breakage of the P-O link by nucleophilic assault is the most effective chemical approach for degrading organophosphate CWA (for example, hydrolysis). Zr-MOFs, which can operate as Lewis acids to enhance the phosphorus centers' reactivity, can be utilized to hydrolyze organophosphate CWAs. Additionally, the —OH groups or any other functional group on linkers may be employed as Lewis acid catalysts.[60,281,282] Operating the nucleophilic (such as OH^- as well as H_2O) or providing assistance for the exit of the leaving group are also ways to speed up the reaction. By DFT, Chen and Snurr studied the catalytic mechanism for hydrolysis of gas-phase of organophosphates onto NU-1000 in great detail.[267] Zr-MOFs have been shown to catalyze the gas-phase sarin and dimethyl phosphate (DMMP) hydrolysis, and the whole reaction process, together with the energy distribution.[283,284] Chemical laboratories cannot routinely handle sarin since it is highly toxic, on the other hand, DMMP is particularly not an accurate sarin simulant with regard to hydrolytic reactivity.[279,285] Although DMMP is a great sarin simulant with regards to adsorption performance,[286] *p*-nitrophenol dimethyl phosphate (also known as methyl paraoxon) was selected instead, and the catalytic hydrolysis route of DMNP was traced out on the NU-1000. According to some reports, it began at the NU-1000 node and involved removing a molecule of water to establish an unlocked binding site on Zr.[287,288] DMNP molecules (**Figure 28**) first attach to open Zr sites and are then susceptible to the nucleophilic

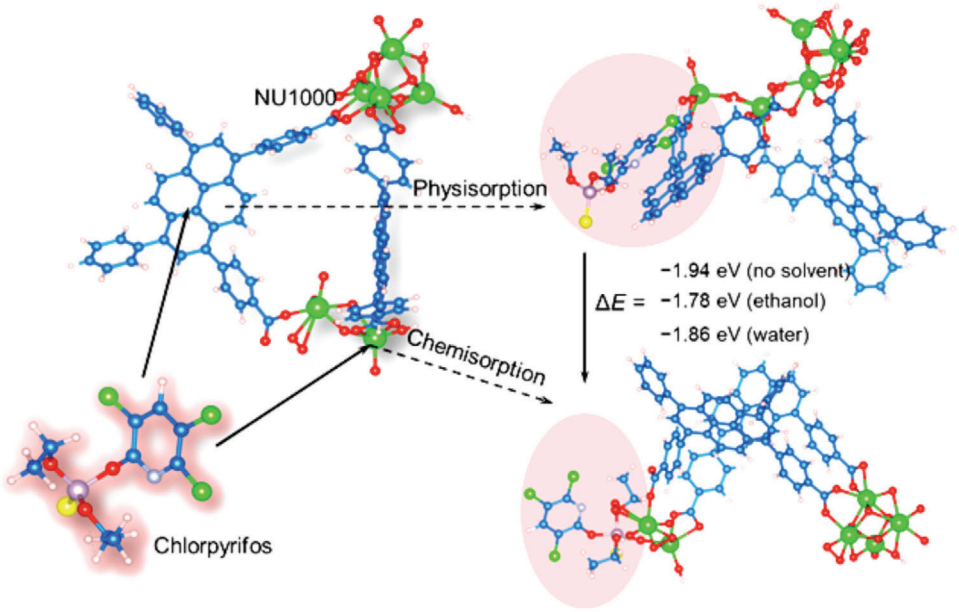

Figure 27. Quantum chemical calculations result for NU-1000/chlorpyrifos interactions: adsorbtion of chlorpyrifos on the NU-1000 linkers and the Zr nodes via physisorption mode and chemisorption mode, respectively. Reproduced with permission.[277] Copyright 2022, American Chemical Society.

assault of water molecules. After this phase, the penta-coordinate phosphorus center (INT 1) positions the leaving group in an axial place.[289,290] Dimethyl phosphoric acid (DMPA) is produced by reacting Zr—O with hydrogen on the node and then being desorbed when the leaving group has left via the —OH group on the node.

5.5. Desulfurization

Desulfurization is a serious issue in the petroleum industry, considering the strict legislation and incrementing awareness about environmental problems.[291,292] Yu et al. developed an approach to synthesize a hydrodesulfurization catalyst by loading MoS_2 in NU-1000 using ALD at extraordinary desulfurization activity and high stability.[293] Catalytic oxidative desulfurization of NU-1000 was also assessed by Zheng and coworkers in the presence of H_2O_2 which revealed excellent efficiency and good stability.[51, 294]

5.6. Photocatalytic Degradation

Natural photosynthetic light-harvesting complexes can store visible-region solar photons and quickly deliver them to chemical catalysts and energy-converting electrodes at the highest efficiency.[295] In a study in 2021, Goswami et al. found that NU-1000 could absorb energy and deliver it to acceptors/donors of electrons by serving as an antenna.[296] These results verified the ability of NU-1000 and other MOFs with the same properties to offer a large "antenna" capable of immobilizing catalysts on the MOF nodes, hence, opening new horizons in the field of solar energy conversion.

Photocatalytic degradation of organic pollutants such as antibiotics in wastewater is a promising green approach, with high performance, cost-effectiveness, and sustainability.[297] Abazari et al. developed a hybrid NU-1000@$ZnIn_2S_4$ (NU@ZIS) nanocomposite core/shell with superior sono-photocatalytic behavior to degrade tetracycline (TC) antibiotics in aqueous media. The improved activity of NU@ZIS was ascribed to the heterojunction formation between ZIS and NU and these components' synergistic effects, resulting in outstanding radical production which facilitated the transfer of Z-scheme charge carrier while decreasing the charge carrier recombination.[298] In addition, the catalyst offered good biocompatibility and sono-photocatalytic performance for the decontamination of different water resources due to the cytotoxicity of NU@ZIS composites along with the aquatic toxicity against *E.coli* after the photocatalytic reaction (**Figure 29**).

Photocatalytic oxidation of sulfide into sulfoxide has been considered an interesting environmentally compatible route for chemical transformations and degradation of toxic chemicals.[299] Hou et al. introduced the synthesis of a series of In_2S_3/NU-1000 heterojunctions with high efficiency in the visible-light-driven photocatalytic oxidation of sulfide.[300] They attributed the significant rise in the photocatalytic activity to the creation of Z-scheme heterojunctions In_2S_3/NU-1000 which enhanced the visible light absorption, shortened the charge transfer distance, improved charge transfer efficiency, and promoted redox potentials for effective provision of $^1O_2$ and $^\bullet O_2$ active species as shown in following mechanism (**Figure 30**).

Liu et al. employed NU-1000 as a heterogeneous photocatalyst to degrade 2-chloroethyl ethyl sulfide (CEES).[301] They also assessed the generation of $^1O_2$ by NU-1000 which selectively oxidized CEES to the CEESO with no toxic sulfone by-products. The large pores and three-dimensional structure of NU-1000 facilitated the products and substrates diffusion in addition to enhancing the generation of singlet oxygen through isolating and heterogenizing moieties of pyrene in an ordered array.[302,303] Knapp et al. prepared NU-1000 with UO_2^{2+} grafted on its nodes to be

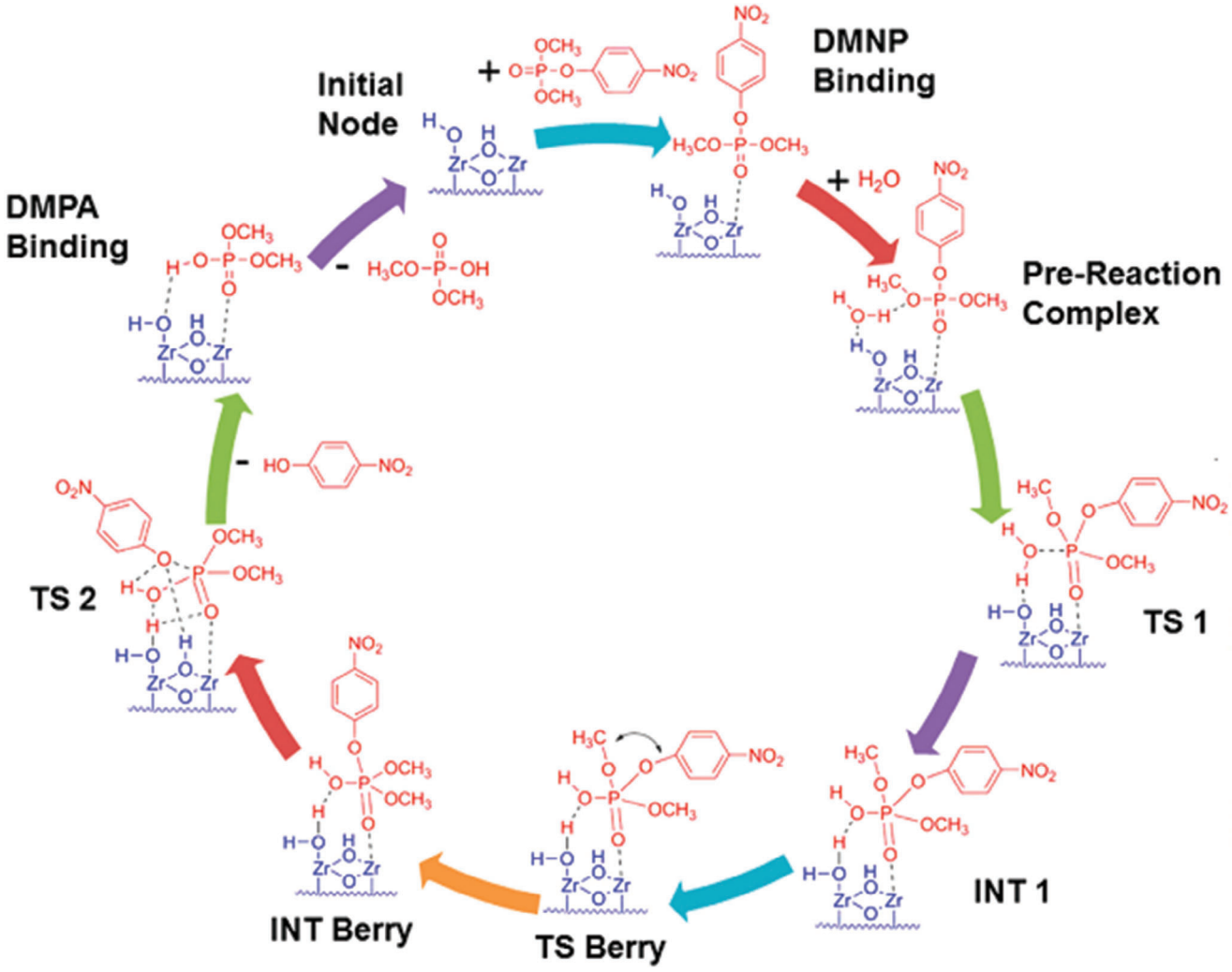

Figure 28. Complete cycle of catalytic reaction for DMNP hydrolysis in the gas phase using the NU-1000 catalyst. Reproduced with permission.[267] Copyright 2020, American Chemical Society.

used in the oxidation of 4-methoxybenzyl alcohol via visible light photocatalysis. Their developed system showed superior activity due to the interactions between the H_4TBAPy linkers and uranyl ions.[304]

Biological potential showed a remarkable improvement upon the enhancement of atom-transfer radical addition (ATEA) with the photocatalytic method to olefins.[305] The negative reductive potential of perfluoroalkyl iodide can prevent the production of perfluoroalkyl radicals through the transfer of a single electron in the photocatalyst from the excited state. Zhang et al. offered a photocatalytic strategy capable of simultaneous integration of the perfluoroalkyl and iodo groups into olefins via the application of a heterogeneous NU-1000-based photocatalyst under LED irradiation.[306] Lee et al. incorporated protoporphyrin IX as a photosensitizer into NU-1000 through SALI which showed an enhanced photocatalytic production of singlet oxygen and thus, superior degradation of 2-chloroethyl ethyl sulfide (CEES) under UV and blue light. Their developed system also expanded the effective spectral visible range of light that can be used by NU-1000.[307]

Quantum dots and metal clusters as diverse photo-redox species can be introduced into the MOFs pores for improving their photoactivity.[308,309] The encapsulation of nanoclusters in MOFs has been taken into account due to its promising potential for photocatalysis. Truhlar et al. did a computational study and confirmed that Cd_6Se_6@NU-1000 can facilitate transfer of electrons from the organic linkers to the inorganic clusters, resulting in charge separation.[108] Substitution on the linker can adjust the position of the bands and the bandgap of the composite (Cd_6Se_6@NU-1000), allowing for visible light water splitting. The charge separation in the MOF can prolong the life of the excited states, improving photocatalytic activity. Peters and colleagues observed an increment in photocatalytic hydrogen evolution by NU-1000 with encapsulating few-atom clusters of nickel sulfide in the NU-1000 pores.[107] Cao et al. succeeded in the synthesis of CdS@NU-1000 and CdS@NU-1000/1% RGO nanocomposites with enhanced photocatalytic behavior by a factor of ~10 in comparison with the commercial CdS.[111] These composites of MOFs offer effective charge separation, reflecting the applicability of the theory to alleviate the absorption of visible light and

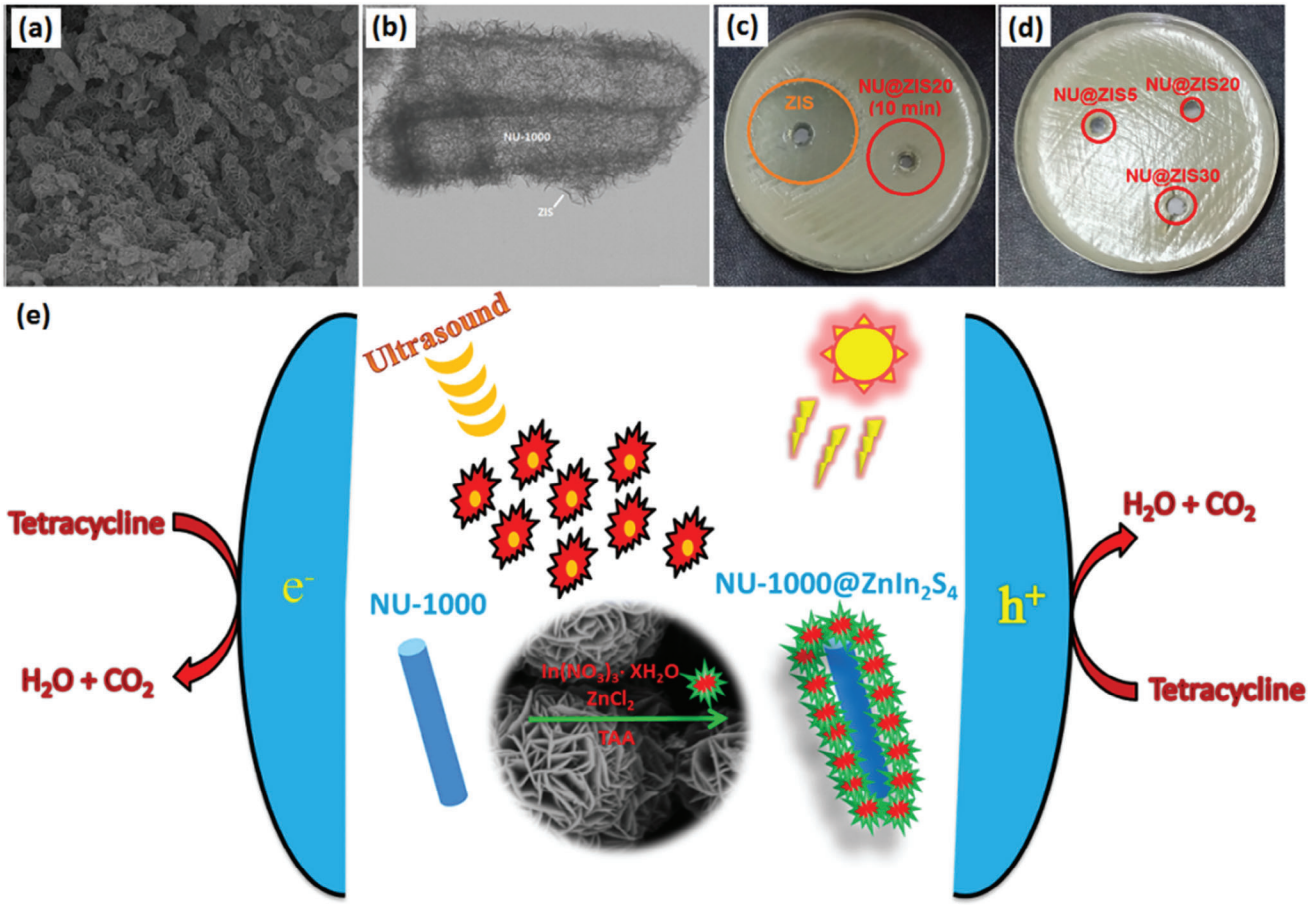

Figure 29. a) FE-SEM and b) TEM images of NU@ZIS nanocomposites, c,d) aquatic toxicity against *E.coli* of water solutions after degradation of tetracycline over samples by agar-well diffusion experiments, and e) proposed mechanism for degradation of tetracycline over NU@ZIS heterojunction. Reproduced with permission.[298] Copyright 2021, American Chemical Society.

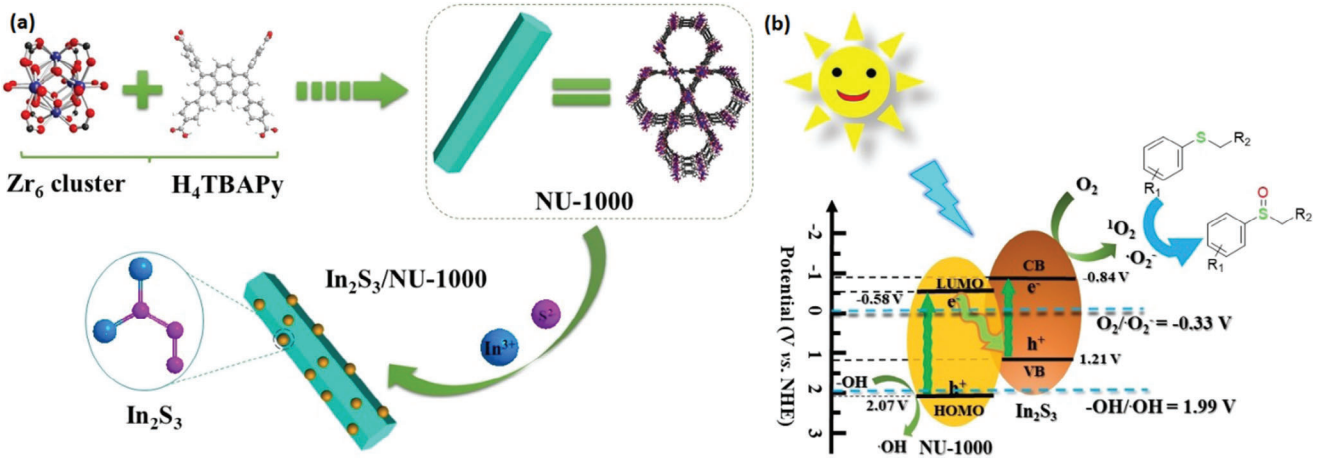

Figure 30. a) Schematic illustration of In_2S_3/NU-1000 heterojunction preparation, and b) the Z-scheme mechanism of charge transfer processes for oxidation of sulfide over heterojunction of In_2S_3/NU-1000. Reproduced with permission.[300] Copyright 2022, WILEY-VCH.

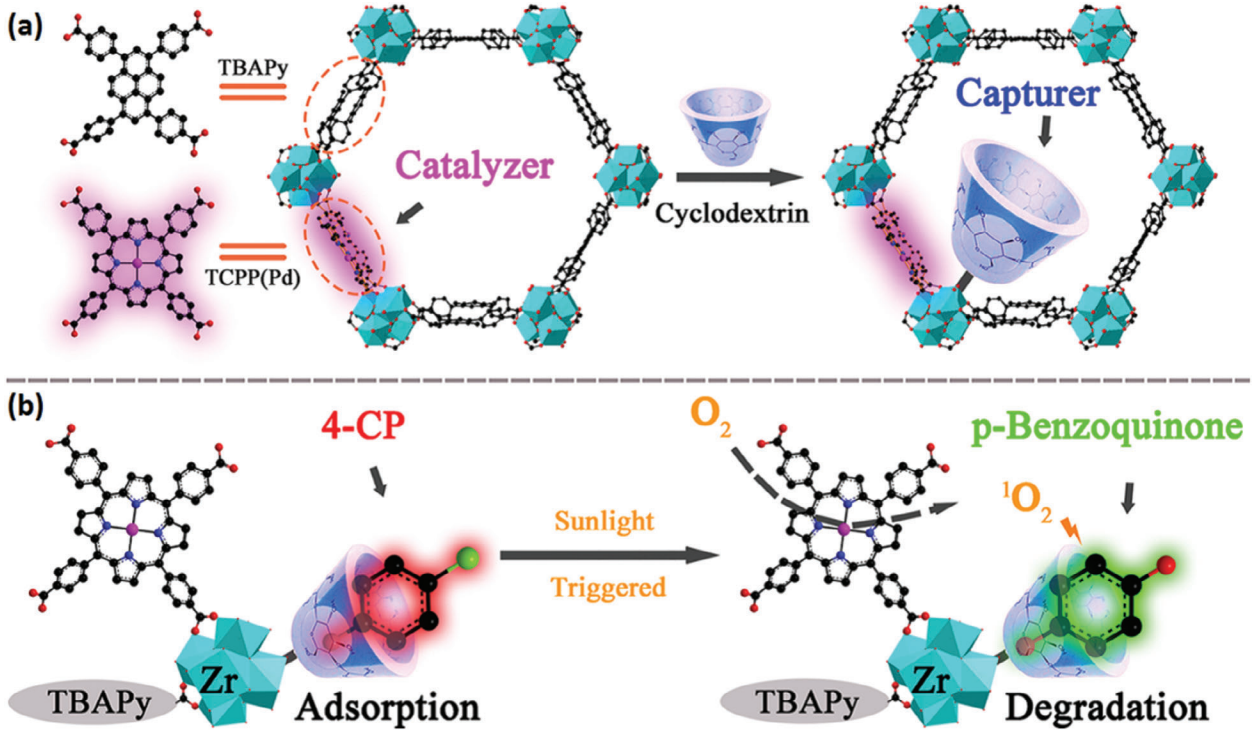

Figure 31. a) Spatial Structures of CMCD@NU-1000-TCPP(Pd) and b) the adsorption and phototriggered $^1O_2$-induced for degradation of 4-chlorophenol using CMCD@NU-1000-TCPP(Pd). Reproduced with permission.[311] Copyright 2021, American Chemical Society.

adjust the band edge position for a specific photocatalytic reaction (i.e. splitting of water and reduction of CO_2).

As a model of toxic chlorophenols, 4-chlorophenol (4-CP) has found widespread agricultural and industrial applications. Even trace levels of 4-CP are extremely genotoxic, carcinogenic, and non-biodegradable.[310] In a study conducted in 2021, Gu et al. prepared CMCD@NU-1000-TCPP (Pd) for 4-CP degradation and adsorption in H_2O. Their system contributed to the transformation of the O_2 into $^1O_2$ if exposed to light. The produced $^1O_2$ rapidly reacted with 4-CP to yield less toxic products.[311] β-CMCD and TCPP(Pd) respectively served as the capturer and photodegradation promoters to reach the MOF-based adsorption–degradation integrator (**Figure 31**). CMCD@NU-1000-TCPP (Pd) managed in rapid entrapment of >60% 4-CP in 5 min, realizing an outstanding adsorption capacity (296 mg g^{-1}).

As a class of compound, imines play a critical role in the synthesis of nitrogen-bearing chemicals such as dyes and pharmaceuticals. Imines' actions can be described through the photocatalytic oxidative coupling of amine with an oxidative reagent upon light exposure to fulfill the requirements of green chemistry and resolve the global energy issue.[312] It makes no sense. A CdS@Nu-1000 heterojunction was prepared by Hou et al. in 2021 for high-efficiency photocatalytic oxidative coupling of amines (**Figure 32**). An improvement was detected in the photocatalytic activity of CdS@Nu-1000 which can be due to their wider photoresponse range, efficient carrier separation, and good decoupling of redox reactions. Such a drastic improvement in photocatalytic behavior can be due to the mesoporous channels, high surface area, and properly dispersed heterojunction.[313]

The rise in the use of nitrates has led to serious health hazards. The Environmental Protection Agency has determined the maximum allowable nitrate concentration in drinking water as 10 mg L^{-1}.[314] Choi et al. prepared an NU-1000-based catalyst containing iron thiolate clusters to photocatalytically reduce nitrate to a less toxic and more valuable product: ammonium NH^{4+}.[315]

5.7. Biomedical Applications

A thorough understanding of the interactions of biological molecules with materials can remarkably help in the expansion

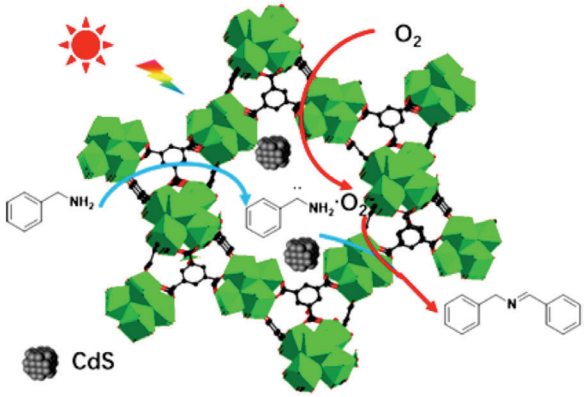

Figure 32. Photocatalytic oxidative coupling of amines under CdS@Nu-1000 nanoconposites. Reproduced with permission.[313] Copyright 2021, American Chemical Society.

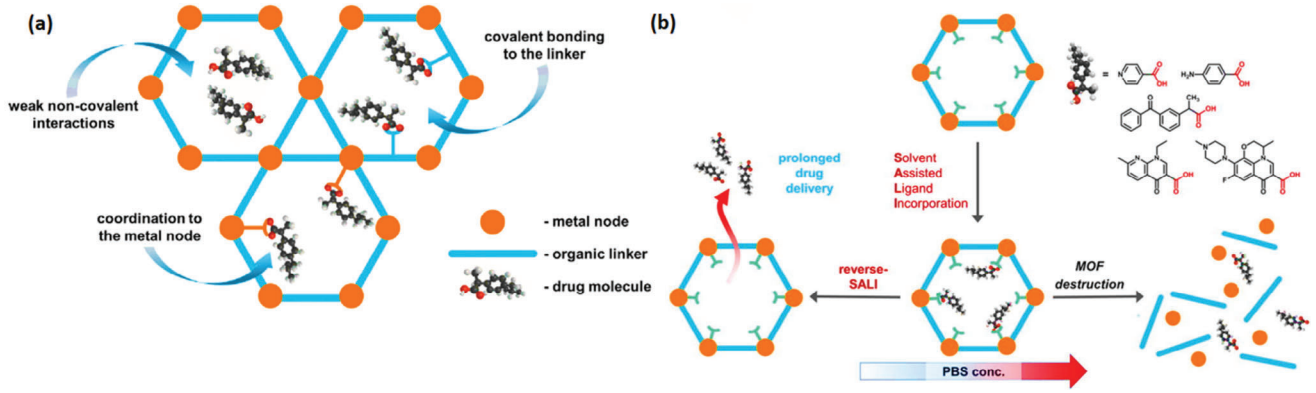

Figure 33. a) Strategies for drug encapsulation in MOFs and b) release routes of drug from guest@NU-1000 carrier. Reproduced with permission.[319] Copyright 2018, Elsevier.

and design of adsorbents for diverse applications.[316] In 2022, Loosen et al., considered various peptides to evaluate the nature of these interactions and determine factors involved in the peptides adsorption onto Zr-MOFs of various structures and surface features.[317] According to the experimental results, hydrophilicity affected the adsorption of peptides in the presence of Zr(IV) sites and linker nature in MOFs. Experimental investigations also revealed that in peptides protected at the C—N terminus, interactions of hydrophobicity and repulsion promoted the adsorption of NU-1000 with higher hydrophobic properties. Owing to their diversity in the amino acid chain and interactions such as sulfur, carboxylate, and M^{+}-π, they were effective in adsorption which can be mainly assigned to the nature of linkers and connectivity in the nodes.

Pang et al. substituted the H_4TBAPy ligand in NU-1000 with tetrakis(4-carboxyphenyl)porphyrin for photodynamic therapy applications through a post-synthetic modification route.[318] Owing to its less toxicity and good photodynamic behavior, the modified NU-1000 showed outstanding anti-tumor activity in vitro and in vivo. Bury et al. managed to anchor three carboxylate-containing model drugs in the pore of NU-1000: levofloxacin, ketoprofen, and nalidixic acid, i.e. guest@NU-1000 materials (**Figure 33**) using the SALI method. Their results indicated the stability of NU-1000 in phosphate concentrations of the blood plasma while releasing the drugs with no decomposition in the MOF framework. The drug release kinetics showed a strong dependence on the guest molecule size. The figure illustrates the pathways of drug encapsulation and drug release of guest@NU-1000.[319]

Chemotherapy is one of the gold-standard approaches in the treatment of cancers. Zhao et al. synthesized NU-1000 particles of diverse sizes by changing the type of solvent and content of the modulator.[320] The nanoscale NU-1000 systems managed to load ≈35 wt.% of DOX with a long release profile (over 2 weeks) attributable to its superior biocompatibility and large pores. The in vivo assessments have shown the benefits of NU-1000 as a carrier of chemotherapy drugs due to its extraordinary efficacy of antitumor activity.

The large pore size of NU-1000 promotes effective drug loading while controllable drug release is achievable through its instability in phosphate buffer saline (PBS).[321] To deliver Calcein, NU-901, and NU-1000 were used by Fairen-Jimenez et al.[322] Farha and colleagues also succeeded in protein delivery by NU-1000.[323] They also characterized the structural properties of these systems to evaluate their capability to enter host cells. NU-1000 serves as a host of the protein and their colloidal stability and cellular entry can be ascribed to their dense functionalization and oligonucleotide-rich surfaces. Insulin in comparison with native protein showed great loading and a ten-fold increment in cellular studies on the absorption (**Figure 34a**). NU-1000 also reported efficient uremic elimination from human serum albumin.[324] They assigned the large NU-1000 adsorption capacity to its robust adsorption sites of hydrophobic sandwiched by two ligands of pyrene and the OH^{-} and H_2O molecules on the clusters of NU-1000, which can establish H...H bonds with polar functional groups of the guest molecules. In human serum albumin, NU-1000 also removed almost all *p*-cresyl sulfates. Uremic toxins can bind to *p*-cresyl sulfates (Figure 34b). Howarth et al. showed the 56 mg g^{-1} adsorption capacity for aqueous sulfate using NU-1000. They observed no interference from competitive anions such as Cl^{-}, Br^{-}, I^{-}, and NO_3^{-}.[325]

Levodopa (LD) is an amino acid that acts as a precursor in the formation of several neurotransmitters. Sensitive and selective detection of LD is a vital issue in clinical samples.[326] Polypyrrole integration by post-synthetic methods on NU-1000 was reported by Biswas et al. which involved adsorption of pyrrole and subsequently oxidative polymerization to achieve PPy@NU-1000.[327] For LD detection, a modified glassy carbon electrode was prepared from PPy@NU-1000. The developed sensor showed high reproducibility, sensitivity, selectivity, and stability for LD detection in the presence of interfering species. Using HPLC, a great recovery was obtained in the range of 99.3-101.6% for the analysis of human serum.

As the final —OH group of NU-1000 may be functionalized with active metal ions or other functional groups, the use of NU-1000 in adsorption, catalysis, gas separation as well as sensing, can be employed by this feature.[51,70,169,219,322] Intercalating into DNA, the drug doxorubicin hydrochloride (also known as DOX), which is extensively used to treat cancer, prevents the generation of nucleic acids and, as a result, limits the production of cancer cells. There are many possible applications for NU-1000 in the biomedicine field.[321] Phosphate buffered saline (PBS) with its instability makes it ideal for regulated drug release, while the large pore size facilitates high-efficiency drug loading.[321]

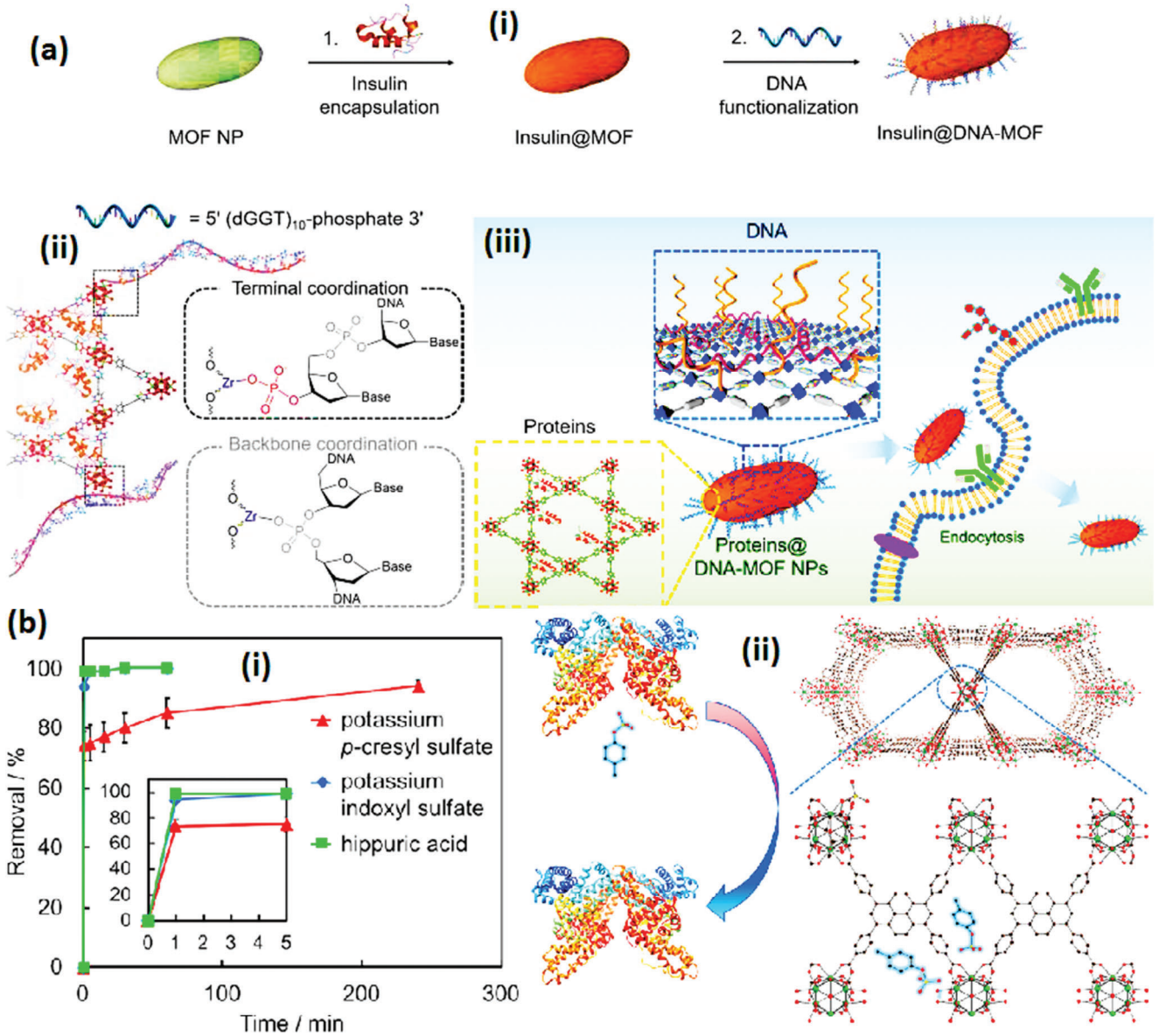

Figure 34. a) i) Encapsulation of insulin in NU-1000 channels along with functionalization of DNA surface, ii) DNA functionalization of insulin encapsulated NU-1000 nanoparticles, and iii) cellular uptake by insulin@DNA-NU-1000 nanoparticles. Reproduced with permission.[323] Copyright 2019, American Chemical Society. b) The removal efficiency of i) uremic toxins and ii) *p*-cresyl sulfate by hydrophobic adsorption sites of NU-1000. Reproduced with permission.[324] Copyright 2019, American Chemical Society.

Fairen-Jimenez and co-workers NU-1000 were used as calcein delivery carriers.[322] Delivering proteins was accomplished by Farha and colleagues using NU-1000.[323] In addition, they found that NU-1000 was able to eliminate uremic toxins from human serum albumin, according to their findings.[324] This drug delivery method for DOX was tested for its anticancer effects using produced NU-1000 nanoparticles as drug carriers. Finally, Zhao et al. reported that the solvent species changed to produce different-sized NU-1000 nanoparticles.[320] ND@PEG was tested in vivo for its anticancer effectiveness.[328,329] Mice that had tumors were given one of the following treatments: PBS (the control group), DOX, NU-1000, or ND@PEG (where ND stands for DOX@NU1000 and PEG refers to polyethylene glycol). Each group included a total of four mice. It was necessary to employ intratumoral injections to administer NU-1000 because of the unstable nature of the drug, and each group of mice was given two treatments throughout the course of the 14-day treatment period. The volumes of the tumors in the DOX and ND@PEG groups were significantly lower compared to those in the PBS and NU-1000 groups (**Figure 35**a–c). It was shown that ND@PEG-treated mice had the lowest growth rate of tumor out of the four groups, showing that the use of NU-1000 as a drug carrier boosted the therapeutic effect, which may be related to its high permeability, biocompatibility, dispersibility, and retention.[330] It was demonstrated that NU-1000 has strong in vivo biocompatibility since the body weight of the mice in each group rose to

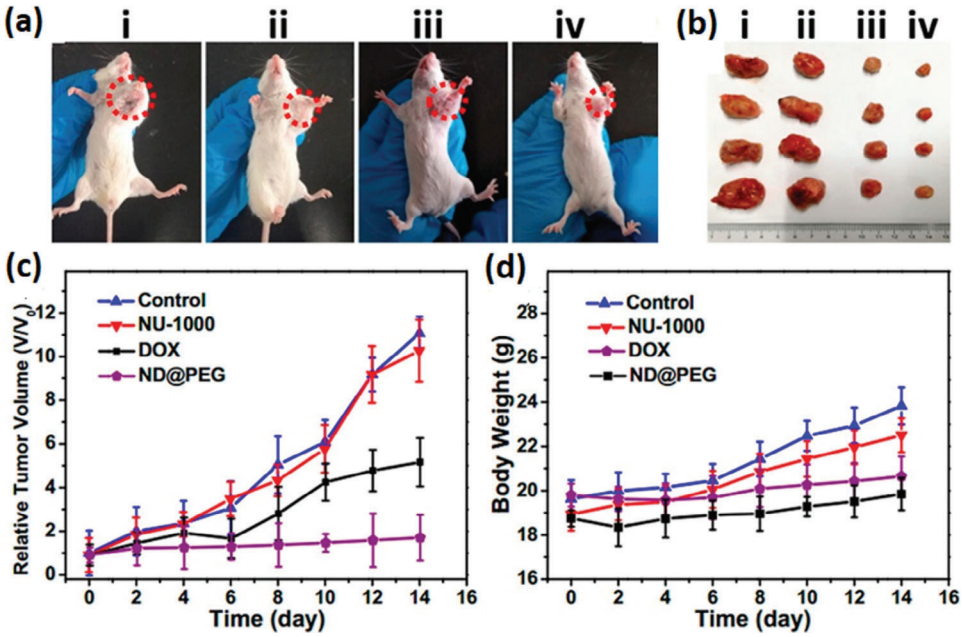

Figure 35. a) Images of mice, b) excised tumors: i) PBS (control), ii) NU-1000, iii) DOX, iv) ND@PEG. c) Relative tumor volume, d) mice body weight following PBS therapy, NU-1000, DOX, and ND@PEG treatment (a–d). Reproduced with permission.[320] Copyright 2019, American Chemical Society.

varied degrees, which corresponded to the tumor size in each group. (Figure 35d).

5.8. Magnetic Resonance

Owing to its superior spatiotemporal resolution, unlimited depth penetration, and desirable safety profile, magnetic resonance imaging (MRI) has been widely utilized as a biomedical imaging modality.[331] McLeod et al. prepared Gd(III)-functionalized NU-1000 materials to be applied as an MRI contrast agent.[330]

5.9. Removal of Metals

Industrial wastewater and domestic sewage may contain high levels of heavy metal ions, posing serious environmental risks.[332] Among different MOFs, Zr-MOFs have found extensive applications for removing the pollutants from H_2O because of their thermal stability and ability to preserve the structure in aqueous medium as a consequence of the robust interactions between the carboxylic ligands and the clusters of Zr^{4+}. Also, the modification sites for binding to the functional molecules can be provided by unsaturated nodes of Zr.[65] Also, by using solvent-assisted ligand incorporation, the different aromatic acids and carboxylic acids were incorporated into the NU-1000.[333] For the MOFs synthesis to increment the metal ions adsorption new strategies have been applied. Lin et al. applied a one-pot approach to preparing Zr-MOFsSH(O) by functionalized molecules and modulators of ALA (**Figure 36**, strategy 2). Accordingly, carboxyl and thiol groups can be employed as an alternative to modulators and also as functionalized molecules. In the course of the synthesis, the coordination of Zr^{4+} with SH occurs. For comparison, they also made the Zr-MOFsSH(O) by the post-synthetic modification (Zr-MOFs-SH(P), Figure 36, strategy 1). According to their findings, modified Zr-MOFs, PCN-224-MAA(P), exhibited 139 mg g^{-1} adsorption capacity, possibly because of the difficulties in the coordination of Zr^{4+} with the groups of SH. Thanks to its high mercapto group contents, modified ZrMOFs-SH(O) showed a greater adsorption capacity for Hg^{2+} ions compared to Zr-MOFs-SH(P).[334]

Sb(III) cation is another toxic metal ion whose toxicity is ≈ 10 times greater than Sb(V). Hence, an efficient remediation method for Sb^{+3} and Sb^{+5} oxyanions can ensure the safety of humans in Sb-polluted regions.[335] Chen et al. assessed seven types of Zr-MOFs and observed the high-efficiency removal capacity of NU-1000 for both Sb^{+3} (137 mg g^{-1}) and Sb^{+5} (288 mg g^{-1}) along with fast adsorption kinetics, much greater than the majority of previously reported antimony adsorbents.[336] The terminal hydroxyl groups on the fretworks of NU-1000 play an important role in the adsorption of Sb^{+3} or Sb^{+5} (**Figure 37**). The highest adsorption capacity of 259 mg g^{-1} was obtained for $Sb(OH)_6^-$ adsorption and extraction from H_2O by Rangwani et al. They also reported the interaction of $Sb(OH)_6^-$ with the nodes of Zr_6 in NU-1000. Moreover, an increment in the content of adsorbed ions reinforced the analyte-node interactions.[337]

Selenite (SeO_3^{2-}) and selenate (SeO_4^{2-}) are natural species whose trace levels are vital for humans.[338] Given the possible danger of elevated levels of selenium, the U.S. Environmental Protection Agency (EPA) has declared the highest acceptable level of selenium in drinking water (50 ppb). Howarth and coworkers examined the adsorption and removal capacity of several Zr-MOFs for selenite and selenate anions in aqueous media. Accordingly, NU-1000 showed the fastest uptake rates and the highest adsorption capacity for both selenite and selenate ions which

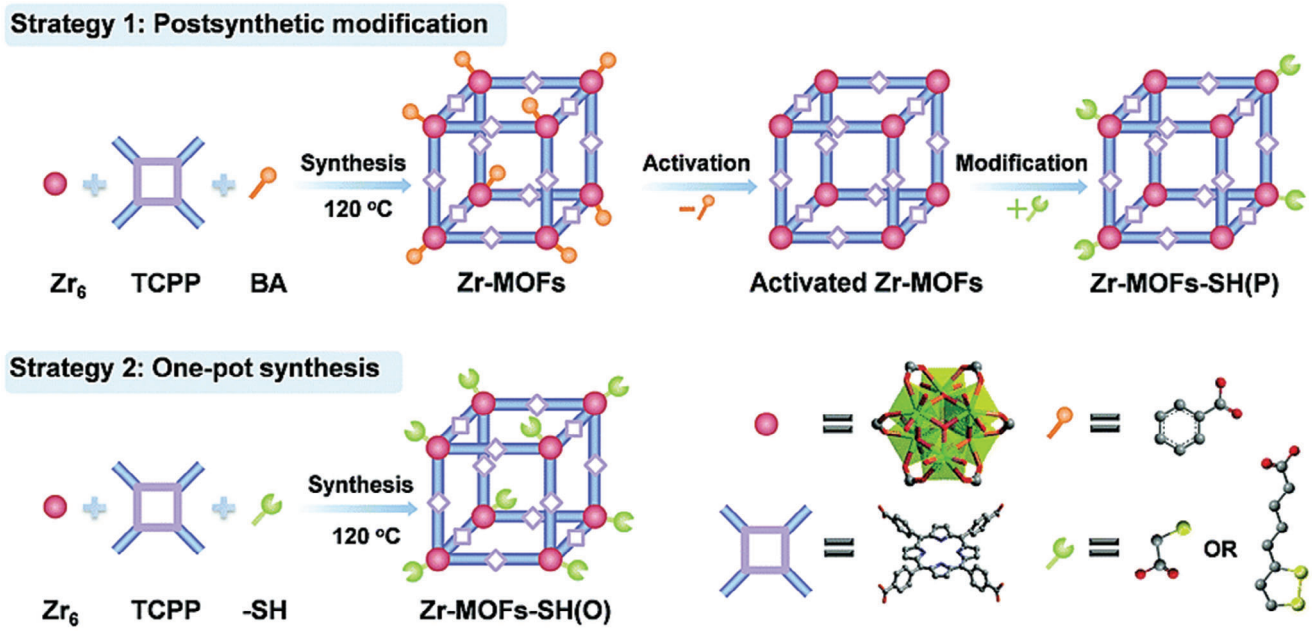

Figure 36. Two strategies for synthesis of Zr-MOFsSH(O) via 1) the postsynthetic modification and 2) the one-pot synthesis. Reproduced with permission.[334] Copyright 2019, Royal Society of Chemistry.

could be assigned to the higher adsorption sites and the node in a bridging (η^2-μ_2) fashion of NU-1000.[339]

Dichromate ($Cr_2O_7^{2-}$) is a common contaminant in industrial effluents. Lin et al. probed the ability of six MOFs with high stability in aqueous solutions with large surface areas to adsorb and separate $Cr_2O_7^{2-}$.[340] Their findings revealed the efficiency of NU-1000 as a photoluminescent sensor of $Cr_2O_7^{2-}$ with a vast linear range (1.8–340 μM) and a low detection limit (1.8 μM) in aqueous environments.

Uranium accumulation in mine drainage and acidic wastewater of nuclear fuel cycles line radioactive liquid waste as another toxic metal ion.[341] An effective uranium recovery method is a demanding challenge due to the high acidity and radioactivity as well as complicated coexisting fission nuclide elements in the mentioned liquid wastes.[342] In 2021, Zhang et al. prepared phosphine oxide architectures confined in the pores of Nu-1000 to bind with uranium in strong HNO_3 environments.[343] Their system showed a great uranium adsorption capacity (80 mg g^{-1} in 1 M HNO_3) with abundant ligand sites and ultrafast sorption rates.

5.10. Removal of Organic Compounds

The wastewater pollutants must be efficiently managed as they are continuously released into limited freshwater resources, posing serious threats to the terrestrial, aquatic, and aerial flora and fauna.[344] Organic arsenic acids (OAAs) must be removed from

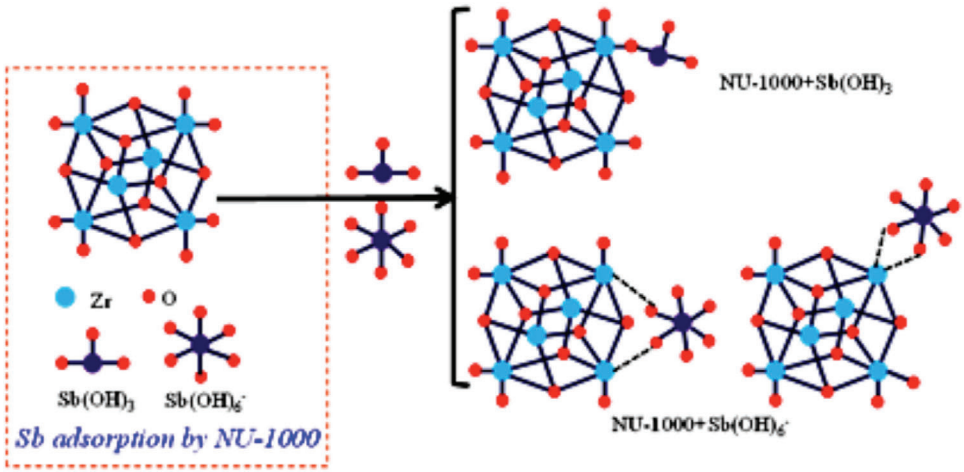

Figure 37. Presentation of Sb^{+3} and Sb^{+5} binding modes to the NU-1000 nodes. Reproduced with permission.[336] Copyright 2017, American Chemical Society.

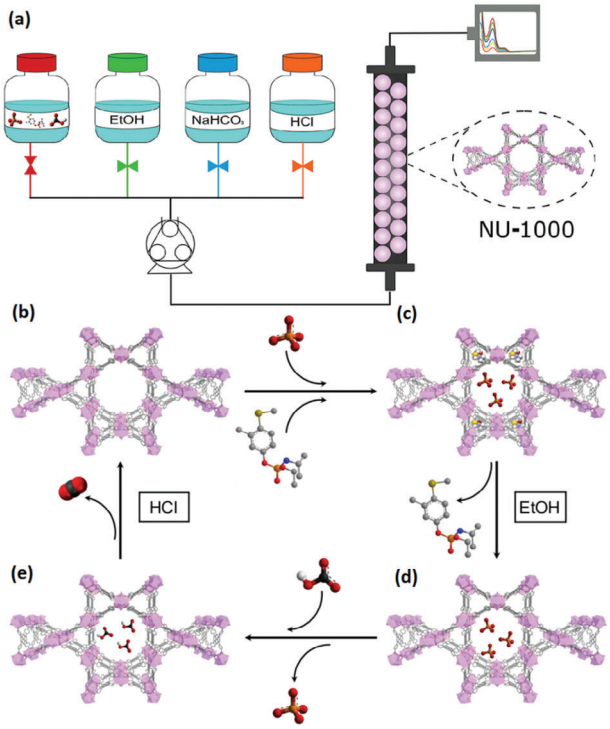

Figure 38. a) The experimental setup for the dynamic studies by NU-1000 loaded HPLC column, a) methodology for the reversible and selective capturing of fenamiphos and phosphate and their recovery, b) The simultaneous adsorption procedure, c) Fenamiphos desorption with ethanol, d) ion exchange of phosphate with HCO_3^-, and e) Reproduction of NU-1000 by treatment with HCl. Reproduced with permission.[347] Copyright 2021, Elsevier.

water due to their capability to form toxic inorganic arsenic compounds via biotic and abiotic degradations.[345] Lin and colleagues evaluated the adsorptive removal ability of 7 Zr-MOFs for several OAAs models such as roxarsone (ROX) and *p*-arsanilic acid (ASA) in an aqueous medium. According to their results, coordination interactions between the sample and ASA are dominant forces, while the synergistic impact of the electrostatic, hydrogen bonds, and $\pi-\pi$ interactions governed the adsorption of ASA on Zr-MOFs. The mild structural differences in Zr-MOFs explain their different adsorptive removal trends.[346] Maldonado et al. explored the efficiency of NU-1000 in adsorbing two P-based water pollutants: organophosphorus pesticides such as fenamiphos and phosphate in aqueous environments.[347] They designed a three-step strategy for fenamiphos and phosphate anions separate quantitative recovery and secret adsorbent regeneration (**Figure 38**).

Atrazine is a water pollutant whose extensive application, persistency, and environmental mobility have led to the contamination of surface and groundwater resources.[348] Akpinar et.al examined different Zr-MOFs with diverse pore sizes, framework topologies, linker π-system sizes, and chemical functionality to reach the highest atrazine removal with the highest rate. They observed the maximum capacity in NU-1000 within 1 min possibly because of its large pores and the abundant $\pi-\pi$ interaction sites at the linkers based on pyrene.[58]

Per- and polyfluoroalkyl substances (PFASs) are members of a new class of toxic contaminants whose bioaccumulation and persistent nature pose serious hazards.[349] In 2021, Li et al. systematically evaluated the acid adsorption of perfluoroalkyl compounds and reported NU-1000 as an efficient PFAS sorbent in aqueous environments with adsorption capacity as high as 620 mg g^{-1}.[350] Accordingly, the adsorption of PFAS is governed by ionic interactions with the eight-connected NU-1000 nodes. A series of mesoporous MOFs was examined by Zheng et al. for the adsorption of R134a (CH_2FCF_3) fluorocarbon. They observed extraordinary fluorocarbon uptake of ≈170 wt.% for NU-1000 (almost saturation). They also assessed fluorocarbon adsorption based on morphology or topology of pores and expressed that pore volume and surface area alone cannot be a proper measure. Enhanced R134a adsorption capability was recorded in the hierarchical structures encompassing a combination of meso and microporous channels.[351]

Polycyclic aromatic hydrocarbons (PAHs) arise from the incomplete combustion of organic matter.[352] As one of the main pollutants, PAHs have adverse effects on the ecosystem and humans.[353] Ning et al. evaluated several tetraphenyl-pyrene-based MOFs (NU-1000, NU-901, and ROD-7) for fluorescent detection of PAHs. Only NU-1000 exhibited fluorescent responses to acenaphthylene, pyrene, and fluoranthene in the form of quenching, enhancement with redshift, and enhancement with blueshift, respectively. The emissions of NU-901 and ROD-7, however, revealed no variations upon exposure to the tested PAHs. The distinct fluorescent response of these MOFs can be attributed to the variation of their excited energies due to their diverse framework topologies which determine the thermodynamic feasibility of response processes.[354]

As a broad-spectrum herbicide, glyphosate can harm human cells.[355] Different sizes of UiO-67 and NU-1000 were prepared by Pankajakshan et al. (from nanometer to micrometer) to examine their potential in eliminating glyphosate from aqueous environments. According to their findings, Zr_6 clusters have the potential for specific adsorption due to the presence of hydroxyl groups and terminal water as active sites. Glyphosate had stronger interactions with NU-1000 attributable to lower distance of Zr···O− P and its great adsorption energy. Such an increase in NU-1000 capacity and rate of adsorption could be ascribed to the increment in the external surface area and the decrement of the diffusion barrier.[59]

In another study, Yu et al. assessed three Zr-MOFs (NU-1000, MOF-525, and UiO-66) with high stability in aqueous medium with various topologies and size of pores to remove tetracycline.[356] The best adsorption rate was recorded for NU-1000. The pore nature and topology drastically influenced the adsorption activity of MOFs. They also reported that MOFs with *csq* topology possess a better mass transfer, leading to an augmented adsorption rate.

5.11. Luminescence in Nu-1000

Luminescent materials due to their superiorities over probes based on solution have been extensively utilized for bio-/chemosensing.[357] Luminescent materials are stable and portable, and non-invasive while providing real-time detection, tunable shape

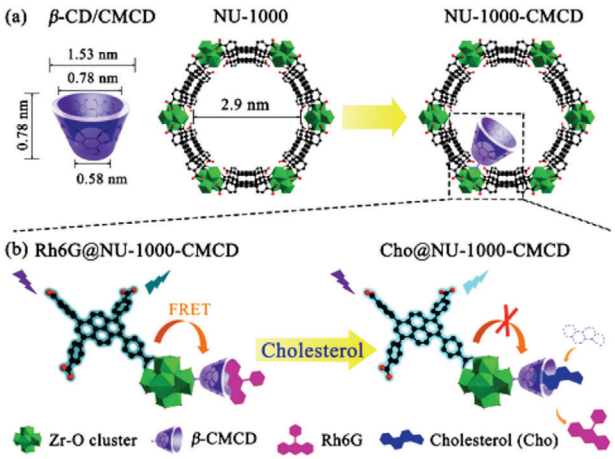

Figure 39. a) Dimensional and structural parameters of NU-1000, β-CD/CMCD, and NU-1000-CMCD. b) The schematically sensing mechanism of Rh6G@NU-1000-CMCD for the CDHS with carboxymethyl b-cyclodextrin as the recognition sites. Reproduced with permission.[359] Copyright 2019, Royal Society of Chemistry.

and size, and recyclability. Additionally, Lu et al. described selective and sensitive detection for various chemical/biological species through the use of functional materials and common luminophores assembly or special luminophores with a recognition moiety.[358] An efficient and accurate solution to check the cholesterol level in human serum is highly essential since cholesterol is responsible for vital tasks as a lipid. In cellular membranes cholesterol maintains fluidity and structural integrity; it also serves as a precursor in the biosynthesis of steroids and bile acids. Gong et al. fabricated a substitution-type luminescent NU-1000 probe for fast and precise CDHS samples.[359] They used carboxymethyl-cyclodextrin (β-CMCD) as a bridge of FRET and a substitution entrapper for the CDHS (**Figure 39**). Rh_6G@NU-1000-CMCD with open structure facilitated the diffusion of cholesterol across the framework, hence, decrement the LOD to 0.4 μM while broadening the linear range. Owing to its superior structural stability and intense fluorescence signal, the developed system offered the possibility of cholesterol detection with proper repeatability and reliability.

It is also possible to gain information about the structure between polymer and filler at the MOF-polymer interface by changing optical signals after excitation in mixed-matrix membranes. This approach provides a novel strategy to obtain information about interspecies interactions.[360,361] In 2022, Wang et al. prepared high-performance mixed-matrix membranes for high-speed visible-light communication by combining various luminescent NU-1000−polymers with unique photoluminescent behavior and strong spectral overlap.[362] Their results offered a suitable approach to designing high-speed visible-light communication in addition to promoting mixed-matrix membranes for novel applications.

As a urinary metabolite of PAHs, 1-hydroxypyrene can be used as a biomarker in the detection of human intoxication of PAH carcinogens.[363] A sensitive simple 1-hydroxypyrene sensor with a fast response is highly favorable. Zhou et.al studied the microcrystalline NU-1000 sensitivity with fluorescent pyrene cores for urinary 1-hydroxypyrene luminescent detection. The NU-1000 pyrene core operates as the converter of signal and significantly quenches luminescence upon exposure to 1-hydroxypyrene due to the impressive transfer of charge between cores of pyrene and highly conjugated 1-hydroxypyrene via $\pi-\pi$ interactions. Additionally, the pore confinement impacts on channel size of NU-1000 facilitates the preconcentration of 1-hydroxypyrene, facilitating the contact of 1-hydroxypyrene with NU-1000, thus, increasing the efficiency of detection.[364]

6. Outlook and Perspectives

Environmental pollution and energy shortage are two vital issues of today's world and have been attracting the attention of researchers throughout the globe. The significance of the energy crisis is continuously increasing with the population growth and industrialization of societies. In this regard, the enlargement of more advanced techniques with high efficiency and high durability compounds sounds crucial. Zr-MOFs are one of these materials. Thanks to its structural flexibility, high stability, and interesting performance, Zr-MOF has found significance. To understand the performance of Zr-MOFs, important challenges such as porosity control, composition, and topological and crystalline structures have to be addressed. Its diverse clusters and linkers promote its stability and structural adjustability, making it suitable for specific applications. According to the literature, five types of clusters have been reported for Zr-MOFs including Zr_6O_8, Zr_8O_6, ZrO_6, ZrO_7, and ZrO_8. NU-1000 is one of the members of this group of MOFs classified as large pore Zr_6-based MOFs which can serve as a template for special applications. Owing to its high stability (chemical and thermal), NU-1000 is predicted to encompass four anionic hydroxo ligand terminals attached to $Zr_6(\mu_3{-}O)_4(\mu_3{-}OH)_4(H_2O)_4(OH)_4$ clusters to facilitate various reactions. This review addressed the details of advancements made in the modification of the NU-1000 structure to create unique features for various energy- and environment-related purposes. NU-1000 can serve as a proper carrier for various reactions beyond the laboratory scale due to 1) accessibility of hydroxyl/water ligands on the nodes in the NU-1000 structure which can easily combine with the target material promoting the removal of various organic or metallic pollutants, 2) in photo/electrocatalytic applications, the presence of large mesoporous channels can facilitate the diffusion of the electrolyte ions to form a strong bond between the substrate and catalyst which can efficiently affect the performance of the material, 3) high stability under various parameters of reaction with the possibility of reusing the catalyst with no notable loss of activity, and 4) due to the high specific surface area of NU-1000, its abundant active sites are more accessible; moreover, its structural adjustability can promote synergistic effect between the catalytic centers, further affecting the performance of the catalyst. Furthermore, due to the possibility of functionalization of the cluster and linkers, it can serve as an electrode or provide special light-affected activities. Structurally, NU-1000 could be an ideal template for diverse applications, making it an effective and efficient choice. This review summarizes the studies on NU-1000 and provides a comprehensive discussion of the structure and properties of NU-1000 with some promising strategies to foster further improvements in future research. Concerning its synthesis, various synthesis strategies of NU-1000 are discussed including

post-synthetic modifications, isoreticular expansion, modulated synthesis, and topology-based design. Regarding the ongoing advancements in this field, NU-1000 structures with various types of SBUs will emerge in the years to come. By designing and introducing novel ligands, various types of Zr-MOFs can be developed, leading to the ever-increasing growth of the members of this family of MOFs with unique properties, further promoting their applications. Despite these predictions, these strategies are developed based on trial and error and a deep understanding of their mechanisms requires a long time; thus, no definite comment can be made now. Therefore, further research in this field is highly justified. Due to the excellent and unique structural properties of NU-1000 including high porosity and ideal stability, researchers are studying this high-potential material for diverse applications including drug delivery, gas separation and adsorption, electrochemistry, photochemistry, fluorescence sensing, catalysis, and many other applications. Zr-MOFs, including NU-1000, are at the beginning of their development journey compared to other types of MOFs including Cu-MOFs, Cr-MOFs, Al-MOFs, Zn-MOFs, and ZIFs. This group of materials dominates MOFs due to their stability and unique structure. Moreover, scalable synthesis of NU-1000 is possible by green and cost-effective methods with ideal repeatability and performance, day-by-day progress is also observed in this field. The mentioned advancements have led to the mass production of NU-1000 with desirable and ideal stability, stating the high potential for various commercial applications. A huge step forward in the application of MOFs occurs when these materials gain a special position in practical applications.

7. Opportunities and Challenges

Advancements in the applications of NU-1000 require extensive research and attempts. Several major challenges should be also overcome to achieve this goal. Some of the challenges are listed below:

1) Despite the extensive applications of NU-1000, the studies on the different aspects of these applications are not balanced and these studies are mainly focused on the environment and energy. Moreover, the overall performance of NU-1000 in practical applications is not understandable.
2) Preparation of catalysts and electrode materials based on NU-1000 for energy purposes, innovative, economic, and efficient approaches are required to shift their production from lab scale to practical scale.
3) Computational simulations and advanced characterizations are required for a deeper understanding of the relationship between structure and activity in NU-1000 for energy-related applications.
4) The electrocatalytic performance of NU-1000 in most of the reports was on a laboratory scale and their current industrial scale was not investigated.
5) Experimental and computational investigations are of crucial significance in the understanding of the unique role of NU-1000 in electrocatalytic reactions and the design of efficient electrocatalysts in the future.
6) The poor conductivity of NU-1000 is one of the main challenges in its application as an electrocatalyst or electrode material for energy purposes which can limit its applications.
7) Computational studies on the electrocatalytic performance of NU-1000 are very rare. Future works in this field can further clarify the performance of this material as an electrocatalyst.
8) NU-1000 has not been employed in all energy and environment applications. By further elucidation of different aspects of this material, its application can be developed in these fields as well.
9) The biomedical applications of these materials are challenged by the side effects arising from the accumulated system by the passage of time which can be resolved by the efficient designs to decline the accumulations in future studies.

In the end, we hope that this review motivates and encourages researchers to further studies with more attractive ideas to find diverse applications for these unique materials. These attempts should be directed to further add to the applications of these materials and promote the industrialization of this valuable class of materials.

Acknowledgements

This work was supported by the University of Maragheh, Iran's National Elites Foundation, and Iran National Science Foundation (project number: 4025093). The authors were also grateful for the financial support. Majed A. Bajaber expresses their appreciation to the Deanship of Scientific Research at King Khalid University, Saudi Arabia, for funding this work through a research group program under grant number RGP. 2/428/44. [Correction added on April 11, 2024, after first online publication: Affiliations were corrected.]

Open access publishing facilitated by Queensland University of Technology, as part of the Wiley - Queensland University of Technology agreement via the Council of Australian University Librarians.

Conflict of Interest

The authors declare no conflict of interest.

Keywords

advanced materials, functional applications, micro-/meso-poros unique structureity, Zr-Metal–organic frameworks

Received: July 26, 2023
Revised: November 8, 2023
Published online: November 23, 2023

[1] X. Luo, R. Abazari, M. Tahir, W. K. Fan, A. Kumar, T. Kalhorizadeh, A. M. Kirillov, A. R. Amani-Ghadim, J. Chen, Y. Zhou, *Coord. Chem. Rev.* **2022**, *461*, 214505.
[2] S. Sanati, A. Morsali, H. García, *Energy Environ. Sci.* **2022**, *15*, 3119.
[3] H. R. Lim, H. S. Kim, R. Qazi, Y. T. Kwon, J. W. Jeong, W. H. Yeo, *Adv. Mater.* **2020**, *32*, 1901924.
[4] G. Zhang, D. Chen, N. Li, Q. Xu, H. Li, J. He, J. Lu, *Angew. Chem., Int. Ed.* **2020**, *132*, 8332.
[5] X. Pu, H. Wang, D. Zhao, H. Yang, X. Ai, S. Cao, Z. Chen, Y. Cao, *Small* **2019**, *15*, 1805427.

[6] D. P. Dubal, O. Ayyad, V. Ruiz, P. Gomez-Romero, *Chem. Soc. Rev.* **2015**, *44*, 1777.
[7] N. Uddin, H. Zhang, Y. Du, G. Jia, S. Wang, Z. Yin, *Adv. Mater.* **2020**, *32*, 1905739.
[8] Y. Chen, M. Cheng, C. Lai, Z. Wei, G. Zhang, L. Li, C. Tang, L. Du, G. Wang, H. Liu, *Small* **2023**, *19*, 2205902.
[9] Y. S. Yu, X. Zhang, J. W. Liu, Y. Lee, X. S. Li, *Energy Environ. Sci.* **2021**, *14*, 5611.
[10] E. Gong, S. Ali, C. B. Hiragond, H. S. Kim, N. S. Powar, D. Kim, H. Kim, S. I. In, *Energy Environ. Sci.* **2022**, *15*, 880.
[11] A. Khandelwal, D. Maarisetty, S. S. Baral, *Renewable Sustainable Energy Rev.* **2022**, *167*, 112693.
[12] X. Ge, C. Gu, X. Wang, J. Tu, *J. Mater. Chem. A* **2017**, *5*, 8209.
[13] A. M. Tokmachev, D. V. Averyanov, I. A. Karateev, I. S. Sokolov, O. E. Parfenov, V. G. Storchak, *Adv. Funct. Mater.* **2020**, *30*, 2002691.
[14] S. K. Yadav, G. K. Grandhi, D. P. Dubal, J. C. de Mello, M. Otyepka, R. Zbořil, R. A. Fischer, K. Jayaramulu, *Small* **2020**, *16*, 2004891.
[15] Y. Hu, R. Abazari, S. Sanati, M. Nadafan, C. L. Carpenter-Warren, A. M. Z. Slawin, Y. Zhou, A. M. Kirillov, *ACS Appl. Mater. Interfaces* **2023**, *15*, 37300.
[16] J. Wang, R. Abazari, S. Sanati, A. Ejsmont, J. Goscianska, Y. Zhou, D. P. Dubal, *Small* **2023**, *19*, 2300673.
[17] Y. Zhou, R. Abazari, J. Chen, M. Tahir, A. Kumar, R. R. Ikreedeegh, E. Rani, H. Singh, A. M. Kirillov, *Coord. Chem. Rev.* **2022**, *451*, 214264.
[18] Z. Lei, Y. Xue, W. Chen, W. Qiu, Y. Zhang, S. Horike, L. Tang, *Adv. Energy Mater.* **2018**, *8*, 1801587.
[19] S. Sanati, R. Abazari, J. Albero, A. Morsali, H. García, Z. Liang, R. Zou, *Angew. Chem., Int. Ed.* **2021**, *60*, 11048.
[20] S. K. Yadav, G. K. Grandhi, D. P. Dubal, J. C. de Mello, M. Otyepka, R. Zbořil, R. A. Fischer, K. Jayaramulu, *Small* **2020**, *16*, 2004891.
[21] Y. Pan, S. Sanati, R. Abazari, V. Navvar Noveiri, J. Gao, A. M Kirillov, *Inorg. Chem.* **2022**, *61*, 20913.
[22] R. Pétuya, S. Durdy, D. Antypov, M. W. Gaultois, N. G. Berry, G. R. Darling, A. P. Katsoulidis, M. S. Dyer, M. J. Rosseinsky, *Angew. Chem., Int. Ed.* **2022**, *61*, e202114573.
[23] S. Yuan, L. Zou, J. S. Qin, J. Li, L. Huang, L. Feng, X. Wang, M. Bosch, A. Alsalme, T. Cagin, *Nat. Commun.* **2017**, *8*, 1.
[24] R. Abazari, A. R. Amani-Ghadim, A. M. Z. Slawin, C. L. Carpenter-Warren, A. M. Kirillov, *Inorg. Chem.* **2022**, *61*, 9514.
[25] M. Yuan, J. Chen, H. Zhang, Q. Li, L. Zhou, C. Yang, R. Liu, Z. Liu, S. Zhang, G. Zhang, *Energy Environ. Sci.* **2022**, *15*, 2084.
[26] R. Abazari, S. Sanati, A. Morsali, *Inorg. Chem.* **2022**, *61*, 3396.
[27] Z. Wang, J. H. Zhang, J. J. Jiang, H. P. Wang, Z. W. Wei, X. Zhu, M. Pan, C. Y. Su, *J. Mater. Chem. A* **2018**, *6*, 17698.
[28] K. Kang, L. Li, M. Zhang, X. Zhang, L. Lei, C. Xiao, *Inorg. Chem.* **2021**, *60*, 16420.
[29] N. Al Amery, H. R. Abid, S. Al-Saadi, S. Wang, S. Liu, *Mater. Today Chem.* **2020**, *17*, 100343.
[30] Y. Pan, S. Sanati, M. Nadafan, R. Abazari, J. Gao, A. M. Kirillov, *Inorg. Chem.* **2022**, *61*, 18873.
[31] K. Jayaramulu, M. Horn, A. Schneemann, H. Saini, A. Bakandritsos, V. Ranc, M. Petr, V. Stavila, C. Narayana, B. Scheibe, Š. Kment, M. Otyepka, N. Motta, D. Dubal, R. Zbořil, R. A. Fischer, *Adv. Mater.* **2021**, *33*, 2004560.
[32] T. Kalhorizadeh, B. Dahrazma, R. Zarghami, S. Mirzababaei, A. M. Kirillov, R. Abazari, *New J. Chem.* **2022**, *46*, 9440.
[33] R. Abazari, E. Yazdani, M. Nadafan, A. M. Kirillov, J. Gao, A. M. Z. Slawin, C. L. Carpenter-Warren, *Inorg. Chem.* **2021**, *60*, 9700.
[34] R. Abazari, G. Salehi, A. R. Mahjoub, *Ultrason. Sonochem.* **2018**, *46*, 59.
[35] Y. Li, Y. Xu, W. Yang, W. Shen, H. Xue, H. Pang, *Small* **2018**, *14*, 1704435.
[36] Y. Pan, R. Abazari, J. Yao, J. Gao, *J. Phys. Energy* **2021**, *3*, 032010.
[37] Y. Zhang, H. Liu, F. Gao, X. Tan, Y. Cai, B. Hu, Q. Huang, M. Fang, X. Wang, *EnergyChem* **2022**, *4*, 100078.
[38] X. Li, R. Zhou, Z. Wang, M. Zhang, T. He, *J. Mater. Chem. A* **2022**, *10*, 1642.
[39] H. Peng, W. Xiong, Z. Yang, Z. Xu, J. Cao, M. Jia, Y. Xiang, *J. Hazard. Mater.* **2022**, *432*, 128684.
[40] M. Moayed Mohseni, M. Jouyandeh, S. Mohammad Sajadi, A. Hejna, S. Habibzadeh, A. Mohaddespour, N. Rabiee, H. Daneshgar, O. Akhavan, M. Asadnia, M. Rabiee, S. Ramakrishna, R. Luque, M. Reza Saeb, *Chem. Eng. J.* **2022**, *449*, 137700.
[41] N. Rabiee, M. Atarod, M. Tavakolizadeh, S. Asgari, M. Rezaei, O. Akhavan, A. Pourjavadi, M. Jouyandeh, E. C. Lima, A. Hamed Mashhadzadeh, A. Ehsani, S. Ahmadi, M. R. Saeb, *Microporous Mesoporous Mater.* **2022**, *335*, 111670.
[42] V. Guillerm, M. Eddaoudi, *Acc. Chem. Res.* **2021**, *54*, 3298.
[43] Z. Chen, H. Jiang, M. Li, M. O'Keeffe, M. Eddaoudi, *Chem. Rev.* **2020**, *120*, 8039.
[44] Z. Chen, P. Li, X. Zhang, M. R. Mian, X. Wang, P. Li, Z. Liu, M. O'Keeffe, J. F. Stoddart, O. K. Farha, *Nano Res.* **2021**, *14*, 376.
[45] Z. Chen, K. O. Kirlikovali, P. Li, O. K. Farha, *Acc. Chem. Res.* **2022**, *55*, 579.
[46] P. K. Chattaraj, H. Lee, R. G. Parr, *J. Am. Chem. Soc.* **1991**,*113*, 1855.
[47] A. Demessence, D. M. D'Alessandro, M. L. Foo, J. R. Long, *J. Am. Chem. Soc.* **2009**, *131*, 8784.
[48] J. P. Zhang, A. X. Zhu, R. B. Lin, X. L. Qi, X. M. Chen, *Adv. Mater.* **2011**, *23*, 1268.
[49] P. Ji, J. B. Solomon, Z. Lin, A. M. Wilders, R. F. Jordan, W. Lin, *J. Am. Chem. Soc.* **2017**, *139*, 11325.
[50] T. He, X. Xu, B. Ni, H. Wang, Y. Long, W. Hu, X. Wang, *Nanoscale* **2017**, *9*, 19209.
[51] H.-Q. Zheng, Y.-N. Zeng, J. Chen, R.-G. Lin, W.-E. Zhuang, R. Cao, Z.-J. Lin, *Inorg. Chem.* **2019**, *58*, 6983.
[52] Y. Yang, Z. Niu, H. Li, Y. Ma, Y. Zhang, H. Wang, *Dalton Trans.* **2018**, *47*, 6538.
[53] V. Bon, I. Senkovska, M. S. Weiss, S. Kaskel, *CrystEngComm* **2013**, *15*, 9572.
[54] M. Nakhaei, K. Akhbari, A. Davoodi, *CrystEngComm* **2021**, *23*, 8538.
[55] M. J. Katz, Z. J. Brown, Y. J. Colon, P. W. Siu, K. A. Scheidt, R. Q. Snurr, J. T. Hupp, O. K. Farha, *Chem. Commun.* **2013**, *49*, 9449.
[56] F. P. Kinik, A. O. Guerrero, D. Ongari, C. P. Ireland, B. Smit, *Chem. Soc. Rev.* **2021**, *50*, 3143.
[57] L. Yang, P. Cai, L. Zhang, X. Xu, A. A. Yakovenko, Q. Wang, J. Pang, S. Yuan, X. Zou, N. Huang, Z. Huang, H. C. Zhou, *J. Am. Chem. Soc.* **2021**, *143*, 12129.
[58] I. Akpinar, R. J. Drout, T. Islamoglu, S. Kato, J. Lyu, O. K. Farha, *ACS Appl. Mater. Interfaces* **2019**, *11*, 6097.
[59] A. Pankajakshan, M. Sinha, A. A. Ojha, S. Mandal, *ACS Omega* **2018**, *3*, 7832.
[60] J. E. Mondloch, M. J. Katz, W. C. Isley Iii, P. Ghosh, P. Liao, W. Bury, G. W. Wagner, M. G. Hall, J. B. DeCoste, G. W. Peterson, R. Q. Snurr, C. J. Cramer, J. T. Hupp, O. K. Farha, *Nat. Mater.* **2015**, *14*, 512.
[61] Y. Liu, S. Y. Moon, J. T. Hupp, O. K. Farha, *ACS Nano* **2015**, *9*, 12358.
[62] Y. Dong, J. Zhang, Y. Yang, J. Wang, B. Hu, W. Wang, W. Cao, S. Gai, D. Xia, K. Lin, R. Fan, *Nano Energy* **2022**, *97*, 107184.
[63] Y. Bai, Y. Dou, L. H. Xie, W. Rutledge, J. R. Li, H. C. Zhou, *Chem. Soc. Rev.* **2016**, *45*, 2327.
[64] N. Yuan, X. Gong, W. Sun, C. Yu, *Chemosphere* **2021**, *267*, 128863.
[65] Q. Du, R. Rao, F. Bi, Y. Yang, W. Zhang, Y. Yang, N. Liu, X. Zhang, *Surf. Interfaces* **2022**, *28*, 101647.
[66] K. Ahmad, M. A. Nazir, A. K. Qureshi, E. Hussain, T. Najam, M. S. Javed, S. S. A. Shah, M. K. Tufail, S. Hussain, N. A. Khan, H. U. R. Shah, M. Ashfaq, *Mater. Sci. Eng. B* **2020**, *262*, 114766.
[67] T. C. Wang, N. A. Vermeulen, I. S. Kim, A. B. F. Martinson, J. F. Stoddart, J. T. Hupp, O. K. Farha, *Nat. Protoc.* **2016**, *11*, 149.

[68] J. H. Cavka, S. Jakobsen, U. Olsbye, N. Guillou, C. Lamberti, S. Bordiga, K. P. Lillerud, *J. Am. Chem. Soc.* **2008**, *130*, 13850.
[69] H. Noh, C. W. Kung, K.-i. Otake, A. W. Peters, Z. Li, Y. Liao, X. Gong, O. K. Farha, J. T. Hupp, *ACS Catal.* **2018**, *8*, 9848.
[70] J. E. Mondloch, W. Bury, D. Fairen-Jimenez, S. Kwon, E. J. DeMarco, M. H. Weston, A. A. Sarjeant, S. T. Nguyen, P. C. Stair, R. Q. Snurr, O. K. Farha, J. T. Hupp, *J. Am. Chem. Soc.* **2013**, *135*, 10294.
[71] S. P. Desai, J. Ye, J. Zheng, M. S. Ferrandon, T. E. Webber, A. E. Platero-Prats, J. Duan, P. Garcia-Holley, D. M. Camaioni, K. W. Chapman, M. Delferro, O. K. Farha, J. L. Fulton, L. Gagliardi, J. A. Lercher, R. L. Penn, A. Stein, C. C. Lu, *J. Am. Chem. Soc.* **2018**, *140*, 15309.
[72] I. Hod, P. Deria, W. Bury, J. E. Mondloch, C. W. Kung, M. So, M. D. Sampson, A. W. Peters, C. P. Kubiak, O. K. Farha, J. T. Hupp, *Nat. Commun.* **2015**, *6*, 1.
[73] G. Yilmaz, K. M. Yam, C. Zhang, H. J. Fan, G. W. Ho, *Adv. Mater.* **2017**, *29*, 1606814.
[74] Z. Lu, R. Wang, Y. Liao, O. K. Farha, W. Bi, T. R. Sheridan, K. Zhang, J. Duan, J. Liu, J. T. Hupp, *Chem. Commun.* **2021**, *57*, 3571.
[75] P. Deria, D. A. Gómez-Gualdrón, I. Hod, R. Q. Snurr, J. T. Hupp, O. K. Farha, *J. Am. Chem. Soc.* **2016**, *138*, 14449.
[76] D. Feng, Z. Y. Gu, Y. P. Chen, J. Park, Z. Wei, Y. Sun, M. Bosch, S. Yuan, H. C. Zhou, *J. Am. Chem. Soc.* **2014**, *136*, 17714.
[77] D. Feng, Z. Y. Gu, J. R. Li, H. L. Jiang, Z. Wei, H. C. Zhou, *Angew. Chem., Int. Ed.* **2012**, *51*, 10307.
[78] D. Feng, W. C. Chung, Z. Wei, Z. Y. Gu, H. L. Jiang, Y. P. Chen, D. J. Darensbourg, H. C. Zhou, *J. Am. Chem. Soc.* **2013**, *135*, 17105.
[79] T. E. Webber, W. G. Liu, S. P. Desai, C. C. Lu, D. G. Truhlar, R. L. Penn, *ACS Appl. Mater. Interfaces* **2017**, *9*, 39342.
[80] Z. Hu, I. Castano, S. Wang, Y. Wang, Y. Peng, Y. Qian, C. Chi, X. Wang, D. Zhao, *Cryst. Growth Des.* **2016**, *16*, 2295.
[81] A. Schaate, P. Roy, A. Godt, J. Lippke, F. Waltz, M. Wiebcke, P. Behrens, *Chem. Eur. J.* **2011**, *17*, 6643.
[82] Z. Hu, Y. Peng, Z. Kang, Y. Qian, D. Zhao, *Inorg. Chem.* **2015**, *54*, 4862.
[83] S. S. Rajasree, J. Yu, S. M. Pratik, X. Li, R. Wang, A. S. Kumbhar, S. Goswami, C. J. Cramer, P. Deria, *J. Am. Chem. Soc.* **2022**, *144*, 1396.
[84] X. J. Kong, T. He, J. Zhou, C. Zhao, T. C. Li, X. Q. Wu, K. Wang, J. R. Li, *Small* **2021**, *17*, 2005357.
[85] W. Cheng, X. Tang, Y. Zhang, D. Wu, W. Yang, *Trends Food Sci. Technol.* **2021**, *112*, 268.
[86] G. Férey, C. Serre, C. Mellot-Draznieks, F. Millange, S. Surblé, J. Dutour, I. Margiolaki, *Angew. Chem., Int. Ed.* **2004**, *116*, 6456.
[87] G. Férey, C. Mellot-Draznieks, C. Serre, F. Millange, J. Dutour, S. Surblé, I. Margiolaki, *Science* **2005**, *309*, 2040.
[88] X. C. Huang, Y. Y. Lin, J. P. Zhang, X. M. Chen, *Angew. Chem., Int. Ed.* **2006**, *45*, 1557.
[89] C. Wang, X. Liu, N. K. Demir, J. P. Chen, K. Li, *Chem. Soc. Rev.* **2016**, *45*, 5107.
[90] B. Bueken, H. Reinsch, N. Heidenreich, A. Vandekerkhove, F. Vermoortele, C. EA Kirschhock, N. Stock, D. De Vos, R. Ameloot, *CrystEngComm* **2017**, *19*, 4152.
[91] N. C. Burtch, I. M. Walton, J. T. Hungerford, C. R. Morelock, Y. Jiao, J. Heinen, Y. S. Chen, A. A. Yakovenko, W. Xu, D. Dubbeldam, K. S. Walton, *Nat. Chem.* **2020**, *12*, 186.
[92] S. Yuan, J. Peng, Y. Zhang, Y. Shao-Horn, *J. Phys. Chem. C* **2019**, *123*, 28266.
[93] J. Shen, R. Fan, Y. Wang, J. Zhou, C. Chen, Z. Wei, S. Ju, T. Qian, Y. Peng, M. Shen, *Energy Environ. Sci.* **2022**, *15*, 3051.
[94] D. P. Dubal, N. R. Chodankar, D. H. Kim, P. Gomez-Romero, *Chem. Soc. Rev.* **2018**, *47*, 2065.
[95] S. P. Tripathy, S. Subudhi, A. Ray, P. Behera, A. Bhaumik, K. Parida, *Langmuir* **2022**, *38*, 1766.
[96] Y. Wang, Y. Fu, S. You, X. Li, L. Zhao, C. Qin, X. Wang, *CrystEngComm* **2021**, *23*, 8115.
[97] L. Xin, D. Zhang, K. Qu, Y. Lu, Y. Wang, K. Huang, Z. Wang, W. Jin, Z. Xu, *Adv. Func. Mater.* **2021**, *31*, 2104629.
[98] D. Zhang, W. He, J. Ye, X. Gao, D. Wang, J. Song, *Small* **2021**, *17*, 2005149.
[99] T. N. Do, C. You, J. Kim, *Energy Environ. Sci.* **2022**, *15*, 169.
[100] K. H. Ng, S. Y. Lai, C. K. Cheng, Y. W. Cheng, C. C. Chong, *Chem. Eng. J.* **2021**, *417*, 128847.
[101] A. K Singh, C. Das, A. Indra, *Coord. Chem. Rev.* **2022**, *465*, 214516.
[102] E. Safaralizadeh, S. Janitabar Darzi, A. R. Mahjoub, R. Abazari, *Res. Chem. Intermed.* **2017**, *43*, 1197.
[103] X. Li, K. Gao, B. Mo, J. Tang, J. Wu, H. Hou, *Inorg. Chem.* **2021**, *60*, 1352.
[104] Y. Liang, H. Jiang, H. Lin, C. Wang, K. Yu, C. Wang, J. Lv, B. Zhou, *Chem. Eng. J.* **2023**, *466*, 143220.
[105] L. Jiao, Y. Dong, X. Xin, R. Wang, H. Lv, *J. Mater. Chem. A* **2021**, *9*, 19725.
[106] L. Jiao, Y. Dong, X. Xin, L. Qin, H. Lv, *Appl. Catal. B: Environ.* **2021**, *291*, 120091.
[107] J. D. Xiao, H. L. Jiang, *Small* **2017**, *13*, 1700632.
[108] A. W. Peters, Z. Li, O. K. Farha, J. T. Hupp, *ACS Appl. Mater. Interfaces* **2016**, *8*, 20675.
[109] H. Noh, Y. Yang, S. Ahn, A. W. Peters, O. K. Farha, J. T. Hupp, *J. Electrochem. Soc.* **2019**, *166*, H3154.
[110] P. P. Bag, X. S. Wang, P. Sahoo, J. Xiong, R. Cao, *Catal. Sci. Technol.* **2017**, *7*, 5113.
[111] I. Choudhuri, D. G. Truhlar, *J. Phys. Chem. C* **2020**, *124*, 8504.
[112] P. M. Rajaitha, S. Hajra, K. Mistewicz, S. Panda, M. Sahu, D. Dubal, Y. Yamauchi, H. J. Kim, *J. Mater. Chem. A* **2020**, *10*, 15906.
[113] A. Nasu, A. Sakuda, T. Kimura, M. Deguchi, A. Tsuchimoto, M. Okubo, A. Yamada, M. Tatsumisago, A. Hayashi, *Small* **2022**, *18*, 2203383.
[114] Y. Li, S. Guo, T. Jin, Y. Wang, F. Cheng, L. Jiao, *Nano Energy* **2019**, *63*, 103821.
[115] W. Yan, H. Ma, X. Zhao, Y. Zhang, P. Vishniakov, X. Wang, X. Zhong, *Small* **2023**, *19*, 2208270.
[116] W. Zhong, B. Xiao, Z. Lin, Z. Wang, L. Huang, S. Shen, Q. Zhang, L. Gu, *Adv. Mater.* **2021**, *33*, 2007894.
[117] J. McAllister, N. A. G. Bandeira, J. C. McGlynn, A. Y. Ganin, Y. F. Song, C. Bo, H. N. Miras, *Nat. Commun.* **2019**, *10*, 370.
[118] Z. Li, N. M. Schweitzer, A. B. League, V. Bernales, A. W. Peters, A. B. Getsoian, T. C. Wang, J. T. Miller, A. Vjunov, J. L. Fulton, J. A. Lercher, C. J. Cramer, L. Gagliardi, J. T. Hupp, O. K. Farha, *J. Am. Chem. Soc.* **2016**, *138*, 1977.
[119] A. W. Peters, K. Otake, A. E. Platero-Prats, Z. Li, M. R. DeStefano, K. W. Chapman, O. K. Farha, J. T. Hupp, *ACS Appl. Mater. Interfaces* **2018**, *10*, 15073.
[120] H. Noh, Y. Yang, X. Zhang, T. A. Goetjen, Z. H. Syed, Z. Lu, S. Ahn, O. K. Farha, J. T. Hupp, *ChemElectroChem* **2020**, *7*, 509.
[121] X. Zhang, R. Lin, X. Meng, W. Li, F. Chen, J. Hou, *Inorg. Chem.* **2021**, *60*, 9987.
[122] X. Zhao, P. Pachfule, S. Li, J. R. J. Simke, J. Schmidt, A. Thomas, *Angew. Chem.* **2018**, *130*, 9059.
[123] X. Wang, W. Zhou, Y.-P. Wu, J.-W. Tian, X. K. Wang, D. D. Huang, J. Zhao, D. S. Li, *J. Alloys Compd.* **2018**, *753*, 228.
[124] A. Howe, T. Liseev, M. Gil-Sepulcre, C. Gimbert-Suriñach, J. Benet-Buchholz, A. Llobet, S. Ott, *Mater. Adv.* **2022**, *3*, 4227.
[125] R. H. Palmer, C. W. Kung, J. Liu, O. K. Farha, J. T. Hupp, *Langmuir* **2018**, *34*, 14143.
[126] C. W. Kung, J. E. Mondloch, T. C. Wang, W. Bury, W. Hoffeditz, B. M. Klahr, R. C. Klet, M. J. Pellin, O. K. Farha, J. T. Hupp, *ACS Appl. Mater. Interfaces* **2015**, *7*, 28223.
[127] S. Sanati, R. Abazari, A. Morsali, *Chem. Commun.* **2020**, *56*, 6652.

[128] Y. X. Duan, F. L. Meng, K. H. Liu, S. S. Yi, S. J. Li, J. M. Yan, Q. Jiang, *Adv. Mater.* **2018**, *30*, 1706194.
[129] Y. Zhang, R. Yang, H. Li, Z. Zeng, *Small* **2022**, *18*, 2203759.
[130] X. Wang, M. Fan, Y. Guan, Y. Liu, M. Liu, T. N. V. Karsili, J. Yi, X. D. Zhou, J. Zhang, *J. Mater. Chem. A* **2021**, *9*, 22710.
[131] S. L. Hou, J. Dong, X. L. Jiang, Z. H. Jiao, B. Zhao, *Angew. Chem., Int. Ed.* **2019**, *58*, 577.
[132] S. Y. Lee, H. Jung, N. K. Kim, H. S. Oh, B. K. Min, Y. J. Hwang, *J. Am. Chem. Soc.* **2018**, *140*, 8681.
[133] C. W. Kung, C. O. Audu, A. W. Peters, H. Noh, O. K. Farha, J. T. Hupp, *ACS Energy Lett.* **2017**, *2*, 2394.
[134] D. Sun, Y. Fu, W. Liu, L. Ye, D. Wang, L. Yang, X. Fu, Z. Li, *Chem. Eur. J.* **2013**, *19*, 14279.
[135] K. Sonowal, N. Nandal, P. Basyach, L. Kalita, S. L. Jain, L. Saikia, *J. CO2 Utiliz.* **2022**, *57*, 101905.
[136] K. Zhang, S. Goswami, H. Noh, Z. Lu, T. Sheridan, J. Duan, W. Dong, J. T. Hupp, *J. Photochem. Photobiol.* **2022**, *10*, 100111.
[137] Y. He, Z. Chang, S. Wu, Y. Qiao, S. Bai, K. Jiang, P. He, H. Zhou, *Adv. Energy Mater.* **2018**, *8*, 1802130.
[138] S. Nanda, A. Manthiram, *Energy Environ. Sci.* **2020**, *13*, 2501.
[139] K. Kim, T. Kim, J. H. Moon, *Small* **2022**, *18*, 2201416.
[140] B. Liu, V. S. Thoi, *Chem. Mater.* **2020**, *32*, 8450.
[141] G. Hai, H. Wang, *Coord. Chem. Rev.* **2022**, *469*, 214670.
[142] R. Abazari, S. Sanati, N. Li, J. Qian, *Inorg. Chem.* **2023**, *62*, 18680.
[143] N. S. Bobbitt, E. Li, R. Q. Snurr, *Braz. J. Chem. Eng.* **2022**, *39*, 919.
[144] M. Oschatz, M. Antonietti, *Energy Environ. Sci.* **2018**, *11*, 57.
[145] C. Peng, D. Yu, L. Wang, X. Yu, Z. Zhao, *J. Mate. Chem. A* **2021**, *9*, 12947.
[146] E. Martínez-Ahumada, M. L. Díaz-Ramírez, M. d. J. Velásquez-Hernández, V. Jancik, I. A. Ibarra, *Chem. Sci.* **2021**, *12*, 6772.
[147] S. Han, Y. Huang, T. Watanabe, S. Nair, K. S. Walton, D. S. Sholl, J. C. Meredith, *Microporous Mesoporous Mater.* **2013**, *173*, 86.
[148] M. Wen, G. Li, H. Liu, J. Chen, T. An, H. Yamashita, *Environ. Sci.: Nano* **2019**, *6*, 1006.
[149] P. Brandt, S. H. Xing, J. Liang, G. Kurt, A. Nuhnen, O. Weingart, C. Janiak, *ACS Appl. Mate. Interfaces* **2021**, *13*, 29137.
[150] S. Gorla, M. L. Díaz-Ramírez, N. S. Abeynayake, D. M. Kaphan, D. R. Williams, V. Martis, H. A. Lara-García, B. Donnadieu, N. Lopez, I. A. Ibarra, V. Montiel-palma, *ACS Appl. Mate. Interfaces* **2020**, *12*, 41758.
[151] G. Mercuri, M. Moroni, S. Galli, G. Tuci, G. Giambastiani, T. Yan, D. Liu, A. Rossin, *ACS Appl. Mater. Interfaces* **2021**, *13*, 58982.
[152] X. Xia, G. Hu, W. Li, S. Li, *ACS Appl. Nano Mater* **2019**, *2*, 6022.
[153] L. Luconi, G. Mercuri, T. Islamoglu, A. Fermi, G. Bergamini, G. Giambastiani, A. Rossin, *J. Mater. Chem. C* **2020**, *8*, 7492.
[154] T. M. Gür, *Energy Environ. Sci.* **2018**, *11*, 2696.
[155] B. Tahir, M. Tahir, N. A. S. Amin, *Appl.Catal. B: Environ.* **2019**, *248*, 167.
[156] M. B. Kim, P. K. Thallapally, *J. Coord. Chem.* **2021**, *74*, 216.
[157] S. Vandenbrande, T. Verstraelen, J. J. Gutiérrez-Sevillano, M. Waroquier, V. Van Speybroeck, *J. Phys. Chem. C* **2017**, *121*, 25309.
[158] G. O. Vissers, W. Zhang, O. E. Vilches, W. G. Liu, H. S. Yu, D. G. Truhlar, C. T. Campbell, *J. Phys. Chem. C* **2019**, *123*, 6586.
[159] J. H. Kang, T. U. Yoon, S. Y. Kim, M. B. Kim, H. J. Kim, H. C. Yang, Y. S. Bae, *Microporous Mesoporous Mater.* **2019**, *281*, 84.
[160] J. Liu, Z. Lu, Z. Chen, M. Rimoldi, A. J. Howarth, H. Chen, S. Alayoglu, R. Q. Snurr, O. K. Farha, J. T. Hupp, *ACS Appl. Mater. Interfaces* **2021**, *13*, 20081.
[161] H. Chen, Z. Chen, O. K. Farha, R. Q. Snurr, *ACS Sustainable Chem. Eng.* **2019**, *7*, 18242.
[162] R. Ge, X. X. Li, S. T. Zheng, *Coord. Chem. Rev.* **2021**, *435*, 213787.
[163] P. Chen, X. He, M. Pang, X. Dong, S. Zhao, W. Zhang, *ACS Appl. Mater. Interfaces* **2020**, *12*, 20429.
[164] P. R. Chauhan, S. C. Kaushik, S. K. Tyagi, *Renew. Sustain. Energy Rev.* **2022**, *154*, 111808.
[165] S. Wang, X. Xia, S. Li, *Appl. Therm. Eng.* **2021**, *189*, 116707.
[166] Z. Liu, G. An, X. Xia, S. Wu, S. Li, L. Wang, *J. Mater. Chem. A* **2021**, *9*, 6188.
[167] M. Yabushita, N. A. Grosso-Giordano, A. Fukuoka, A. Katz, *ACS Appl. Mater. Interfaces* **2018**, *10*, 39670.
[168] M. Yabushita, P. Li, V. Bernales, H. Kobayashi, A. Fukuoka, L. Gagliardi, O. K. Farha, A. Katz, *Chem. Commun.* **2016**, *52*, 7094.
[169] M. Yabushita, P. Li, H. Kobayashi, A. Fukuoka, O. K. Farha, A. Katz, *Chem. Commun.* **2016**, *52*, 11791.
[170] M. Yabushita, P. Li, K. A. Durkin, H. Kobayashi, A. Fukuoka, O. K. Farha, A. Katz, *Langmuir* **2017**, *33*, 4129.
[171] M. Yabushita, G. Papa, P. Li, A. Fukuoka, O. K. Farha, B. A. Simmons, A. Katz, *Fuel Process. Technol.* **2020**, *197*, 106189.
[172] R. Wang, C. Ching, W. R. Dichtel, D. E. Helbling, *Environ. Sci. Technol. Lett.* **2020**, *7*, 954.
[173] R. Li, S. Alomari, T. Islamoglu, O. K. Farha, S. Fernando, S. M. Thagard, T. M. Holsen, M. Wriedt, *Environ. Sci. Technol.* **2021**, *55*, 15162.
[174] M. Ding, X. Cai, H. L. Jiang, *Chem. Sci.* **2019**, *10*, 10209.
[175] S. Yuan, L. Feng, K. Wang, J. Pang, M. Bosch, C. Lollar, Y. Sun, J. Qin, X. Yang, P. Zhang, Q. Wang, L. Zou, Y. Zhang, L. Zhang, Y. Fang, J. Li, H. C. Zhou, *Adv. Mater.* **2018**, *30*, 1704303.
[176] L. Yang, K. B. Idrees, Z. Chen, J. Knapp, Y. Chen, X. Wang, R. Cao, X. Zhang, H. Xing, T. Islamoglu, O. K. Farha, *ACS Appl. Nano Mater.* **2021**, *4*, 4346.
[177] E. Vargas L, R. Q. Snurr, *Langmuir* **2015**, *31*, 10056.
[178] L. Zou, Y. S. Wei, C. C. Hou, C. Li, Q. Xu, *Small* **2021**, *17*, 2004809.
[179] Y. Yang, X. Zhang, S. Kanchanakungwankul, Z. Lu, H. Noh, Z. H. Syed, O. K. Farha, D. G. Truhlar, J. T. Hupp, *J. Am. Chem. Soc.* **2020**, *142*, 21169.
[180] K. Otake, Y. Cui, C. T. Buru, Z. Li, J. T. Hupp, O. K. Farha, *J. Am. Chem. Soc.* **2018**, *140*, 8652.
[181] F. Tian, H. Zhang, S. Liu, T. Wu, J. Yu, D. Wang, X. Jin, C. Peng, *Appl.Catal. B: Environ.* **2021**, *285*, 119834.
[182] J. Ye, L. Gagliardi, C. J. Cramer, D. G. Truhlar, *J. Catal.* **2017**, *354*, 278.
[183] V. Bernales, D. Yang, J. Yu, G. Gümüşlü, C. J. Cramer, B. C. Gates, L. Gagliardi, *ACS Appl. Mater. Interfaces* **2017**, *9*, 33511.
[184] J. Ye, L. Gagliardi, C. J. Cramer, D. G. Truhlar, *J. Catal.* **2018**, *360*, 160.
[185] S. Pellizzeri, M. Barona, V. Bernales, P. Miró, P. Liao, L. Gagliardi, R. Q. Snurr, R. B. Getman, *Catal. Today* **2018**, *312*, 149.
[186] J. Liu, J. Ye, Z. Li, K. Otake, Y. Liao, A. W. Peters, H. Noh, D. G. Truhlar, L. Gagliardi, C. J. Cramer, O. K. Farha, J. T. Hupp, *J. Am. Chem. Soc.* **2018**, *140*, 11174.
[187] Y. Zhang, X. Kang, Z. Jian, *Nat. Commun.* **2022**, *13*, 725.
[188] T. A. Goetjen, J. G. Knapp, Z. H. Syed, R. A. Hackler, X. Zhang, M. Delferro, J. T. Hupp, O. K. Farha, *Catal. Sci. Technol.* **2022**, *12*, 1619.
[189] X. Wang, X. Zhang, R. Pandharkar, J. Lyu, D. Ray, Y. Yang, S. Kato, J. Liu, M. C. Wasson, T. Islamoglu, Z. Li, J. T. Hupp, C. J. Cramer, L. Gagliardi, O. K. Farha, *ACS Catal.* **2020**, *10*, 8995.
[190] S. P. Desai, J. Ye, T. Islamoglu, O. K. Farha, C. C. Lu, *Organometallics* **2019**, *38*, 3466.
[191] L. R. Redfern, Z. Li, X. Zhang, O. K. Farha, *ACS Appl. Nano Mater.* **2018**, *1*, 4413.
[192] A. E. Platero-Prats, A. B. League, V. Bernales, J. Ye, L. C. Gallington, A. Vjunov, N. M. Schweitzer, Z. Li, J. Zheng, B. L. Mehdi, A. J. Stevens, A. Dohnalkova, M. Balasubramanian, O. K. Farha, J. T. Hupp, N. D. Browning, J. L. Fulton, D. M. Camaioni, J. A. Lercher, D. G. Truhlar, L. Gagliardi, C. J. Cramer, K. W. Chapman, *J. Am. Chem. Soc.* **2017**, *139*, 10410.
[193] S. T. Madrahimov, J. R. Gallagher, G. Zhang, Z. Meinhart, S. J. Garibay, M. Delferro, J. T. Miller, O. K. Farha, J. T. Hupp, S. T. Nguyen, *ACS Catal.* **2015**, *5*, 6713.

[194] V. Bernales, A. B. League, Z. Li, N. M. Schweitzer, A. W. Peters, R. K. Carlson, J. T. Hupp, C. J. Cramer, O. K. Farha, L. Gagliardi, *J. Phys. Chem. C* **2016**, *120*, 23576.
[195] H. Shabbir, S. Pellizzeri, M. Ferrandon, I. S. Kim, N. A. Vermeulen, O. K. Farha, M. Delferro, A. B. F. Martinson, R. B. Getman, *Catal. Sci. Technol.* **2020**, *10*, 3594.
[196] Y. Wang, P. Hu, J. Yang, Y. A. Zhu, D. Chen, *Chem. Soc. Rev.* **2021**, *50*, 4299.
[197] C. A. Gaggioli, J. Sauer, L. Gagliardi, *J. Am. Chem. Soc.* **2019**, *141*, 14603.
[198] D. R. Pahls, M. A. Ortuño, P. H. Winegar, C. J. Cramer, L. Gagliardi, *Inorg. Chem.* **2017**, *56*, 8739.
[199] M. C. Simons, M. A. Ortuño, V. Bernales, C. A. Gaggioli, C. J. Cramer, A. Bhan, L. Gagliardi, *ACS Catal.* **2018**, *8*, 2864.
[200] Y. B. Huang, M. Shen, X. Wang, P. Huang, R. Chen, Z. J. Lin, R. Cao, *J. Catal.* **2016**, *333*, 1.
[201] H. Noh, Y. Cui, A. W. Peters, D. R. Pahls, M. A. Ortuno, N. A. Vermeulen, C. J. Cramer, L. Gagliardi, J. T. Hupp, O. K. Farha, *J. Am. Chem. Soc.* **2016**, *138*, 14720.
[202] K. Berijani, A. Morsali, J. T. Hupp, *Catal. Sci. Technol.* **2019**, *9*, 3388.
[203] Z. Li, A. W. Peters, V. Bernales, M. A. Ortuño, N. M. Schweitzer, M. R. DeStefano, L. C. Gallington, A. E. Platero-Prats, K. W. Chapman, C. J. Cramer, L. Gagliardi, J. T. Hupp, O. K. Farha, *ACS Cent. Sci.* **2017**, *3*, 31.
[204] Z. Li, A. W. Peters, A. E. Platero-Prats, J. Liu, C. W. Kung, H. Noh, M. R. DeStefano, N. M. Schweitzer, K. W. Chapman, J. T. Hupp, O. K. Farha, *J. Am. Chem. Soc.* **2017**, *139*, 15251.
[205] D. Yang, S. O. Odoh, T. C. Wang, O. K. Farha, J. T. Hupp, C. J. Cramer, L. Gagliardi, B. C. Gates, *J. Am. Chem. Soc.* **2015**, *137*, 7391.
[206] M. K. Samantaray, E. Pump, A. Bendjeriou-Sedjerari, V. D'Elia, J. D. Pelletier, M. Guidotti, R. Psaro, J. M. Basset, *Chem. Soc. Rev.* **2018**, *47*, 8403.
[207] W. Han, L. H. Shao, X. J. Sun, Y. H. Liu, F. M. Zhang, Y. Wang, P. Y. Dong, G. L. Zhang, *Appl.Catal. B: Environ.* **2022**, *317*, 121710.
[208] B. Yang, K. Sharkas, L. Gagliardi, D. G. Truhlar, *Catal. Sci. Technol.* **2019**, *9*, 7003.
[209] S. Sanati, A. Morsali, H. García, *Inter. J. Hydrogen Energy* **2023**, *48*, 14749.
[210] R. C. Klet, T. C. Wang, L. E. Fernandez, D. G. Truhlar, J. T. Hupp, O. K. Farha, *Chem. Mater.* **2016**, *28*, 1213.
[211] I. S. Kim, J. Borycz, A. E. Platero-Prats, S. Tussupbayev, T. C. Wang, O. K. Farha, J. T. Hupp, L. Gagliardi, K. W. Chapman, C. J. Cramer, A. B. F. Martinson, *Chem. Mater.* **2015**, *27*, 4772.
[212] J. M. Lownsbury, I. A. Santos-López, W. Zhang, C. T. Campbell, H. S. Yu, W. G. Liu, C. J. Cramer, D. G. Truhlar, T. Wang, J. T. Hupp, O. K. Farha, *J. Phys. Chem. C* **2016**, *120*, 16850.
[213] N. E. Thornburg, Y. Liu, P. Li, J. T. Hupp, O. K. Farha, J. M. Notestein, *Catal. Sci. Technol.* **2016**, *6*, 6480.
[214] M. D. Korzyński, D. F. Consoli, S. Zhang, Y. Román-Leshkov, M. Dincaˇ, *J. Am. Chem.Soc.* **2018**, *140*, 6956.
[215] Y. Feng, Y. Xu, S. Liu, D. Wu, Z. Su, G. Chen, J. Liu, G. Li, *Coord. Chem. Rev.* **2022**, *459*, 214414.
[216] Y. Chen, F. Jiménez-Ángeles, B. Qiao, M. D. Krzyaniak, F. Sha, S. Kato, X. Gong, C. T. Buru, Z. Chen, X. Zhang, N. C. Gianneschi, M. R. Wasielewski, M. Olvera de la Cruz, O. K. Farha, *J. Am. Chem. Soc.* **2020**, *142*, 18576.
[217] R. Zhang, X. Yan, K. Fan, *Acc. Mater. Res.* **2021**, *2*, 534.
[218] J. Moons, A. Loosen, C. Simms, F. de Azambuja, T. N. Parac-Vogt, *Nanoscale* **2021**, *13*, 12298.
[219] P. Li, R. C. Klet, S. Y. Moon, T. C. Wang, P. Deria, A. W. Peters, B. M. Klahr, H. J. Park, S. S. Al-Juaid, J. T. Hupp, O. K. Farha, *Chem. Commun.* **2015**, *51*, 10925.
[220] D. A. Wood, C. Nwaoha, B. F. Towler, *J. Nat. Gas Sci. Eng.* **2012**, *9*, 196.
[221] R. Gupta, A. Mishra, Y. Thirupathaiah, A. K. Chandel, *Biomass Conversion. Biorefin.* **2022**, *16*, 1.
[222] S. Ahn, S. L. Nauert, K. E. Hicks, M. A. Ardagh, N. M. Schweitzer, O. K. Farha, J. M. Notestein, *ACS Catal.* **2020**, *10*, 2817.
[223] L. N. Ma, L. Zhang, W. F. Zhang, Z. H. Wang, L. Hou, Y. Y. Wang, *Inorg. Chem.* **2022**, *61*, 2679.
[224] R. A. Hackler, R. Pandharkar, M. S. Ferrandon, I. S. Kim, N. A. Vermeulen, L. C. Gallington, K. W. Chapman, O. K. Farha, C. J. Cramer, J. Sauer, L. Gagliardi, A. B. F. Martinson, M. Delferro, *J. Am. Chem. Soc.* **2020**, *142*, 20380.
[225] J. Liu, Z. Li, X. Zhang, K.-i. Otake, L. Zhang, A. W. Peters, M. J. Young, N. M. Bedford, S. P. Letourneau, D. J. Mandia, J. W. Elam, O. K. Farha, J. T. Hupp, *ACS Catal.* **2019**, *9*, 3198.
[226] M. Yabushita, P. Li, T. Islamoglu, H. Kobayashi, A. Fukuoka, O. K. Farha, A. Katz, *Ind. Eng. Chem. Res.* **2017**, *56*, 7141.
[227] N. Zheng, X. He, R. Hu, R. Wang, Q. Zhou, Y. Lian, Z. Hu, *Appl.Catal. B: Environ.* **2022**, *307*, 121157.
[228] C. T. Buru, M. C. Wasson, O. K. Farha, *ACS Appl. Nano Mater* **2019**, *3*, 658.
[229] Z. Thiam, E. Abou-Hamad, B. Dereli, L. Liu, A. H. Emwas, R. Ahmad, H. Jiang, A. A. Isah, P. B. Ndiaye, M. Taoufik, Y. Han, L. Cavallo, J. M. Basset, M. Eddaoudi, *J. Am. Chem. Soc.* **2020**, *142*, 16690.
[230] L. Dai, Y. Wang, Y. Liu, C. He, R. Ruan, Z. Yu, L. Jiang, Z. Zeng, Q. Wu, *Sci. Total Environ.* **2020**, *749*, 142386.
[231] J. Sun, Y. Wang, *ACS Catal.* **2014**, *4*, 1078.
[232] V. Paluka, T. Maihom, M. Probst, J. Limtrakul, *Phys. Chem. Chem. Phys.* **2020**, *22*, 13622.
[233] M. A. Ortuño, V. Bernales, L. Gagliardi, C. J. Cramer, *J. Phys. Chem. C* **2016**, *120*, 24697.
[234] K. Sorimachi, M. Terada, *J. Am. Chem. Soc.* **2008**, *130*, 14452.
[235] S. Ahn, S. L. Nauert, C. T. Buru, M. Rimoldi, H. Choi, N. M. Schweitzer, J. T. Hupp, O. K. Farha, J. M. Notestein, *J. Am. Chem. Soc.* **2018**, *140*, 8535.
[236] H. Beyzavi, R. C. Klet, S. Tussupbayev, J. Borycz, N. A. Vermeulen, C. J. Cramer, J. F. Stoddart, J. T. Hupp, O. K. Farha, *J. Am. Chem. Soc.* **2014**, *136*, 15861.
[237] A. Cadiau, K. Adil, P. M. Bhatt, Y. Belmabkhout, M. Eddaoudi, *Science* **2016**, *353*, 137.
[238] B. C. Bukowski, F. A. Son, Y. Chen, L. Robison, T. Islamoglu, R. Q. Snurr, O. K. Farha, *Chem. Mater.* **2022**, *34*, 4134.
[239] Y. Shi, G. Wang, J. Mei, C. Xiao, D. Hu, A. Wang, Y. Song, Y. Ni, G. Jiang, A. Duan, *ACS Omega* **2020**, *5*, 15576.
[240] J. Dai, K. Li, Z. Feng, J. Xu, Y. Chen, H. Zhang, Z. Zhang, *J. Phys. Chem. C* **2020**, *124*, 24713.
[241] H. Chen, R. Q. Snurr, *Langmuir* **2020**, *36*, 1372.
[242] T. Ikuno, J. Zheng, A. Vjunov, M. Sanchez-Sanchez, M. A. Ortuño, D. R. Pahls, J. L. Fulton, D. M. Camaioni, Z. Li, D. Ray, B. L. Mehdi, N. D. Browning, O. K. Farha, J. T. Hupp, C. J. Cramer, L. Gagliardi, J. A. Lercher, *J. Am. Chem. Soc.* **2017**, *139*, 10294.
[243] J. Baek, B. Rungtaweevoranit, X. Pei, M. Park, S. C. Fakra, Y. S. Liu, R. Matheu, S. A. Alshmimri, S. Alshehri, C. A. Trickett, G. A. Somorjai, O. M. Yaghi, *J. Am. Chem. Soc.* **2018**, *140*, 18208.
[244] X. Zhang, Z. Huang, M. Ferrandon, D. Yang, L. Robison, P. Li, T. C. Wang, M. Delferro, O. K. Farha, *Nat. Catal.* **2018**, *1*, 356.
[245] A. B. Thompson, D. R. Pahls, V. Bernales, L. C. Gallington, C. D. Malonzo, T. Webber, S. J. Tereniak, T. C. Wang, S. P. Desai, Z. Li, I. S. Kim, L. Gagliardi, R. L. Penn, K. W. Chapman, A. Stein, O. K. Farha, J. T. Hupp, A. B. F. Martinson, C. C. Lu, *Chem. Mater.* **2016**, *28*, 6753.
[246] N. Couzon, J. Dhainaut, C. Campagne, S. Royer, T. Loiseau, C. Volkringer, *Coord. Chem. Rev.* **2022**, *467*, 214598.

[247] C. T. Buru, M. B. Majewski, A. J. Howarth, R. H. Lavroff, C. W. Kung, A. W. Peters, S. Goswami, O. K. Farha, *ACS Appl. Mater. Interfaces* **2018**, *10*, 23802.
[248] Z. Lu, J. Liu, X. Zhang, Y. Liao, R. Wang, K. Zhang, J. Lyu, O. K. Farha, J. T. Hupp, *J. Am. Chem. Soc.* **2020**, *142*, 21110.
[249] S. Y. Moon, Y. Liu, J. T. Hupp, O. K. Farha, *Angew. Chem.* **2015**, *127*, 6899.
[250] M. R. Momeni, C. J. Cramer, *Chem. Mater.* **2018**, *30*, 4432.
[251] S. J. Garibay, O. K. Farha, J. B. DeCoste, *Chem. Commun.* **2019**, *55*, 7005.
[252] D. F. S. Gallis, J. A. Harvey, C. J. Pearce, M. G. Hall, J. B. DeCoste, M. K. Kinnan, J. A. Greathouse, *J. Mater. Chem. A* **2018**, *6*, 3038.
[253] Y. Liao, T. Sheridan, J. Liu, O. Farha, J. Hupp, *ACS Appl. Mater. Interfaces* **2021**, *13*, 30565.
[254] H. Wang, J. J. Mahle, T. M. Tovar, G. W. Peterson, M. G. Hall, J. B. DeCoste, J. H. Buchanan, C. J. Karwacki, *ACS Appl. Mater. Interfaces* **2019**, *11*, 21109.
[255] A. Atilgan, T. Islamoglu, A. J. Howarth, J. T. Hupp, O. K. Farha, *ACS Appl. Mate. Interfaces* **2017**, *9*, 24555.
[256] A. J. Howarth, C. T. Buru, Y. Liu, A. M. Ploskonka, K. J. Hartlieb, M. McEntee, J. J. Mahle, J. H. Buchanan, E. M. Durke, S. S. Al-Juaid, J. F. Stoddart, J. B. DeCoste, J. T. Hupp, O. K. Farha, *Chem. Eur. J.* **2017**, *23*, 214.
[257] Y. Liao, W. Chen, S. Li, W. Jiao, Y. Si, J. Yu, B. Ding, *Small* **2021**, *17*, 2101639.
[258] M. Schwenk, *Toxicol. Lett.* **2018**, *293*, 253.
[259] Y. Liu, A. J. Howarth, N. A. Vermeulen, S. Y. Moon, J. T. Hupp, O. K. Farha, *Coord. Chem. Rev.* **2017**, *346*, 101.
[260] T. Islamoglu, M. A. Ortuño, E. Proussaloglou, A. J. Howarth, N. A. Vermeulen, A. Atilgan, A. M. Asiri, C. J. Cramer, O. K. Farha, *Angew. Chem., Int. Ed.* **2018**, *57*, 1949.
[261] M. L. Mendonca, R. Q. Snurr, *ACS Catal.* **2020**, *10*, 1310.
[262] M. Kalaj, M. R. Momeni, K. C. Bentz, K. S. Barcus, J. M. Palomba, F. Paesani, S. M. Cohen, *Chem. Commun.* **2019**, *55*, 3481.
[263] T. G. Grissom, A. M. Plonka, C. H. Sharp, A. M. Ebrahim, Y. Tian, D. L. Collins-Wildman, A. L. Kaledin, H. J. Siegal, D. Troya, C. L. Hill, A. I. Frenkel, D. G. Musaev, W. O. Gordon, C. J. Karwacki, M. B. Mitchell, J. R. Morris, *ACS Appl. Mater. Interfaces* **2020**, *12*, 14641.
[264] L. C. Gallington, I. S. Kim, W. G. Liu, A. A. Yakovenko, A. E. Platero-Prats, Z. Li, T. C. Wang, J. T. Hupp, O. K. Farha, D. G. Truhlar, A. B. F. Martinson, K. W. Chapman, *J. Am. Chem. Soc.* **2016**, *138*, 13513.
[265] A. E. Platero-Prats, Z. Li, L. C. Gallington, A W. Peters, J. T. Hupp, O. K. Farha, K. W. Chapman, *Faraday Discuss.* **2017**, *201*, 337.
[266] R. Wang, M. Wen, S. Liu, Y. Lu, L. Makroni, B. Muthiah, T. Zhang, Z. Wang, Z. Wang, *Phys. Chem. Chem. Phys.* **2021**, *23*, 12749.
[267] H. Chen, R. Q. Snurr, *ACS Appl. Mater. Interfaces* **2020**, *12*, 14631.
[268] R. Gil-San-Millan, E. López-Maya, A. E. Platero-Prats, V. Torres-Pérez, P. Delgado, A. W. Augustyniak, M. K. Kim, H. W. Lee, S. G. Ryu, J. AR Navarro, *J. Am. Chem. Soc.* **2019**, *141*, 11801.
[269] M. C. de Koning, M. van Grol, T. Breijaert, *Inorg. Chem.* **2017**, *56*, 11804.
[270] Y. Zhang, X. Zhang, J. Lyu, K.-i. Otake, X. Wang, L. R. Redfern, C. D. Malliakas, Z. Li, T. Islamoglu, B. Wang, O. K. Farha, *J. Am. Chem. Soc.* **2018**, *140*, 11179.
[271] M. C. de Koning, G. W. Peterson, M. van Grol, I. Iordanov, M. McEntee, *Chem. Mater.* **2019**, *31*, 7417.
[272] M. Eddleston, N. A. Buckley, P. Eyer, A. H. Dawson, *Lancet* **2008**, *371*, 597.
[273] M. S. Vera, L. Lagomarsino, M. Sylvester, G. L. Pérez, P. Rodríguez, H. Mugni, R. Sinistro, M. Ferraro, C. Bonetto, H. Zagarese, H. Pizarro, *Ecotoxicology* **2010**, *19*, 710.
[274] X. Zhu, B. Li, J. Yang, Y. Li, W. Zhao, J. Shi, J. Gu, *ACS Appl. Mater. Interfaces* **2015**, *7*, 223.
[275] H. Chen, P. Liao, M. L. Mendonca, R. Q. Snurr, *J. Phys. Chem. C* **2018**, *122*, 12362.
[276] S. Bose, P. S. Kumar, D. V. N. Vo, *Chemosphere* **2021**, *283*, 131447.
[277] A. M. Bondžić, T. D. Lazarević Pašti, I. A. Pašti, B. P. Bondžić, M. D. Momčilović, A. Loosen, T. N. Parac-Vogt, *ACS Appl. Nano Mater.* **2022**, *5*, 3312.
[278] T. C. C. Franca, D. A. S. Kitagawa, S. F. A. Cavalcante, J. A. V. da Silva, E. Nepovimova, K. Kuca, *Novichoks: Int. J. Mol. Sci.* **2019**, *20*, 1222.
[279] C. P. Holstege, M. Kirk, F. R. Sidell, *Crit. Care Clin.* **1997**, *13*, 923.
[280] M. L. Mendonca, R. Q. Snurr, *Chem. Eur. J.* **2019**, *25*, 9217.
[281] N. S. Bobbitt, M. L. Mendonca, A. J. Howarth, T. Islamoglu, J. T. Hupp, O. K. Farha, R. Q. Snurr, *Chem. Soc. Rev.* **2017**, *46*, 3357.
[282] D. Bůžek, J. Demel, K. Lang, *Inorg. Chem.* **2018**, *57*, 14290.
[283] T. Islamoglu, M. A. Ortuño, E. Proussaloglou, A. J. Howarth, N. A. Vermeulen, A. Atilgan, A. M. Asiri, C. J. Cramer, O. K. Farha, *Angew. Chem., Int. Ed.* **2018**, *57*, 1949.
[284] D. Troya, *J. Phys. Chem. C* **2016**, *120*, 29312.
[285] G. Wang, C. Sharp, A. M. Plonka, Q. Wang, A. I. Frenkel, W. Guo, C. Hill, C. Smith, J. Kollar, D. Troya, J. R. Morris, *J. Phys. Chem. C* **2017**, *121*, 11261.
[286] A. M. Ploskonka, J. B. DeCoste, *J. Hazard. Mater.* **2019**, *375*, 191.
[287] M. Agrawal, D. F. Sava Gallis, J. A. Greathouse, D. S. Sholl, *J. Phys. Chem. C* **2018**, *122*, 26061.
[288] H. Chen, P. Liao, M. L. Mendonca, R. Q. J. T. Snurr, *J. Phys. Chem. C* **2018**, *122*, 12362.
[289] D. Yang, V. Bernales, T. Islamoglu, O. K. Farha, J. T. Hupp, C. J. Cramer, L. Gagliardi, B. C. Gates, *J. Am. Chem. Soc.* **2016**, *138*, 15189.
[290] R. S. Berry, *J. Chem. Phys.* **1960**, *32*, 933.
[291] M. C. Capel-Sanchez, J. M. Campos-Martin, J. L. G. Fierro, *Energy Environ. Sci.* **2010**, *3*, 328.
[292] M. Sun, R. Abazari, J. Chen, C. Mustansar Hussain, Y. Zhou, A. M. Kirillov, *ACS Appl. Mater. Interfaces* **2023**, *15*, 52581.
[293] L. Yu, W. G. Cui, Q. Zhang, Z. F. Li, Y. Shen, T. L. Hu, *Mater. Adv.* **2021**, *2*, 1294.
[294] P. Deria, J. E. Mondloch, E. Tylianakis, P. Ghosh, W. Bury, R. Q. Snurr, J. T. Hupp, O. K. Farha, *J. Am. Chem. Soc.* **2013**, *135*, 16801.
[295] Y. Pan, R. Abazari, B. Tahir, S. Sanati, Y. Zheng, M. Tahir, J. Gao, *Coord. Chem. Rev.* **2024**, *499*, 215538.
[296] S. Goswami, J. Yu, S. Patwardhan, P. Deria, J. T. Hupp, *ACS Energy Lett.* **2021**, *6*, 848.
[297] C. Dai, B. Liu, *Energy Environ. Sci.* **2020**, *13*, 24.
[298] R. Abazari, S. Sanati, A. Morsali, A. M. Kirillov, *Inorg. Chem.* **2021**, *60*, 9660.
[299] X. Li, X. Ma, F. Zhang, X. Dong, X. Lang, *Appl. Catal. B: Environ.* **2021**, *298*, 120514.
[300] L. Wang, D. Shen, H. Zhang, B. Mo, J. Wu, H. Hou, *Chem. Eur. J.* **2022**, *28*, 202103466.
[301] Y. Liu, C. T. Buru, A. J. Howarth, J. J. Mahle, J. H. Buchanan, J. B. DeCoste, J. T. Hupp, O. K. Farha, *J. Mater. Chem A* **2016**, *4*, 13809.
[302] L. Zhang, C. Xu, Z. Chen, X. Li, P. Li, *J.Hazard. Mater.* **2010**, *173*, 168.
[303] M. N. Romanias, A. Andrade-Eiroa, R. Shahla, Y. Bedjanian, A. G. Zogka, A. Philippidis, P. Dagaut, *J. Phys. Chem. A* **2014**, *118*, 7007.
[304] J. G. Knapp, X. Zhang, T. Elkin, L. E. Wolfsberg, S. L. Hanna, F. A. Son, B. L. Scott, O. K. Farha, *CrystEngComm* **2020**, *22*, 2097.
[305] T. Xu, C. W. Cheung, X. Hu, *Angew. Chem.* **2014**, *126*, 5010.
[306] T. Zhang, P. Wang, Z. Gao, Y. An, C. He, C. Duan, *RSC Adv.* **2018**, *8*, 32610.
[307] M. S. Lee, S. J. Garibay, A. M. Ploskonka, J. B. DeCoste, *MRS Commun.* **2019**, *9*, 464.
[308] F. Guo, S. Yang, Y. Liu, P. Wang, J. Huang, W. Y. Sun, *ACS Catal.* **2019**, *9*, 8464.

[309] D. Feng, T. F. Liu, J. Su, M. Bosch, Z. Wei, W. Wan, D. Yuan, Y. P. Chen, X. Wang, K. Wang, X. Lian, Z. Y. Gu, J. Park, X. Zou, H. C. Zhou, *Nat. Commun.* **2015**, *6*, 1.
[310] X. Li, J. Shen, C. Wu, K. Wu, *Small* **2019**, *15*, 1805567.
[311] W. Zhang, M. Gong, J. Yang, J. Gu, *Langmuir* **2021**, *37*, 8157.
[312] S. Kobayashi, Y. Mori, J. S. Fossey, M. M. Salter, *Chem. Rev.* **2011**, *111*, 2626.
[313] K. Gao, H. Li, Q. Meng, J. Wu, H. Hou, *ACS Appl. Mater. Interfaces* **2021**, *13*, 2779.
[314] J. Gao, B. Jiang, C. Ni, Y. Qi, Y. Zhang, N. Oturan, M. A. Oturan, *Appl.Catal. B: Environ.* **2019**, *254*, 391.
[315] H. Choi, A. W. Peters, H. Noh, L. C. Gallington, A. E. Platero-Prats, M. R. DeStefano, M. Rimoldi, S. Goswami, K. W. Chapman, O. K. Farha, J. T. Hupp, *ACS Appl. Energy Mater.* **2019**, *2*, 8695.
[316] P. O. Saboe, E. Conte, M. Farell, G. C. Bazan, M. Kumar, *Energy Environ. Sci.* **2017**, *10*, 14.
[317] A. Loosen, F. de Azambuja, T. N. Parac-Vogt, *Mate. Adv.* **2022**, *3*, 2475.
[318] X. Zhao, Z. Zhang, X. Cai, B. Ding, C. Sun, G. Liu, C. Hu, S. Shao, M. Pang, *ACS Appl. Mater. Interfaces* **2019**, *11*, 7884.
[319] M. Pander, A. Żelichowska, W. Bury, *Polyhedron* **2018**, *156*, 131.
[320] X. Zhao, S. Liu, C. Hu, Y. Liu, M. Pang, J. Lin, *ACS Appl. Bio Mater.* **2019**, *2*, 4436.
[321] L. Manna, D. J. Milliron, A. Meisel, E. C. Scher, A. P. Alivisatos, *Nat. Mater.* **2003**, *2*, 382.
[322] M. H. Teplensky, M. Fantham, P. Li, T. C. Wang, J. P. Mehta, L. J. Young, P. Z. Moghadam, J. T. Hupp, O. K. Farha, C. F. Kaminski, D. Fairen-Jimenez, *J. Am. Chem. Soc.* **2017**, *139*, 7522.
[323] S. Wang, Y. Chen, S. Wang, P. Li, C. A. Mirkin, O. K. Farha, *J. Am. Chem. Soc.* **2019**, *141*, 2215.
[324] S. Kato, K.-i. Otake, H. Chen, I. Akpinar, C. T. Buru, T. Islamoglu, R. Q. Snurr, O. K. Farha, *J. Am. Chem. Soc.* **2019**, *141*, 2568.
[325] A. J. Howarth, T. C. Wang, S. S. Al-Juaid, S. G. Aziz, J. T. Hupp, O. K. Farha, *Dalton Trans.* **2016**, *45*, 93.
[326] C. L. Mu, D. Wu, H. F. Lu, H. Xie, Q. L. Zhang, *Chin. J. Anal. Chem.* **2017**, *45*, e1726.
[327] S. Biswas, Y. Chen, Y. Xie, X. Sun, Y. Wang, *Mikrochim. Acta* **2020**, *187*, 661.
[328] X. Cai, Z. Xie, B. Ding, S. Shao, S. Liang, M. Pang, J. Lin, *Adv. Sci.* **2019**, *6*, 1900848.
[329] C. Hu, Z. Zhang, S. Liu, X. Liu, M. Pang, *ACS Appl. Mater. Interfaces* **2019**, *11*, 23072.
[330] S. Liu, C. Hu, Y. Liu, X. Zhao, M. Pang, J. Lin, *Chem. Eur. J.* **2019**, *25*, 4315.
[331] J. Ma, X. Ma, L. Xu, *Measurement* **2022**, *200*, 111620.
[332] S. M. McLeod, L. Robison, G. Parigi, A. Olszewski, R. J. Drout, X. Gong, T. Islamoglu, C. Luchinat, O. K. Farha, T. J. Meade, *ACS Appl. Mater. Interfaces* **2020**, *12*, 41157.
[333] P. Deria, W. Bury, J. T. Hupp, O. K. Farha, *Chem. Commun.* **2014**, *50*, 1965.
[334] D. Lin, X. Liu, R. Huang, W. Qi, R. Su, Z. He, *Chem. Commun.* **2019**, *55*, 6775.
[335] L. Kong, Y. Wang, C. B. Andrews, C. Zheng, *Chem. Eng. J.* **2022**, *435*, 134830.
[336] J. Li, X. Li, T. Hayat, A. Alsaedi, C. Chen, *ACS Sustainable Chem. Eng.* **2017**, *5*, 11496.
[337] S. Rangwani, A. J. Howarth, M. R. DeStefano, C. D. Malliakas, A. E. Platero-Prats, K. W. Chapman, O. K. Farha, *Polyhedron* **2018**, *151*, 338.
[338] B. Marouane, M. Klug, K. S. As, J. Engel, S. Reichel, E. Janneck, S. Peiffer, *J. Geochem. Explor.* **2021**, *223*, 106708.
[339] A. J. Howarth, M. J. Katz, T. C. Wang, A. E. Platero-Prats, K. W. Chapman, J. T. Hupp, O. K. Farha, *J. Am. Chem. Soc.* **2015**, *137*, 7488.
[340] Z. J. Lin, H. Q. Zheng, H. Y. Zheng, L. P. Lin, Q. Xin, R. Cao, *Inorg. Chem.* **2017**, *56*, 14178.
[341] T. Chen, K. Yu, C. Dong, X. Yuan, X. Gong, J. Lian, X. Cao, M. Li, L. Zhou, B. Hu, R. He, W. Zhu, X. Wang, *Coord. Chem. Rev.* **2022**, *467*, 214615.
[342] W. Zhang, G. Ye, J. Chen, *J. Mater. Chem. A* **2013**, *1*, 12706.
[343] W. Zhang, X. Dong, Y. Mu, Y. Wang, J. Chen, *J. Mater. Chem. A* **2021**, *9*, 16685.
[344] G. L. Yang, X. L. Jiang, H. Xu, B. Zhao, *Small* **2021**, *17*, 2005327.
[345] M. Karamanlioglu, R. Preziosi, G. D. Robson, *Polym. Degrad. Stab.* **2017**, *137*, 122.
[346] Z. J. Lin, H. Q. Zheng, Y. N. Zeng, Y. L. Wang, J. Chen, G. J. Cao, J. F. Gu, B. Chen, *Chem. Eng. J.* **2019**, *378*, 122196.
[347] L. González, F. J. Carmona, N. M. Padial, J. A. R. Navarro, E. Barea, C. R. Maldonado, *Mater. Today Chem.* **2021**, *22*, 100596.
[348] X. Kong, J. Jiang, J. Ma, Y. Yang, W. Liu, Y. Liu, *Water Res.* **2016**, *90*, 15.
[349] J. Glüge, M. Scheringer, I. T. Cousins, J. C. DeWitt, G. Goldenman, D. Herzke, R. Lohmann, C. A. Ng, X. Trier, Z. Wang, *Environ. Sci. Process. Impacts* **2020**, *22*, 2345.
[350] R. Li, S. Alomari, R. Stanton, M. C. Wasson, T. Islamoglu, O. K. Farha, T. M. Holsen, S. M. Thagard, D. J. Trivedi, M. Wriedt, *Chem. Mater.* **2021**, *33*, 3276.
[351] J. Zheng, D. Barpaga, O. Y. Gutiérrez, N. D. Browning, B. L. Mehdi, O. K. Farha, J. A. Lercher, B. P. McGrail, R. K. Motkuri, *ACS Appl. Energy Mater.* **2018**, *1*, 5853.
[352] G. Lammel, Z. Kitanovski, P. Kukučka, J. Novák, A. M. Arangio, G. P. Codling, A. Filippi, J. Hovorka, J. Kuta, C. Leoni, P. Příbylová, R. Prokeš, O. Sáňka, P. Shahpoury, H. Tong, M. Wietzoreck, *Environ. Sci. Technol.* **2020**, *54*, 2615.
[353] J. Noh, H. Kim, C. Lee, S. J. Yoon, S. Chu, B. O. Kwon, J. Ryu, J. J. Kim, H. Lee, U. H. Yim, J. P. Giesy, J. S. Khim, *Environ. Sci. Technol.* **2018**, *52*, 7910.
[354] D. Ning, Q. Liu, Q. Wang, X. M. Du, Y. Li, W. J. Ruan, *Dalton Trans.* **2019**, *48*, 5705.
[355] P. Shan, J. Hu, M. Liu, Z. Tao, X. Xiao, C. Redshaw, *Coord. Chem. Rev.* **2022**, *467*, 214580.
[356] J. Xia, Y. Gao, G. Yu, *J. Colloid Interface Sci.* **2021**, *590*, 495.
[357] M. K. Javed, A. Sulaiman, M. Yamashita, Z. Y. Li, *Coord. Chem. Rev.* **2022**, *467*, 214625.
[358] W29. Guan, W. Zhou, J. Lu, C. Lu, *Chem. Soc. Rev.* **2015**, *44*, 6981.
[359] M. Gong, J. Yang, Y. Li, Q. Zhuang, J. Gu, *J. Mater. Chem. C* **2019**, *7*, 12674.
[360] P. Duan, J. C. Moreton, S. R. Tavares, R. Semino, G. Maurin, S. M. Cohen, K. Schmidt-Rohr, *J. Am. Chem. Soc.* **2019**, *141*, 7589.
[361] D. Fan, A. Ozcan, N. A. Ramsahye, D. Zhao, G. Maurin, R. Semino, *ACS Mater. Lett.* **2021**, *3*, 344.
[362] J. X. Wang, Y. Wang, I. Nadinov, J. Yin, L. Gutiérrez-Arzaluz, G. Healing, O. Alkhazragi, Y. Cheng, J. Jia, N. Alsadun, V. S. Kale, C. H. Kang, T. K. Ng, O. Shekhah, H. N. Alshareef, O. M. Bakr, M. Eddaoudi, B. S. Ooi, O. F. Mohammed, *J. Am. Chem. Soc.* **2022**, *144*, 6813.
[363] I. Fernández, *Chem. Sci.* **2020**, *11*, 3769.
[364] Y. Zhou, Q. Yang, J. Cuan, Y. Wang, N. Gan, Y. Cao, T. Li, *Analyst* **2018**, *143*, 3628.

Reza Abazari obtained his M.Sc. in Inorganic Chemistry from K.N. Toosi University of Technology (Iran) in 2012 and his Ph.D. degree from Tarbiat Modares University in 2019. Currently, he is working as a Youth Research Professor at the University of Maragheh, Iran. His research interests include the design and synthesis of nanostructured materials based on crystalline porous frameworks for electrochemical energy storage and photocatalytic applications.

Soheila Sanati obtained her Ph.D. degree in Inorganic Chemistry at Azarbaijan Shahid Madani University (Iran) in February 2019. Her research interests mainly focus on the design, synthesis, and applications of layered double hydroxides and metal–organic framework-based nanostructured materials for energy storage and conversion, irradiation thermal treatment, renewable clean energy, and environmental protection applications.

Majed Bajaber After receiving my Ph.D. in Chemistry back in 2020 from the University of New Orleans, USA, he joined King Khalid University in Saudi Arabia as an assistant professor. Recently, he has been honored to lead the Chemistry Department at KKU as well as supervise five laboratories conducting research in multi-disciplinary such as environmental, medicinal, and advanced materials. This year, he received the university's Promising Researcher Award and aspires to be someone who helps the world through science. He wants to inspire generations in Saudi Arabia to be scientists of the future. Research is his work and hobby.

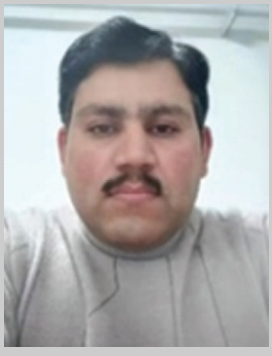

Muhammad Sufyan Javed received his B.S. (2012) and M.S. (2014) degrees from COMSATS University Islamabad, Lahore Campus, and was involved in fuel cells research (Prof. Rizwan Raza). He received his Ph.D. (2017) in degree Condensed Matter Physics under the supervision of Prof. Chenguo Hu. He did his postdoctoral research work at the Department of Physics, Jinan University, China, under the supervision of Prof. Wenjie Mai. Currently, he is working as a Youth Research Professor at the School of Physical Science and Technology, Lanzhou University, China. He has published more than 370 peer-reviewed research articles. His research interests include the synthesis of porous materials, two-dimensional materials, and MXenes for energy conversion and storage devices, especially supercapacitors and multi-ion batteries.

Jinjie Qian earned his Ph.D. degree in 2015 from the Fujian Institute of Research on the Structure of Matter (FJIRSM), Chinese Academy of Sciences, under the supervision of CAS Academician Maochun Hong. Currently serving as an associate professor in the College of Chemistry and Materials Engineering at Wenzhou University, his research focuses on electrochemical investigations into the nanostructures and adjustable morphology of metal–organic frameworks and their derivatives for energy applications.

Deepak Dubal is currently working as a Full Professor at the Queensland University of Technology (QUT), Australia. He is a prolific, well-cited, and multiplefellowship-winning scientist. His achievements are honored by several prestigious fellowships such as Brain Korea-21 (South Korea2011), Alexander von Humboldt (Germany-2012), Marie Curie (Spain-2014), and Australian Future Fellowship (Australia-2018). His research expertise is in the design and development of multifunctional materials for clean energy conversion and storage technologies with a special focus on supercapacitors, lithium-ion batteries, Li-ion capacitors, and electrochemical flow cells. In addition, his team is extending their research area in biomass valorization and battery recycling, aiding the circular economy and sustainable practices.